77

Pressure Estimation of Piezoelectric Rings Embedded Orthogonally in Cylindrical Shells

by

Ching-Yu Lin

B.S., Engineering
National Taiwan University, 1994

Submitted to the Department of Aeronautics and Astronautics Engineering
in Partial Fulfillment of the Requirements for the Degree of
Master of Science in Aeronautics and Astronautics Engineering
at the
Massachusetts Institute of Technology

February 1998

Signature of Author .....
Department of Aeronautics and Astronautics
November 13, 1997

Certified by .....
Professor John Kim Vandiver
Department of Ocean Engineering
Thesis Supervisor

Certified by .....
Professor John Dugundji, Emeritus
Department of Aeronautics and Astronautics
Thesis Supervisor

Accepted by .....
Professor Jaime Peraire
Chairman, Department Graduate Committee

Pressure Estimation of Piezoelectric Rings Embedded Orthogonally in Cylindrical Shells

by

Ching-Yu Lin

Submitted to the Department of Aeronautics and Astronautics Engineering
February, 1998 in partial fulfillment of the
requirement for the Degree of Master Science in
Aeronautics and Astronautics Engineering

Abstract

The goal at this thesis is to estimate the pressure exerted by Navy I and Navy VI type piezoelectric rings under electrical excitation when embedded orthogonally in PVC and steel cylindrical shells. A general mathematical model to estimate the pressure exerted by an elastically bonded piezoelectric ring is developed using electro-mechanical elasticity of piezoelectric materials in cylindrical coordinates. The model shows that this pressure depends not only on the geometry and the material properties of the piezoelectric ring but also on the radial expansion of the piezoelectric ring which is related to the driving point impedance of the surrounding material.

The radial velocity response at any radial position of a circular plate driven by a piezoelectric ring in the center is modeled by solving the wave equation in polar coordinates using Bessel functions. The modeled velocity is validated by experimental measurement. The pressure per unit volt exerted by the piezoelectric ring is estimated as 55 $dB\ re.\ 1\ N/m^2\ /V$ in a 9 cm radius PVC circular plate and 68 $dB\ re.\ 1N/m^2\ /V$ in a 15 cm radius aluminum circular plate.

Based on the study of circular plates and the assumption that the driving point impedance of the piezoelectric ring embedded in the cylindrical shell is the same as that for an infinite circular plate, the pressure per unit volt exerted by piezoelectric ring in the cylindrical shell can be estimated in the same way as that in the circular plate. The pressure per unit volt exerted by the piezoelectric ring is estimated as 68 $dB\ re.\ 1\ N/m^2\ /V$ in a 5 m long, 0.15 m radius steel shell and $55 dB\ re.\ 1\ N/m^2\ /V$ in a 6 m long, 0.2 m radius PVC shell. The near field and far field longitudinal velocity responses on the cylindrical shells are also validated by experimental measurement.

Thesis Supervisor: Dr. John Kim Vandiver
Title: Professor of Ocean Engineering

Thesis Supervisor: Dr. John Dugundji
Title: Professor of Aeronautics and Astronautics, Emeritus

Acknowledgments

I would like to thank Dr. Bondaryk, Professor Vandiver, Professor Dugundji and Professor Spearing for their guidance and encouragement throughout this thesis. I also like to thank Patricia Manning for her help on my experimental work and Mark Hayner for his far field model program. Of course, I am grateful to my parents for their love and support.

This research was funded by Contract N00014-95-0475 from the Office of Naval Research.

Table of Contents

List of Tables

List of Figures

Chapter 1

Introduction

1.1 Motivation

The stealth capability of a submarine which corresponds to its acoustic characteristics is one at the main requirements of submarine design and operation. Thus, the structural acoustic properties of ship and submarine hulls are of high interest to structural acoustics researchers.

Recent structural acoustics research on finite-length submerged shells has quantified the importance of membrane waves in radiation and scattering[1]. Such waves can be compressional, transverse-shear, or flexural, but the first two are of direct importance in the intermediate frequencies where the acoustic wavelength is of the same order as the shell radius. At these intermediate frequencies, compressional and transverse-shear membrane waves are the principal determinants of the shell's radiation and scattering properties, while flexural waves, because they are poorly coupled to the acoustic medium, serve mainly as modifiers of the principal waves.

In order to provide the submarine design community guidance for improved acoustic performance, MIT's Structural Acoustics Group in Ocean Engineering has conducted experimental and theoretical research to explore various modifications to the shell structure, including its frames and bulkheads. The main approach is to study the propagation of compressional and transverse-shear waves in modified cylindrical shells by measuring the response due to different circumferential modal forces.

In the experiment, as illustrated in Figure 1.1, single modes are excited by 12 evenly spaced excitation sources along the circumference of a cylindrical shell. Different modal forces can be simulated by changing the phases of the driving sources. For instance, the zero mode can be simulated by driving 12 sources in the same phase and the first mode can be simulated by driving two neighboring source groups in the opposite phase. The number 12 is determined by Nyquist criteria along the circumference for the frequency range $0 < f < 25KHz$ [2].

Experiments on submerged cylindrical shells in water are costly because due to the large tank facilities required to surround the shell. As a result, before conducting expensive experiments in water, experiments in air are helpful to understand basic wave propagation in the modified cylindrical shell.

Several candidates for in-air excitation devices, proposed by the previous researchers[2], include shakers and piezoelectric rings. Compared to piezoelectric rings, shakers are 2 orders of magnitude more expensive. In addition, heavy mass and large volume make shakers difficult to mount. It is also difficult to drive pure in-plane forces in cylindrical shells with shakers. Two possible ways to mount shakers are illustrated in Figure 1.2. The first method is not suitable because the offset force also induces a moment. In the second method, it is difficult to mount the shaker in the interior cylindrical shell. This also doubles the number of shakers. Subsequently, piezoelectric rings were selected as the driving devices in the cylindrical shell. As illustrated in Figure 1.3, these piezoelectric rings are planted vertically into the cylindrical surface, so they can drive pure in-plane forces in the cylindrical shell. The only drawback of using piezoelectric ring is that the force they exert is not calibrated or known. Therefore, the main motivation in this

thesis is to calibrate or estimate the forces exerted by the piezoelectric rings embedded in the cylindrical shell.

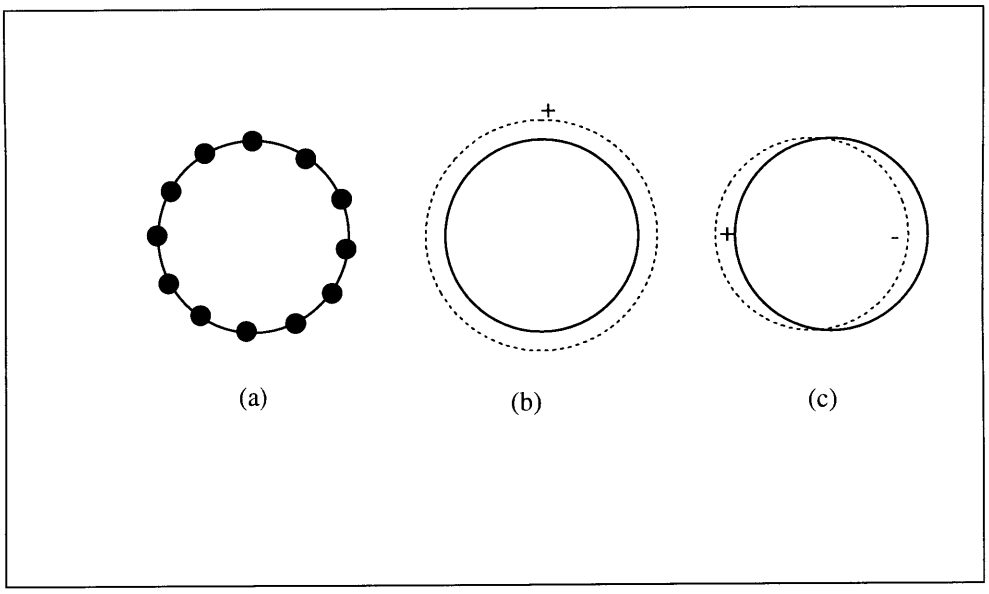

Figure 1.1 Modal Forces: (a) 12 Evenly Spaced Excitation Forces (b) Zero Mode (c) First Mode

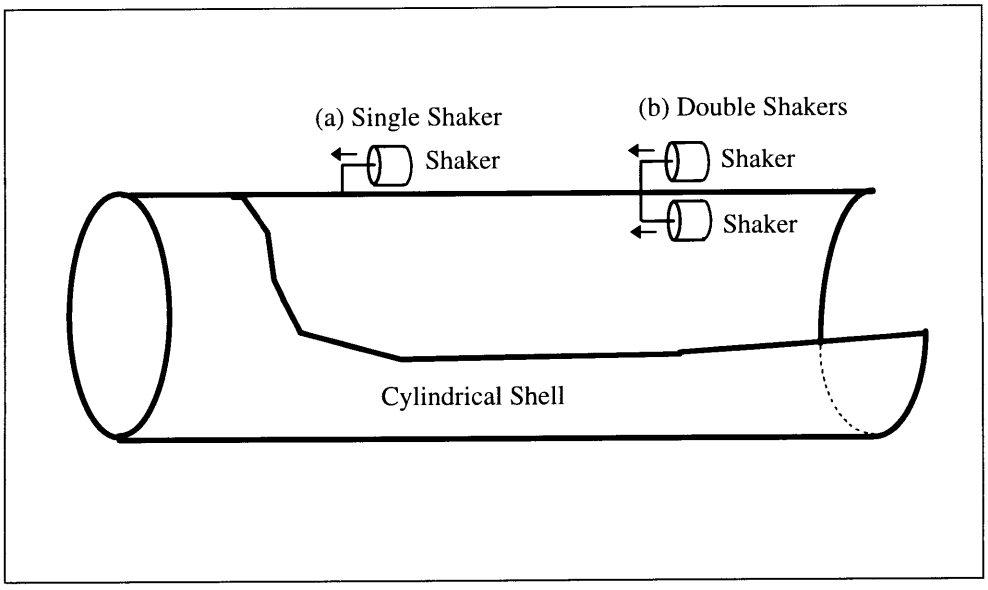

Figure 1.2 Method to Mount the Shaker: (a) Single Shaker (b) Double Shakers

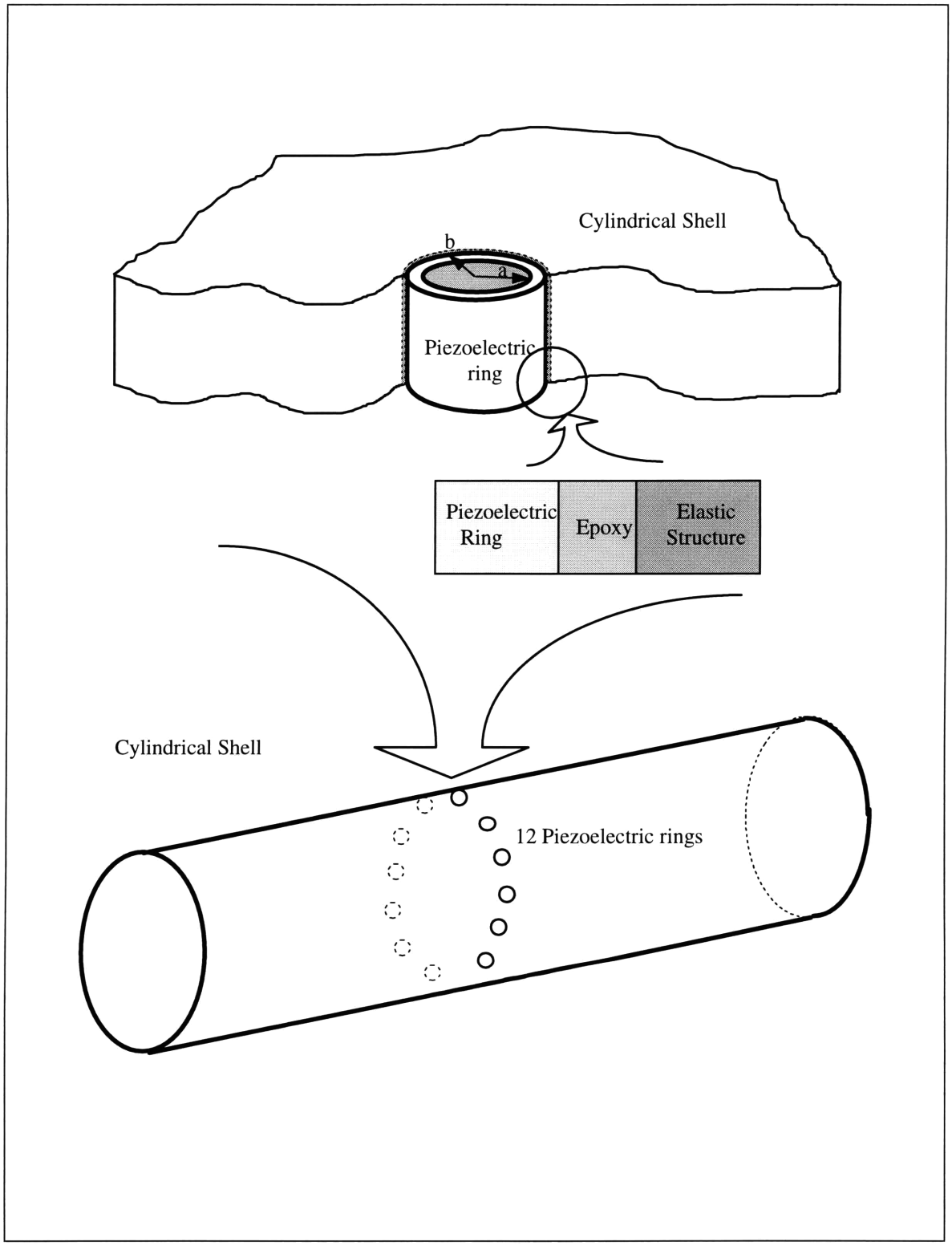

Figure 1.3 Twelve Piezoelectric Ring Sources Planted Vertically in a Cylindrical Shell

1.2 Previous Work

The wave analysis of forced vibration in a cylindrical shell of finite length has been studied by Borgiotii and Rosen using the state vector approach[3]. Propagation of compressional, flexural and shear waves, excited by an array of piezoelectric ring sources, has been successfully measured and compared to this shell theory by Bondaryk[4]. The measurement is presented as velocity per unit voltage; however, the theory is presented as velocity per unit force. Therefore, it is the goal of this thesis to correlate the measurement and the theory by calibrating or estimating the force per unit voltage excited by each piezoelectric ring.

Characteristics of typical piezoelectric materials have been studied for decades. A standard can be found in an IEEE Document.[5] The mechanical vibration and electrical admittance of free piezoelectric cylindrical shells has been studied by Haskin and Walsh[6]; however, piezoelectric rings bonded by elastic material have not been discussed in the literature. Therefore, a general model for elastically bonded piezoelectric rings is developed in this thesis by a modification to the boundary condition.

1.3 Overview of Thesis

Chapter 1 introduces the motivation, previous work and the outline of the thesis. The main approach of this thesis, discussed in Chapter 2, is to develop a general mathematical model to estimate the pressure exerted by elastically bonded piezoelectric rings using the electro-mechanical elasticity of piezoelectric materials in cylindrical coordinates. The model shows that this pressure depends not only on the geometry and

the material properties of the piezoelectric ring but also on the radial expansion of the piezoelectric ring which is related to the driving point impedance of the surrounding material. The stiffer the surrounding material is, the higher the impedance of the surrounding material, so the less the ring expands.

In Chapter 3, the dynamic radial expansion at any radial position of the circular plate, in which a piezoelectric ring is embedded, is modeled by solving the wave equation in cylindrical coordinates using Bessel functions. To illustrate how this circular plate model works, two plates with different materials and radii are studied and taken as examples. The radial velocity response at any radial position of the plate is validated by experimental measurement. Therefore, the pressure per unit voltage exerted by the piezoelectric ring in the circular plate can be calculated using the results from Chapter 2. The calculated pressure per unit voltage exerted by the piezoelectric ring embedded in a 9 cm radius PVC circular plate is about 55 $dB\ re.\ 1\ N/m^2/V$ in the frequency below 20 KHz and almost independent of the frequency except at the two resonant peaks at 5.5 and 14.5 KHz. Similarly, The estimated pressure per unit voltage exerted by the piezoelectric ring embedded in 15 cm radius aluminum circular plate is about 68 $dB\ re.\ 1\ N/m^2/V$ in the frequency range below 20 KHz and almost independent of the frequency except the resonant peak at 12 KHz. These resonant peaks, due to the finite radius of the plate, are also discussed in this chapter.

Based on this fundamental study of piezoelectric rings in circular plates, in the first section of Chapter 4, the pressure per unit voltage exerted by the piezoelectric ring in the cylindrical shell can be estimated in the same way by assuming that the driving point impedance of the ring in a cylindrical shell is the same as that in an infinite circular plate.

Based on this assumption, the calculated longitudinal velocity near the outer surface of the ring in the shell is validated by experimental measurement. A steel and a PVC cylindrical shell are studied and taken as examples in this chapter. The pressure per unit voltage exerted by the single ring is estimated 68 $dB\ re.1\ N/m^2/V$ in the steel shell and 55 $dB\ re.1\ N/m^2/V$ in the PVC shell, and these values are apparently independent of the frequency. In the second section, the far field response is also predicted by integrating the pressure along the ring surface into the unidirectional force and using the state space analysis for the wave propagation in the cylindrical shell developed by Borgiotti and Rosen [3]. The prediction is also validated by experimental measurement. Finally, the conclusion and suggestion for the future work is summarized in Chapter 5.

Chapter 2.

General Physics of Piezoelectric Rings

In this chapter, the general physics of piezoelectric materials is introduced. A mathematical model of a piezoelectric ring bonded by elastic material is derived to examine the pressure and response excited by the ring. The radial velocity response of a piezoelectric ring in air is measured and compared to the model of a free piezoelectric ring. The radial velocity response of epoxy-coated piezoelectric ring is also measured to quantify the effect of epoxy which is used subsequently to connect the piezoelectric ring to elastic materials.

2.1 A Review of Linear Piezoelectricity

Piezoelectric material is generally used as an electro-mechanical transducer whose frequency can range from 0 up to 50MHz [7]. More details can be found in an IEEE Standard[5] and other literature[8]. What follows is a review of the basic physics of piezoelectric materials, including the electro-mechanical constitutive equation, material properties and operating modes.

1. Constitutive Equation

A piezoelectric material has an asymmetric atomic lattice, therefore, exhibiting a dipole moment[7]. Above a certain temperature, known as the Curie point, the dipole directions have random orientations. The dipole may be aligned by applying a strong electric field at a temperature near the Curie point; this process is know as poling. After being polarized, piezoelectric material can change its mechanical dimension when an

electrical field is applied to it. Conversely, an electrical field is generated when this material is subjected to a mechanical deformation. Figure 2.1 defines the coordinates, x_1, x_2 and x_3, of a piezoelectric material corresponding to its polarization. The deformation of a piezoelectric material is contributed to by the strain due to the stress field, T, and the electrical field, E. The strain field, S, can be represented in terms of the stress and the electrical field

$$S = s^E T + dE \tag{2.1}$$

where S is the strain vector denoted as:

$$S = \begin{bmatrix} S_1 \\ S_2 \\ S_3 \\ S_4 \\ S_5 \\ S_6 \end{bmatrix} = \begin{bmatrix} S_{11} \\ S_{22} \\ S_{33} \\ 2S_{23} \\ 2S_{13} \\ 2S_{12} \end{bmatrix},$$

T is the stress vector denoted as:

$$T = \begin{bmatrix} T_1 \\ T_2 \\ T_3 \\ T_4 \\ T_5 \\ T_6 \end{bmatrix} = \begin{bmatrix} T_{11} \\ T_{22} \\ T_{33} \\ T_{23} \\ T_{13} \\ T_{12} \end{bmatrix},$$

E is the electric field vector denoted as:

$$E = \begin{Bmatrix} E_1 \\ E_2 \\ E_3 \end{Bmatrix},$$

d is the piezoelectric constant matrix denoted as:

$$d = \begin{bmatrix} 0 & 0 & d_{31} \\ 0 & 0 & d_{31} \\ 0 & 0 & d_{33} \\ 0 & d_{15} & 0 \\ d_{15} & 0 & 0 \end{bmatrix},$$

s^E is the compliance matrix and the superscript, E, means that the compliance is measured at a constant field (short circuit) and is denoted as:

$$s^E = \begin{bmatrix} s_{11}^E & s_{12}^E & s_{13}^E & 0 & 0 & 0 \\ s_{12}^E & s_{11}^E & s_{13}^E & 0 & 0 & 0 \\ s_{13}^E & s_{13}^E & s_{33}^E & 0 & 0 & 0 \\ 0 & 0 & 0 & s_{44}^E & 0 & 0 \\ 0 & 0 & 0 & 0 & s_{44}^E & 0 \\ 0 & 0 & 0 & 0 & 0 & s_{66}^E \end{bmatrix}.$$

Inversely, the electrical displacement is also contributed by the stress field and the electrical field, so that:

$$D = d_t T + \varepsilon^T E, \tag{2.2}$$

where D is the electric displacement vector denoted as:

$$D = \begin{Bmatrix} D_1 \\ D_2 \\ D_3 \end{Bmatrix},$$

d_t is the transpose of the d matrix, ε^T is the free dielectric constant matrix and the superscript T means that the dielectric constant is measured at a constant stress field and is denoted as:

$$\varepsilon^T = \begin{bmatrix} \varepsilon_{11}^T & 0 & 0 \\ 0 & \varepsilon_{11}^T & 0 \\ 0 & 0 & \varepsilon_{33}^T \end{bmatrix}.$$

Therefore, Equations 2.1 and 2.2 can be written in a matrix form:

$$\begin{bmatrix} S \\ D \end{bmatrix} = \begin{bmatrix} s^E & d \\ d_t & \varepsilon^T \end{bmatrix} \begin{bmatrix} T \\ E \end{bmatrix} \tag{2.3}$$

or

$$\begin{bmatrix} S_1 \\ S_2 \\ S_3 \\ S_4 \\ S_5 \\ S_6 \\ D_1 \\ D_2 \\ D_3 \end{bmatrix} = \begin{bmatrix} s_{11}^E & s_{12}^E & s_{13}^E & 0 & 0 & 0 & 0 & 0 & d_{31} \\ s_{12}^E & s_{11}^E & s_{13}^E & 0 & 0 & 0 & 0 & 0 & d_{31} \\ s_{13}^E & s_{13}^E & s_{33}^E & 0 & 0 & 0 & 0 & 0 & d_{33} \\ 0 & 0 & 0 & s_{44}^E & 0 & 0 & 0 & d_{15} & 0 \\ 0 & 0 & 0 & 0 & s_{44}^E & 0 & d_{15} & 0 & 0 \\ 0 & 0 & 0 & 0 & 0 & s_{66}^E & 0 & 0 & 0 \\ 0 & 0 & 0 & 0 & d_{15} & 0 & \varepsilon_{11}^T & 0 & 0 \\ 0 & 0 & 0 & d_{15} & 0 & 0 & 0 & \varepsilon_{11}^T & 0 \\ d_{31} & d_{31} & d_{33} & 0 & 0 & 0 & 0 & 0 & \varepsilon_{33}^T \end{bmatrix} \begin{bmatrix} T_1 \\ T_2 \\ T_3 \\ T_4 \\ T_5 \\ T_6 \\ E_1 \\ E_2 \\ E_3 \end{bmatrix}, \tag{2.4}$$

which are the well-know constitutive equations of piezoelectric materials. As shown in Equation 2.4, the constitutive equations couple the electrical and mechanical fields using the property constants of piezoelectric material, such as the compliance, s^E, the piezoelectric constant, d, and the dielectric constant, ε^T.

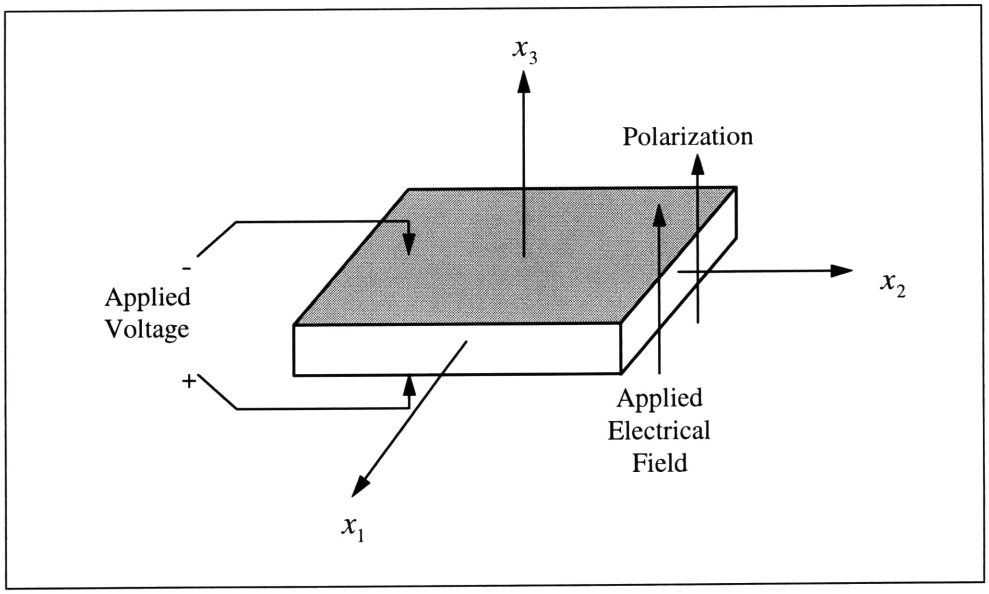

Figure 2.1 Poling Direction of Piezoelectric Material

2. Mode of Operation[9]

With different polarization, load stress and applied voltage, three operation modes of piezoelectric materials are available for different applications. The first one is the longitudinal mode, also called the 3-3 mode, because an electrical field, E_3, is applied along the poling axis and a normal load, T_3, is applied along the poling axis, as illustrated in Figure 2.2(a). If all other stresses are zero, the constitutive equations are simply:

$$\begin{Bmatrix} S_3 \\ D_3 \end{Bmatrix} = \begin{bmatrix} s_{33}^E & d_{33} \\ d_{33} & \varepsilon_{33}^T \end{bmatrix} \begin{Bmatrix} T_3 \\ E_3 \end{Bmatrix} \tag{2.5}$$

The second one is the transverse mode, also called the 3-1 mode, because the electrical field, E_3, is applied along the poling axis and a normal load, T_1, is applied perpendicular to the poling axis, as illustrated in Figure 2.2(b). If all other stresses are zero, the constitutive equations are simply:

$$\begin{Bmatrix} S_1 \\ D_3 \end{Bmatrix} = \begin{bmatrix} s_{11}^E & d_{31} \\ d_{31} & \varepsilon_{33}^T \end{bmatrix} \begin{Bmatrix} T_1 \\ E_3 \end{Bmatrix} \tag{2.6}$$

The third one is the shear mode, also called the 1-5 mode, because the electrical field, E_3, is applied along the poling axis and a shear load, T_5, is applied perpendicular to the poling axis, as illustrated in Figure 2.2(c). If all other stresses are zero, the constitutive equations become:

$$\begin{Bmatrix} S_5 \\ D_1 \end{Bmatrix} = \begin{bmatrix} s_{44}^E & d_{15} \\ d_{15} & \varepsilon_{11}^T \end{bmatrix} \begin{Bmatrix} T_5 \\ E_1 \end{Bmatrix} \tag{2.7}$$

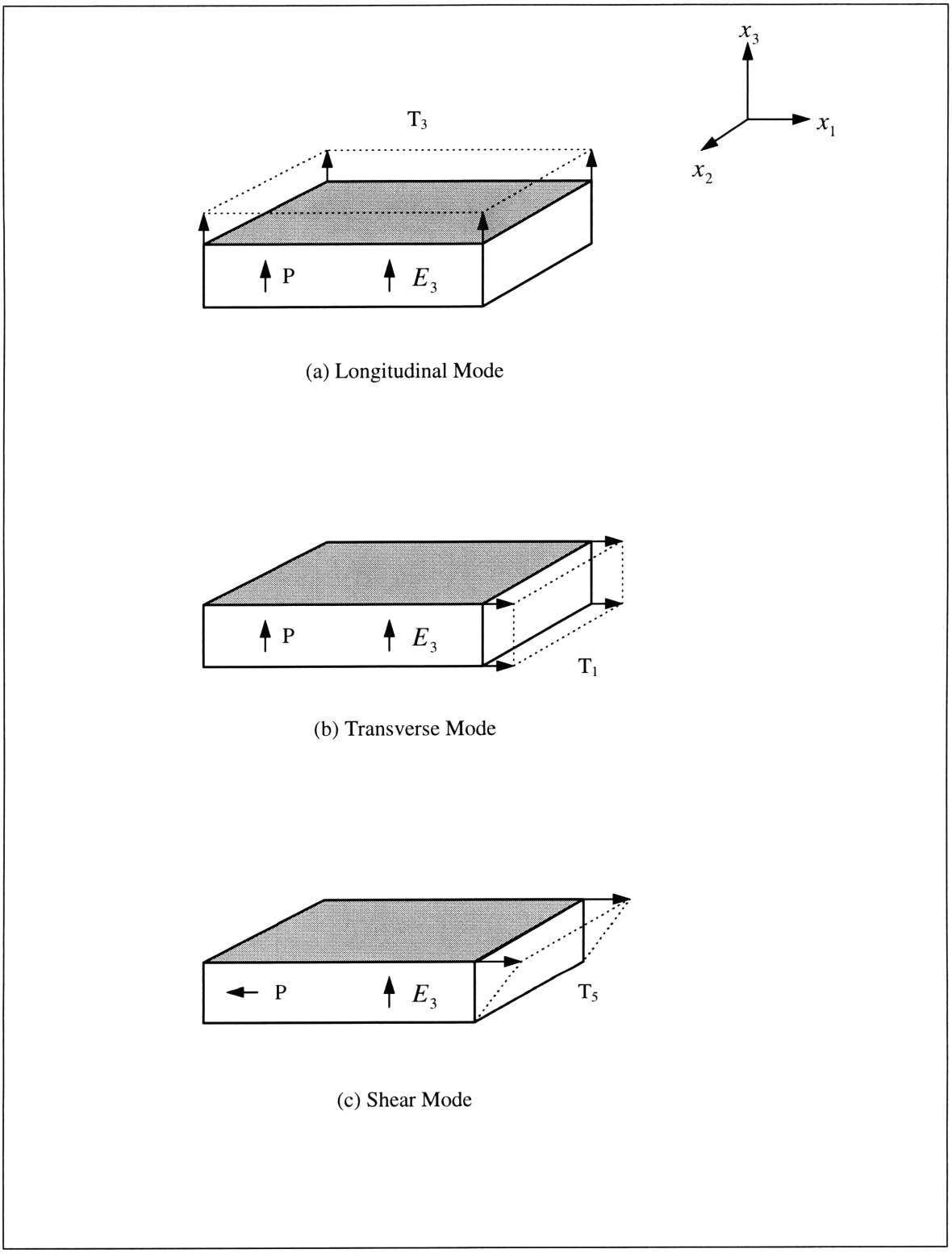

Figure 2.2 Operating Modes of Piezoelectric Materials: (a) Longitudinal Mode (b) Transverse Mode (c) Shear Mode.

3. Material Properties of Typical Piezoelectric Material

Table 2.1 lists the properties of three typical piezoelectric materials. [10] The value of these properties may vary with different manufacturers.

Table 2.1 Material Properties of Typical Piezoelectric Material

Type	Navy I PZT-4	Navy II PZT-5A	Navy VI PZT-5H
$\varepsilon_{33}^T/\varepsilon_0$	1300	1700	3400
$\varepsilon_{11}^T/\varepsilon_0$	1475	1730	3130
d_{31} $(10^{-12} meters/volts)$	-123	-171	-274
d_{33}	289	374	593
d_{15}	496	584	741
s_{11}^E $(10^{-12} meter^2/newton)$	12.3	16.4	16.5
s_{33}^E	15.5	18.8	20.7

where ε_0 is dielectric constant of free space, which is 8.85×10^{-12} $(farads/meter)$

4. Examples

Example 1: Static Problem

As shown in Figure 2.3, a NAVY VI type piezoelectric material, size 5 cm long (L), 1 cm wide (W) and 1 mm thick(t), is polarized along the thickness direction. The material is subject to a 10 N pulling force (F) along the length direction and a 100 volts voltage (v) applied across the thickness. Therefore, the piezoelectric material operates in transverse mode. The displacement due to the applied voltage is of interest in this example.

Case 1: Force Only

If only Force but no voltage is applied on the piezoelectric material, the stress is

$$T_1 = F/A = 1\cdot10^6 (N/m^2),$$

where A is the cross section area, and the electrical field is

$$E_3 = 0,$$

Using Equation 2.6 and Table 2.1, the strain is simply

$$S_1 = s_{11}^E T_1 = 1.65\cdot10^{-5}$$

According to the definition,

$$S_1 = \frac{\Delta L}{L},$$

the displacement along the length direction ΔL is

$$\Delta L = S_1 L = 8.25 \cdot 10^{-7} (m),$$

so the piezoelectric elongates.

Case 2: Both Force and Voltage

If a 10 N force and a 100 volts voltage are applied on the piezoelectric, the stress is

$$T_1 = F/A = 1 \cdot 10^6 (N/m^2)$$

and the electrical field are

$$E_3 = -V/t = -100/0.001 = -10^5 (V/m),$$

Using Equation 2.6 and Table 2.1, the strain is

$$S_1 = s_{11}^E T_1 + d_{31} E_3$$

$$S_1 = 165 \cdot 10^{-7} + 274 \cdot 10^{-7} = 4.39 \cdot 10^{-5}$$

and the displacement is

$$\Delta L = S_1 L = 2.2 \cdot 10^{-6} (m).$$

Therefore, the piezoelectric material elongates due to the applied force and voltage. However, if the voltage is inverted, it can be shown that the piezoelectric material shrinks instead of elongating.

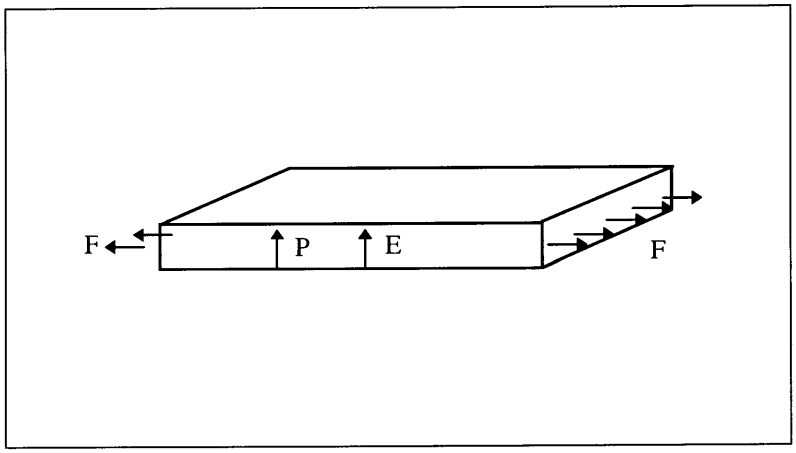

Figure 2.3 One Dimensional Example for Static Piezoelectric Material

Example 2: Radially Polarized Piezoelectric Ring

Figure 2.4 shows a radially polarized piezoelectric ring. The radial (r) and tangential (θ) directions can be set as x_3 and x_1 respectively. The electrical voltage is applied across the wall thickness so that the electric field is applied along the poling direction. If the ring is free and the wall

thickness is small compared to its radius, no radial stress(σ_r or T_3) or other stress exists, but only tangential stress(σ_θ or T_1) exists when the ring expands due to the piezoelectricity. Therefore, the ring operates in the transverse mode, as illustrates in Figures 2.4 and 2.2(b). The details of radially polarized materials are discussed later in this chapter.

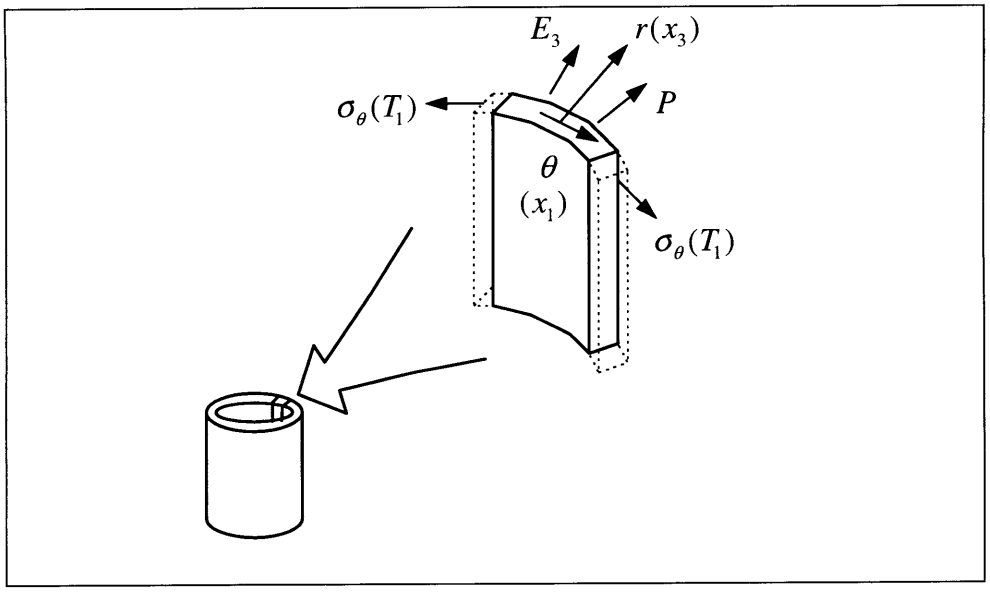

Figure 2.4 Radially Polarized Piezoelectric Ring Operating in the Transverse Mode

The above is a review of general physics of piezoelectric materials. If the constitutive equations, material properties and operating modes are known, most characteristics of the piezoelectric material can be determined. In the following section, a mathematical model for elastically bonded piezoelectric rings is developed using these basic physics.

2.2 Mathematical Model of Elastically Bonded Piezoelectric Rings

In this section, a mathematical model of elastically bonded piezoelectric rings is derived without loss of generality. The piezoelectric ring discussed in this thesis is radially polarized. Figure 2.5 shows the piezoelectric ring embedded in elastic material with a thin layer of epoxy. Although the free ring case has been studied by Haskin et al[6], more emphasis is placed in this section on the boundary condition at the ring's outer surface where the ring is embedded. The derivation starts by defining the coordinates, strain-displacement relationship and constitutive equations, and ends by applying boundary conditions.

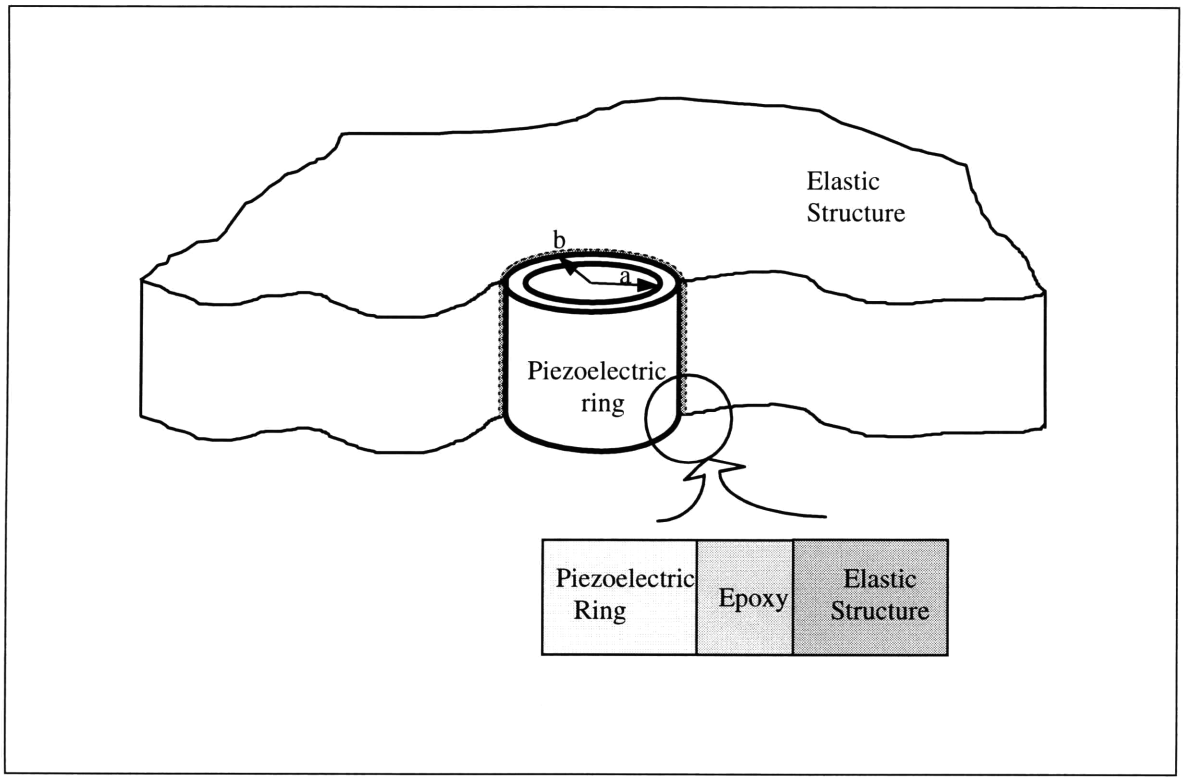

Figure 2.5 Geometry Description of an Elastically Bonded Piezoelectric Ring

1. Defining the Coordinates

The piezoelectric ring used in this thesis is radially polarized, so it expands radially when voltage is applied across the ring wall. The axial deformation of the piezoelectric ring can be assumed small and negligible. Thus, instead of cylindrical coordinates in three dimensions, polar coordinates (r,θ) in two dimensions are used to describe the geometry of the problem, as illustrated in Figure 2.6. Using this polar coordinate system, it is convenient to denote the radial and tangential displacement by u and v, respectively.

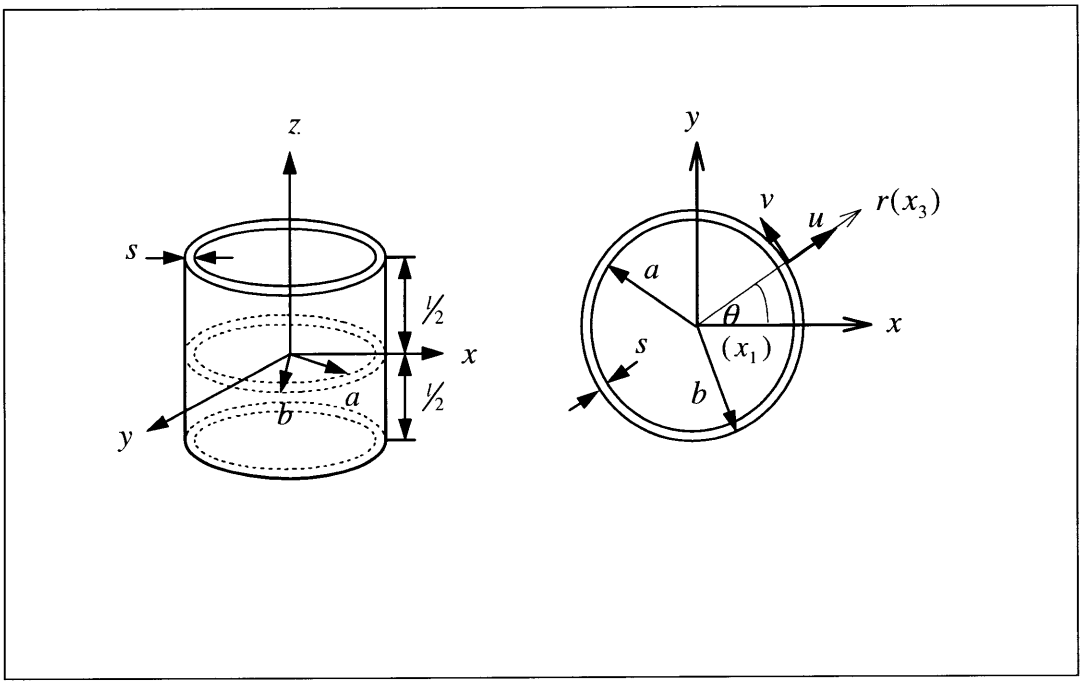

Figure 2.6 Definition of Coordinates

2. Strain-Displacement Relationship

The strain-displacement relationships in polar coordinates are available in general elasticity text [11] and have the form:

$$\varepsilon_r = \frac{\partial u}{\partial r}, \tag{2.8}$$

$$\varepsilon_\theta = \frac{1}{r}\frac{\partial v}{\partial r} + \frac{u}{r}, \tag{2.9}$$

and

$$\gamma_{r\theta} = \frac{1}{r}\frac{\partial u}{\partial \theta} + \frac{\partial v}{\partial r} - \frac{v}{r}. \tag{2.10}$$

where $\varepsilon_r, \varepsilon_\theta$ and $\gamma_{r\theta}$ are radial, tangential and shear strain, respectively. Because of circular symmetry, tangential displacement v and tangential derivatives $\frac{\partial}{\partial \theta}$ are zero, so the tangential strain is simply given by:

$$\varepsilon_\theta = \frac{u}{r}, \tag{2.11}$$

and the shear strain $\gamma_{r\theta}$ is zero. Equation 2.9 shows that the radial strain is the partial derivative of the radial displacement with respect to the radial direction; however, the tangential strain is only the ratio of radial displacement to radial position, as shown in Equation 2.11.

3. Constitutive Equation

According to the Hook's law and considering the lateral deformation, the constitutive equations of a general material in polar coordinates are simply:

$$\varepsilon_r = \frac{1}{E_R}(\sigma_r - \nu_R \sigma_\theta), \tag{2.12}$$

$$\varepsilon_\theta = \frac{1}{E_R}(-\nu_R \sigma_r + \sigma_\theta), \tag{2.13}$$

and

$$\gamma_{r\theta} = \frac{1}{G}\tau_{r\theta}, \tag{2.14}$$

where σ_r, σ_θ and $\tau_{r\theta}$ are radial, tangential and shear stress respectively and G, E_R and ν_R are shear modulus, Young's modulus and Poisson's ratio, respectively. Since the shear strain $\gamma_{r\theta}$ is zero, the shear stress $\tau_{r\theta}$ must be zero, too. Considering the deformation due to the radially polarized piezoelectric, the constitutive equations of piezoelectric materials in polar coordinates can be written as:

$$\varepsilon_r = \frac{1}{E_R}(\sigma_r - \nu_R \sigma_\theta) + d_{33}E_3, \tag{2.15}$$

and

$$\varepsilon_\theta = \frac{1}{E_R}(-\nu_R \sigma_r + \sigma_\theta) + d_{31}E_3, \tag{2.16}$$

where $d_{33}E_3$ and $d_{31}E_3$ are the additional radial and tangential piezoelectric strain components respectively due to the applied electrical field E_3 across the ring wall.

4. Applying Boundary Conditions

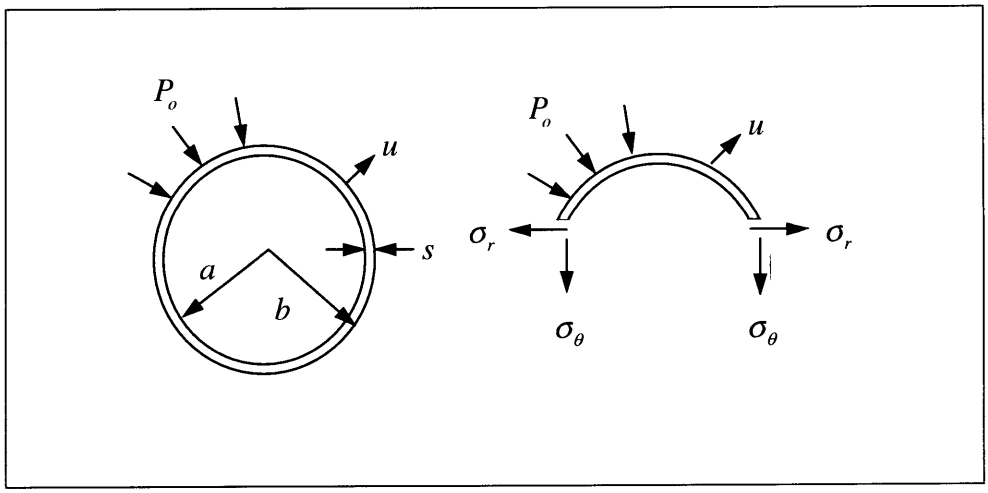

Figure 2.7 Boundary Condition of an Elastically Bonded Ring

The radially polarized piezoelectric ring expands radially when excited by a voltage. Since the piezoelectric ring is bonded, as shown in Figure 2.5, it will be subjected

to a pressure on its outer surface when it expands. Denoting this pressure as P_o on the outer surface, as illustrated in Figure 2.7, the radial and tangential stresses can be written as [11]:

$$\sigma_r = \frac{b^2 P_o}{b^2 - a^2}\left(\frac{a^2}{r^2} - 1\right), \tag{2.17}$$

$$\sigma_\theta = -\frac{b^2 P_o}{b^2 - a^2}\left(\frac{a^2}{r^2} + 1\right). \tag{2.18}$$

where a and b are the inner and the outer radius respectively. Replacing the inner radius , a , by the outer radius, b , and the wall thickness, s :

$$a = b - s, \tag{2.19}$$

and assuming the thickness is much smaller than the outer radius

$$s << b, \tag{2.20}$$

the radial stress component becomes:

$$\sigma_r = \frac{b^2 P_o}{2bs - s^2}\left(\frac{a^2 - r^2}{r^2}\right), \tag{2.21}$$

or

$$\sigma_r \cong \frac{b^2 P_o}{2bs}\left(\frac{a^2 - r^2}{r^2}\right), \tag{2.22}$$

Thus, at $r = a$, $\sigma_r = 0$; and at $r = b$, the radial stress component is simply $\sigma_r \cong P_o$ if $s << b$. Therefore, the radial stress changes from 0 to P_o throughout the wall thickness.

Similarly, replacing a by $b - s$ and using the relation

$$\frac{a^2}{r^2} \cong 1, \qquad a \le r \le b, \tag{2.23}$$

the tangential stress component becomes:

$$\sigma_\theta \cong -\frac{b^2 P_o}{2bs}(\frac{a^2}{r^2}+1), \tag{2.24}$$

or simply

$$\sigma_\theta \cong -P_o \frac{b}{s}. \tag{2.25}$$

This is the familiar tangential stress-pressure relation for a thin cylinder. If the inertia load is considered, substituting P_o with $P_o + \rho s\ddot{u}$ gives the dynamic tangential stress component

$$\sigma_\theta \cong -(P_o + \rho s\ddot{u})\frac{b}{s}. \tag{2.26}$$

Compared to σ_θ, σ_r is negligible for a thin ring, if $s << b$, so that only the tangential stress, σ_θ, exists. Furthermore, as illustrated in Figure 2.4, since the piezoelectric ring is radially polarized and the voltage is applied across the ring wall, the piezoelectric ring operates in the transverse mode, i.e. 3-1 mode. Neglecting σ_r in the constitutive Equation 2.16 yields

$$\varepsilon_\theta = \frac{\sigma_\theta}{E_R} + d_{31}E_3 \tag{2.27}$$

It can be easily shown that Equation 2.27 is the same as the first equation of the transverse mode constitutive equations (2.6) by setting σ_r to T_3 , σ_θ to T_1 and E_R to $1/s_{11}^E$.

Substituting Equations 2.11 and 2.26 into Equation 2.27 and rearranging it give the equation of motion in the radial direction:

$$P_o = -\frac{E_R s}{a^2}(u + \frac{a^2 \rho_R}{E_R}\ddot{u}) + \frac{E_R s}{a} d_{31}E_3 \tag{2.28}$$

Replacing the electrical field, E_3, by the dynamic electrical voltage, $E_3 = \overline{E}_3 e^{i\omega t} = -\overline{V} e^{i\omega t}/s$, the pressure, P_o, by the dynamic pressure, $P_o = \overline{P}_o e^{i\omega t}$,and the radial displacement, u, by the dynamic response, $u = \overline{u} e^{i\omega t}$, the equation of motion for the piezoelectric ring can finally obtained:

$$\overline{P}_o = -\frac{E_R s}{a^2}(1 - \frac{\rho_R a^2}{E_R}\omega^2)\overline{u} - \frac{E_R}{a} d_{31}\overline{V} \qquad (2.29)$$

where i is $\sqrt{-1}$, t is time ($\sec ond$), and ω is circular frequency ($rad / \sec ond$) which is equal to 2π times frequency f (Hz).

It is shown in Equation 2.29 that the radial displacement and pressure interact with each other and depend on the material and the geometry. In addition, the pressure is also dependent upon the ring expansion which is related to the impedance of the surrounding material. If the surrounding material is very compliant, the impedance is small, so the ring expands easily and the pressure exerted by the ring decreases. More details of the piezoelectric ring embedded in a circular plate is discussed in the third chapter. In the next section, a free piezoelectric ring is studied by setting the pressure, P_o, to zero and comparing the result to measurement.

2.3 Free and Epoxy-coated Piezoelectric Ring

Before discussing the influence of the surrounding material, it is interesting to examine the velocity response of a free, i.e. unbounded, piezoelectric ring. An epoxy-coated piezoelectric ring is also studied to quantify the effect of epoxy which is used to connect the piezoelectric ring to the elastic material.

2.3.1 Experimental Setup

Figure 2.8 shows the experimental setup used to measure the transfer function between the radial velocity of the outer surface and the applied voltage across the piezoelectric ring wall. To let the ring vibrate more freely, it is clamped and suspended at its wire 2 cm away from the ring. The piezoelectric ring used in this experiment is a Channel 5700 type, 0.7 mm in wall thickness, 8.0 mm in length and in diameter. Table 2.2 lists the material properties of Channel 5700 type piezoelectric ceramics[12].

As illustrated in Figure 2.8, the whole experiment is controlled by a personal computer software, the Virtual Instruments(VI) by DSP Technology Inc.(DSPT)[13]. This VI software provides the personal computer with control of the SigLab spectrum analyzer and function generator. The connection is by means of Small Computer System Interface(SCSI). The two output channels, named Out1 and Out2, of the SigLab unit can generate various functions such as sine, random or impulse signals, etc. The two input channels, named In1 and In2, of the SigLab unit provide spectral analysis of the input signals.

The radial velocity of the ring is measured in this experiment by a laser Doppler interferometer (LDI) system, manufactured by Polytech. Inc.[14] Using the Doppler effect, the LDI system measures the velocity of the object by calculating the frequency shift between the emitting laser beam and its reflection and then converting this frequency shift into a voltage signal proportional to the measured velocity with 1 mm/s/V sensitivity. Unlike the accelerometer, the LDI system provides a non-contact measurement. No added mass correction is required. Another advantage is that the LDI system can measure the velocity component along the beam direction; thereafter, the radial velocity of the ring

can be easily measured by pointing and focusing the laser beam along the radial direction. The only requirement for this measurement is reflective tape at the measurement point, so that the tape can reflect the laser beam back to the receiver embedded in the LDI system.

For the convenience of illustration, Figure 2.9 shows the corresponding block diagram of the experimental setup in Figure 2.8. A swept sine analysis is used in this experiment to obtain the transfer function between the radial velocity and the applied voltage. Figure 2.10 shows the configuration of swept sine analysis in the SigLab system[13]. SigLab generates a sinusoidal voltage signal V_1 from its first output channel(Out1) in a frequency range from 50 Hz to 20 KHz with a linear increment of 50 Hz, so the ring is excited with 399 discrete frequencies step by step. The voltage control level in this experiment is specified in the first output channel so that every swept sine signal is 4 volts in amplitude . This voltage signal is divided into two channels in parallel. One is fed back to the first input channel(In1) as a reference; the other is magnified to excite the ring by an amplifier with a constant gain K_1, which is 13 or 22.5 dB. This voltage magnified by the amplifier is denoted by V_2 in the block diagram. The radial velocity response, v, of the excited ring is then measured by the LDI system whose output, V_3, is a calibrated voltage signal representing the measured radial velocity with a 1 $V/(mm/s)$ sensitivity, K_2, is fed back to the second input channel(In2) of the SigLab spectrum analyzer. SigLab analyzes this feedback signal using a 20 Hz narrow-band tracking filter whose pass band is centered at the excitation frequency of each step.

It is noted that the input gain settings of two input channels are specified as "Auto", so that the SigLab unit sets the input gains automatically. The only disadvantage of using "Auto" is that the acquisition may take longer because additional amplitude data

must be collected and repeated acquisitions must be processed due to input overloads. To complete a 399 step swept sine analysis in this experiment takes about 100 seconds.

The transfer function between the two input channels can be obtained from VI software by computing the ratio of the cross-spectrum between two input channels and the auto-spectrum of the reference input channel (In1). This transfer function is denoted as G, which is the ratio between V_3 and V_1, and can also be written as

$$G = K_1 X K_2 . \tag{2.30}$$

where

$$G = \frac{V_3}{V_1},\ K_1 = \frac{V_2}{V_1},\ X = \frac{v}{V_2} \text{ and } K_2 = \frac{V_3}{v}.$$

The transfer function, X, between radial velocity of the ring, v, and the driving voltage on the ring, V_2, is of most interest and thus can be determined by:

$$X = \frac{G}{K_1 K_2} \tag{2.31}$$

The gain transfer function of the amplifier and the noise floor of the unexcited system were also measured in the frequency domain. Figure 2.11 shows the gain of amplifier obtained by the same configuration of the free ring experiment except that the output of amplifier was fed back to the second input channel of the SigLab unit and the control voltage level was 0.1 volt. It is shown in Figure 2.11 that the gain of the amplifier was almost independent of frequency in the range of 50 Hz to 20 KHz and was a constant gain of 22.5 dB. Figure 2.12 plots both the transfer function G and the noise floor obtained by the same configuration of the free ring experiment, except that the output channel was disconnected so that the noise floor of the amplifier, the piezoelectric ring and

the LDI system were all included. It is shown in Figure 2.12 that the noise floor is lower than the response by 60dB between 1 and 20KHz and therefore may be ignored.

Table 2.2 Properties and Dimension of the Piezoelectric Rings Used in the Experiment [12]

Type	Channel 5700 (or Navy VI)
Operation Mode	3-1 mode
Piezoelectric Constant (10^{-12} m/V) d_{31}	-250
Elastic Constant (10^{10} N/m^2) $1/s_{11}^E$	6.2
Density (10^3 Kg/m^3)	7.4
Diameter (mm)	8.0
Wall Thickness (mm)	0.7
Length (mm)	8.0

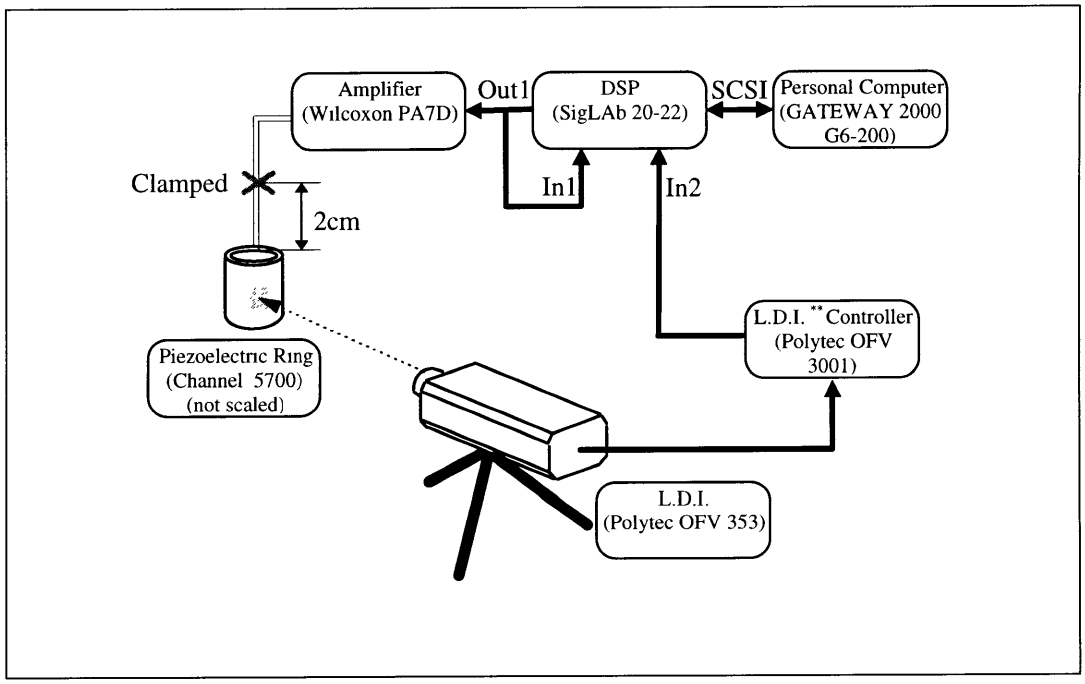

Figure 2.8 Experimental Setup for Unbonded Piezoelectric Ring

** is the abbreviation of "Laser Doppler Interferometer".

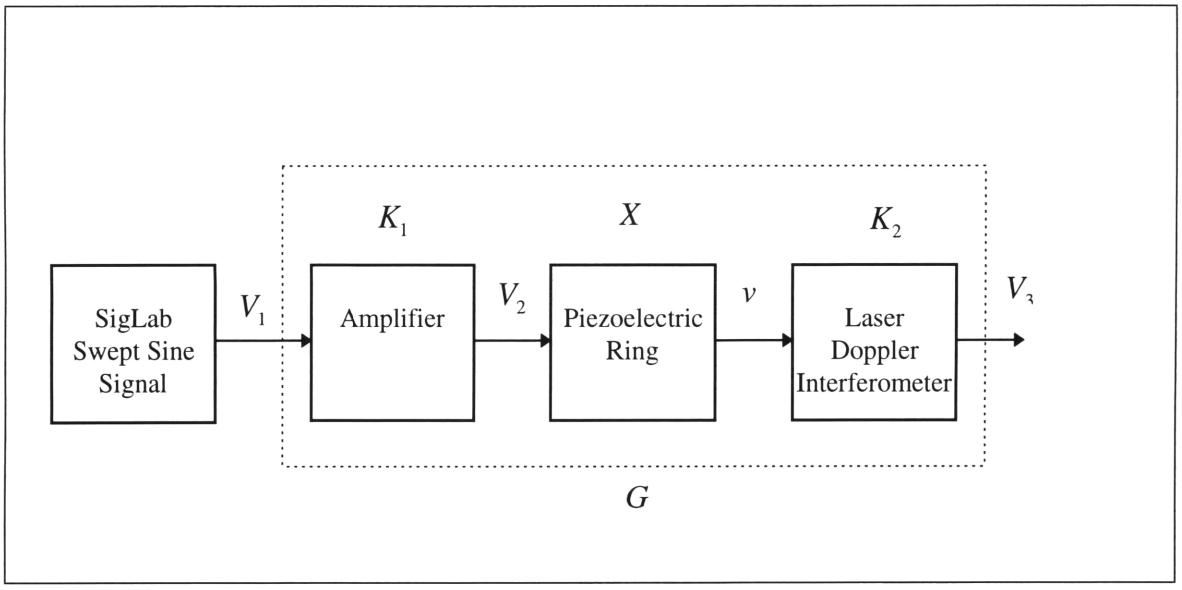

Figure 2.9 Block Diagram of the Experimental Setup

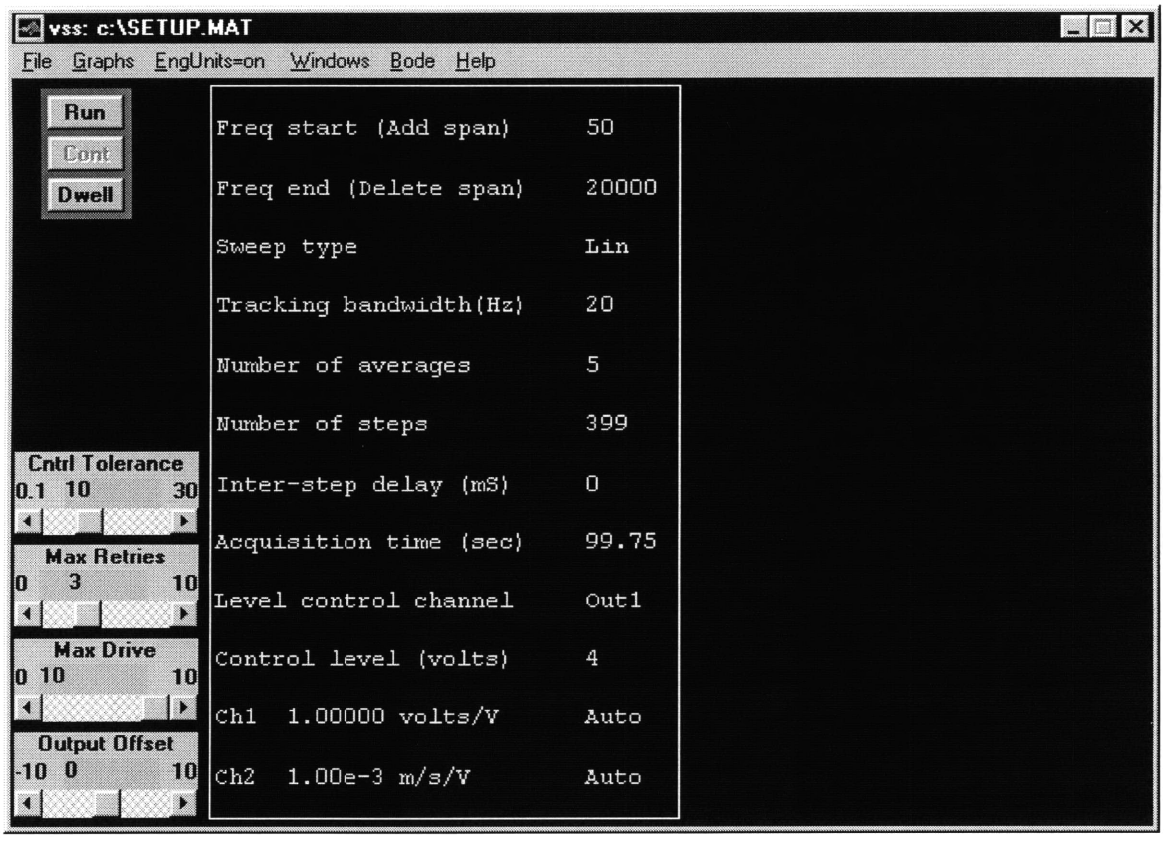

Figure 2.10 Configuration of Swept Sine Analysis in the SigLab System

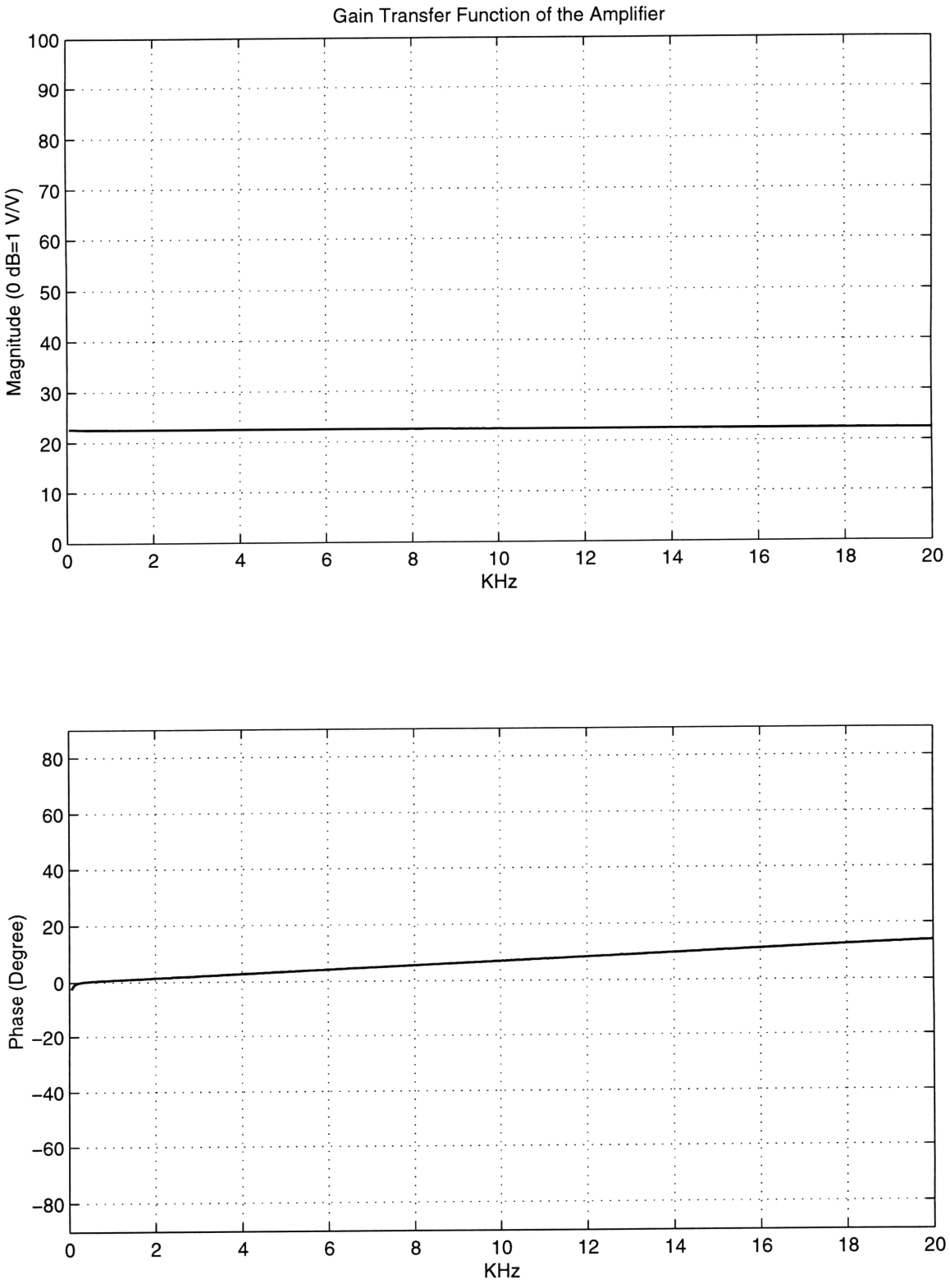

Figure 2.11 Gain Transfer Function of the Amplifier in the Linear Frequency Domain (a) Magnitude (b) Phase

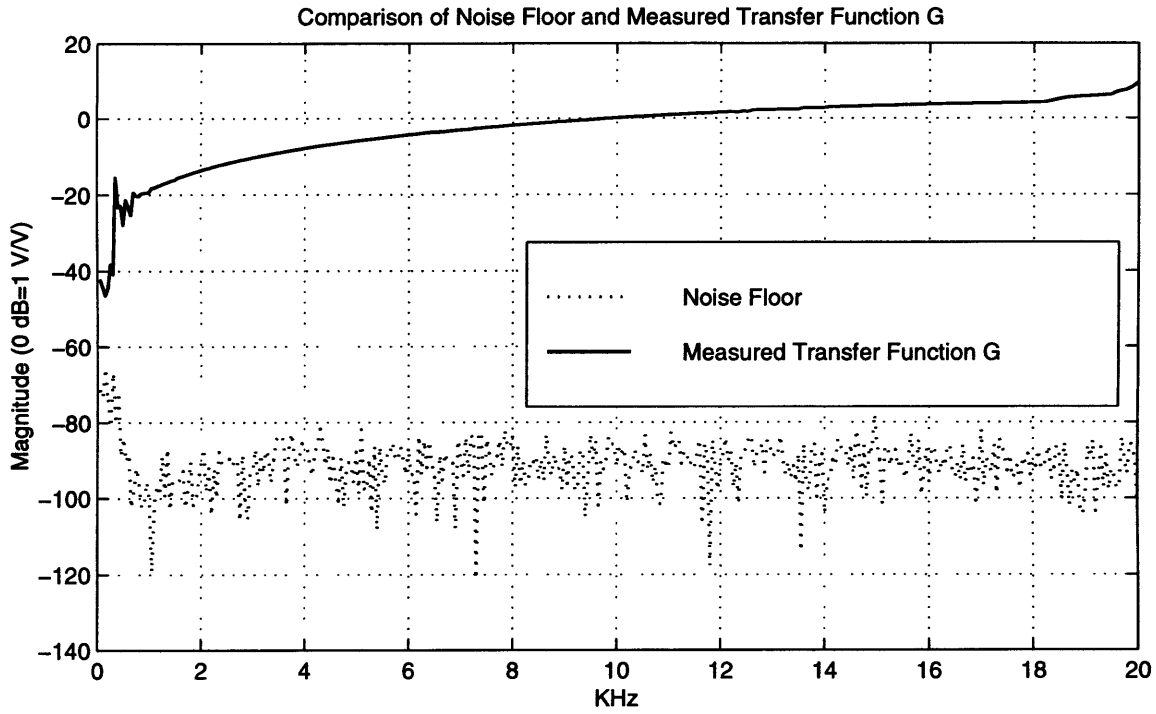

Figure 2.12 Comparison of the Noise Floor and the Measured Transfer Function G

2.3.2 Comparison of Model and Data in Free Case

For the free piezoelectric ring, the pressure in Equation 2.29 can be neglected and the equation of motion becomes:

$$0 = -\frac{E_R s}{a^2}(1 - \frac{\rho_R a^2}{E_R}\omega^2)\bar{u} - \frac{E_R}{a}d_{31}\bar{V}. \tag{2.32}$$

Defining the ring frequency:

$$\omega_R = \sqrt{\frac{E_R}{\rho_R a^2}}, \tag{2.33}$$

rearranging and multiplying Equation 2.32 by complex circular frequency jw, the transfer function between radial velocity and applied voltage is simply

$$\frac{j\omega\bar{u}}{\bar{V}} = \frac{-j\omega d_{31}a/s}{1-\omega^2/\omega_R^2} \tag{2.34}$$

It can be easily shown in Equation 2.34 that the ring resonance occurs when the excitation frequency coincides with the ring frequency. Substituting the material properties listed in Table 2.2, the piezoelectric ring used in this experiment had a ring frequency at about 115 KHz, which is far beyond the frequency range of interest in this project. Therefore, in the frequency range below 20 KHz , the radial displacement response of the free ring is simply a constant and the radial velocity response of the ring is proportional to frequency.

Figures 2.13(a) and 2.14(a) show the comparison between Equation 2.34 and the experimental measurement. As shown in Figure 2.14(a), the dependence of the measured radial velocity response of the ring is the first order in frequency, as discussed earlier. To evaluate the difference between the model and the data, an error analysis is made by subtracting the logarithmic magnitude of the model from the logarithmic magnitude of the data and multiplying by 20. The error analysis between the model and the data, plotted in Figures 2.13(b) and 2.14(b), shows that the model over-estimated the response by 2 dB from 1 to 19 KHz. This 2 dB error is probably due to the difference between the actual value and the nominal value of the piezoelectric constant d_{31}. The nominal piezoelectric constant provided by the manufacturer is $-250 \cdot 10^{-12}(m/V)$; however, the real value may be lower because of aging and other defects. It is reasonable to tune this constant from $-250 \cdot 10^{-12}(m/V)$ to $-200 \cdot 10^{-12}(m/V)$. The piezoelectric constants used in the following discussions were reduced by 20% if not specified otherwise. The tuned model response is also plotted in Figure 2.13 and 2.14.

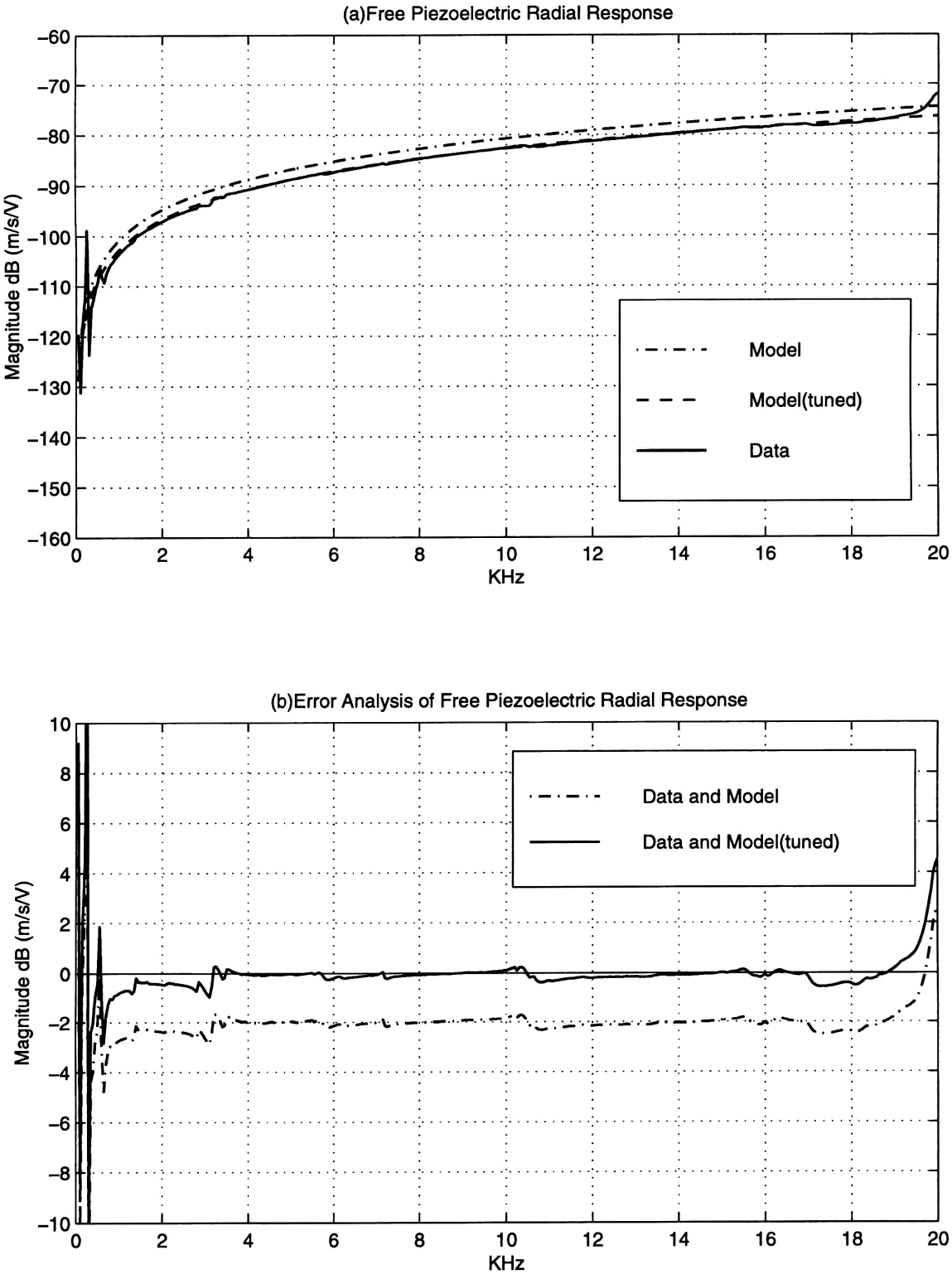

Figure 2.13 Radial Velocity Response per Unit Voltage of the Free Piezoelectric Ring in the Linear Frequency Domain: (a)Comparison of Model and Data, (b)Error Analysis of Model and Data.

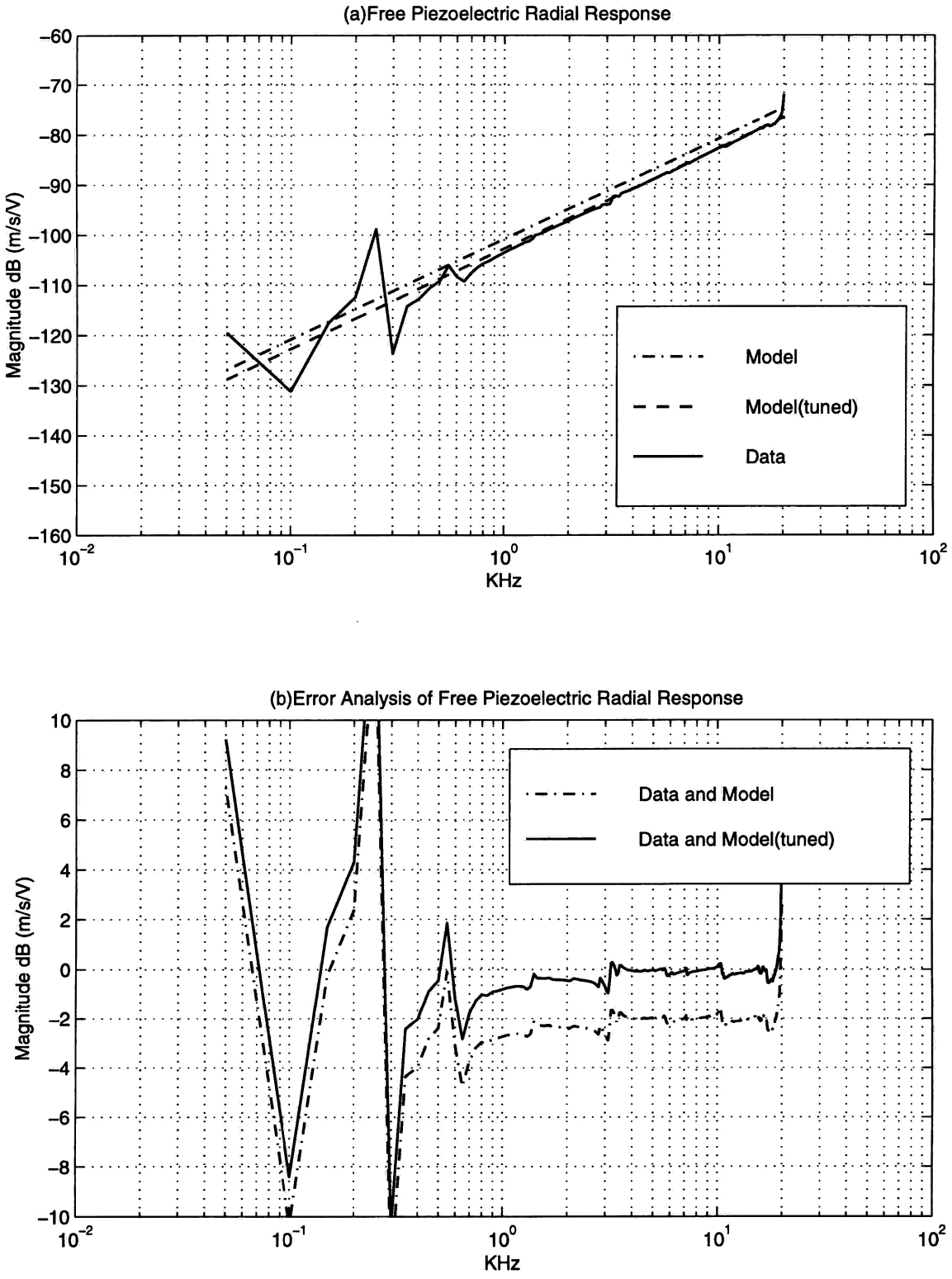

Figure 2.14 Radial Velocity Response per Unit Voltage of the Free Piezoelectric Ring in the Logarithmic Frequency Domain: (a)Comparison of Model and Data, (b)Error Analysis of Model and Data.

2.3.3 Comparison of Free and Epoxy-coated Piezoelectric Ring

Because the piezoelectric ring is bonded to an elastic structure with epoxy for the later experiments, it is important to quantify the influence of this layer. For this reason, a piezoelectric ring was coated with a layer of epoxy, which was as thin as the normal usage in the later experiments (less than approximately 1 mm). Figures 2.15(a) and 2.16(a) show the comparison between the measured response of the free and the epoxy-bounded piezoelectric rings. Figures 2.15(b) and 2.16(b) show the error analysis of the measured response of the free and the epoxy-bounded piezoelectric rings. As shown in the figure, the average difference is about 1dB from 1KHz to 20 KHz so that the effect of the epoxy is negligible. This is because the Young's modulus of epoxy (3~4Gpa) is much smaller than that of piezoelectric material (62Gpa).

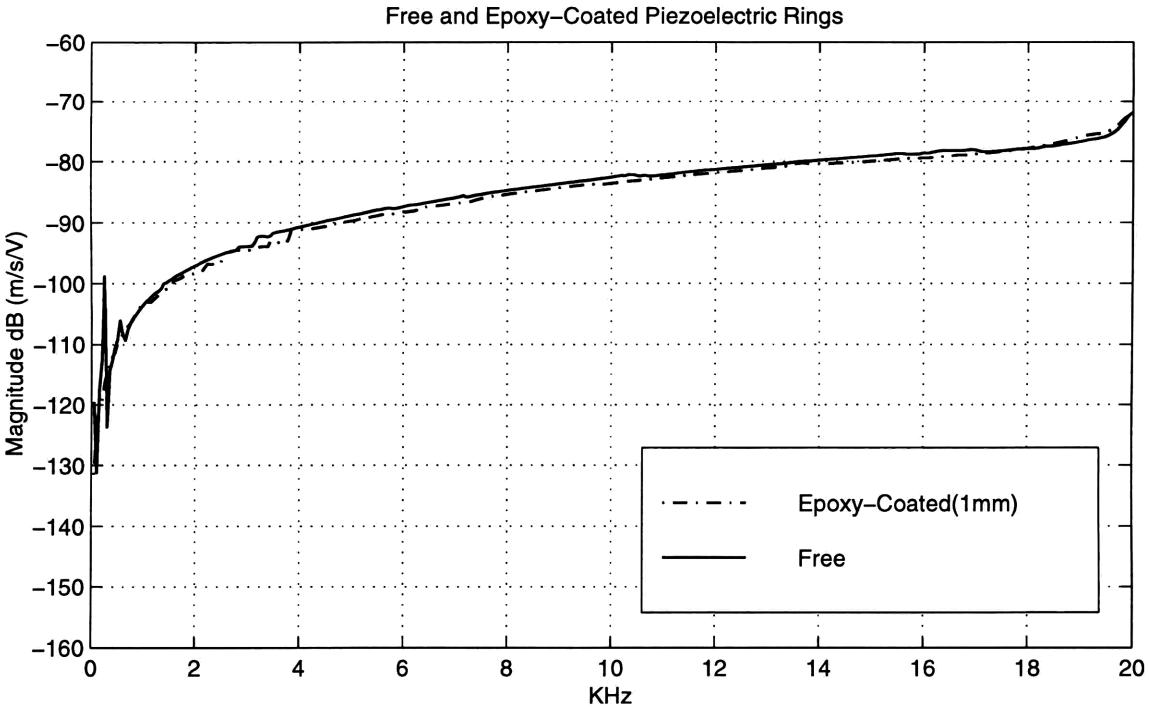

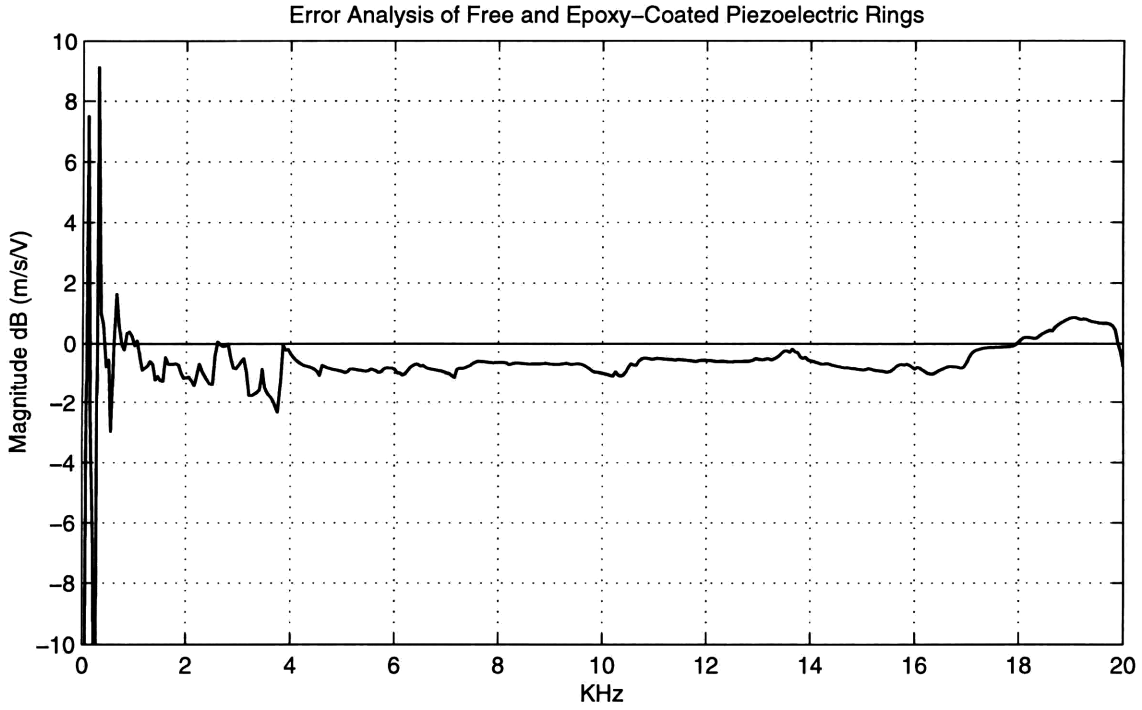

Figure 2.15 Radial Velocity Response per Unit Voltage of the Free and the Epoxy-coated Piezoelectric Rings in the Linear Frequency Domain: (a)Comparison (b)Error Analysis.

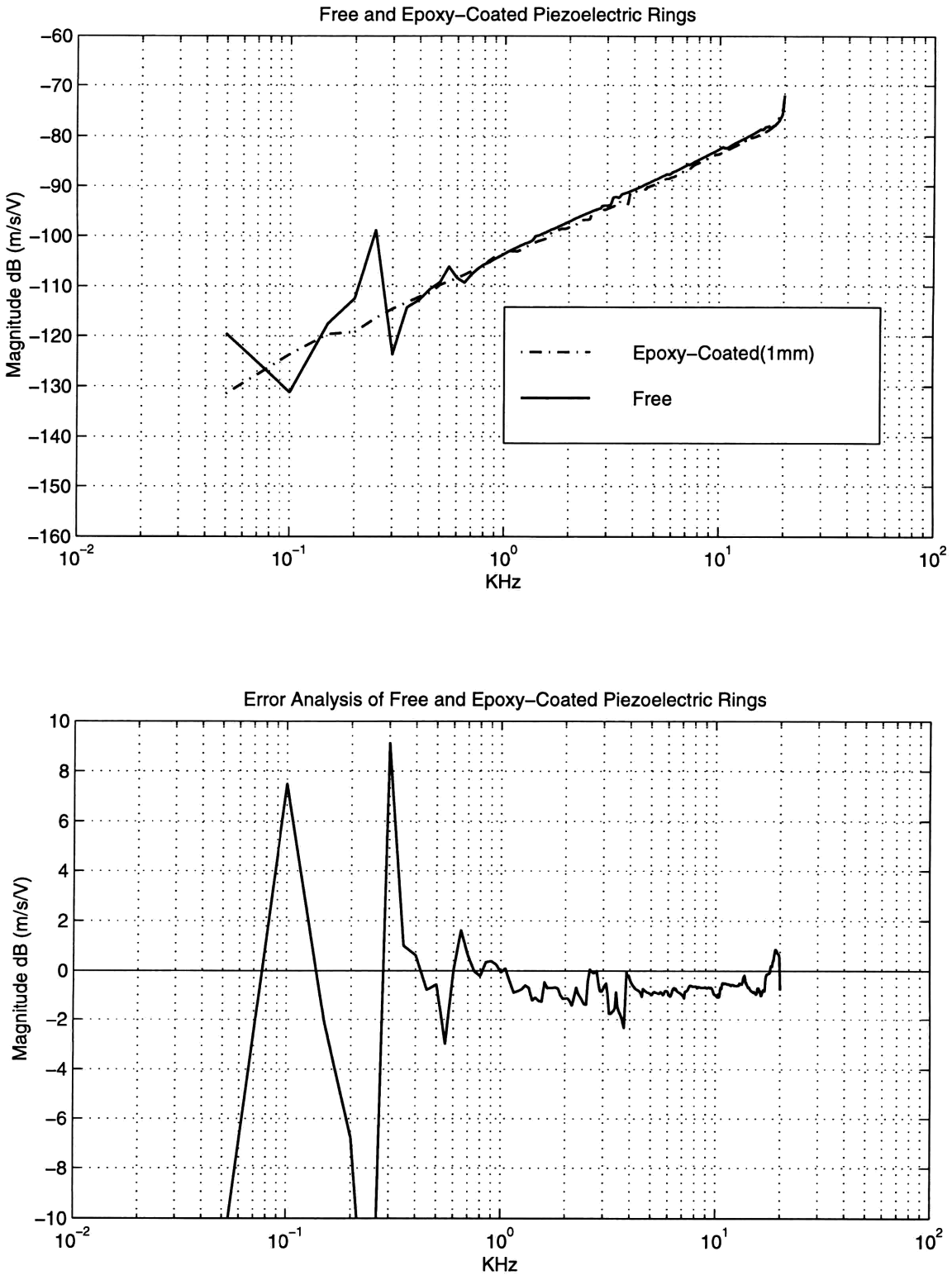

Figure 2.16 Radial Velocity Response per Unit Voltage of the Free and the Epoxy-coated Piezoelectric Rings in the Logarithmic Frequency Domain: (a)Comparison (b)Error Analysis.

Chapter 3.

Piezoelectric Rings in Circular Plates

In this chapter, a circular plate, excited by a piezoelectric ring in the center, is studied to examine the radial velocity response at any arbitrary radial location on the plate. An equation of motion is developed by examining its elasticity in polar coordinates. The solution has the form of a Bessel function. To evaluate this solution, the calculated radial velocity at any radial position is compared to experimental measurements. The comparison shows that the model can predict the response very well if the properties of the plate material, such as aluminum, are accurately defined. Since the model is validated by measurement, the pressure exerted by the piezoelectric ring in the circular plate can be estimated.

3.1 Mathematical Model of a Piezoelectric Ring in a Circular Plate

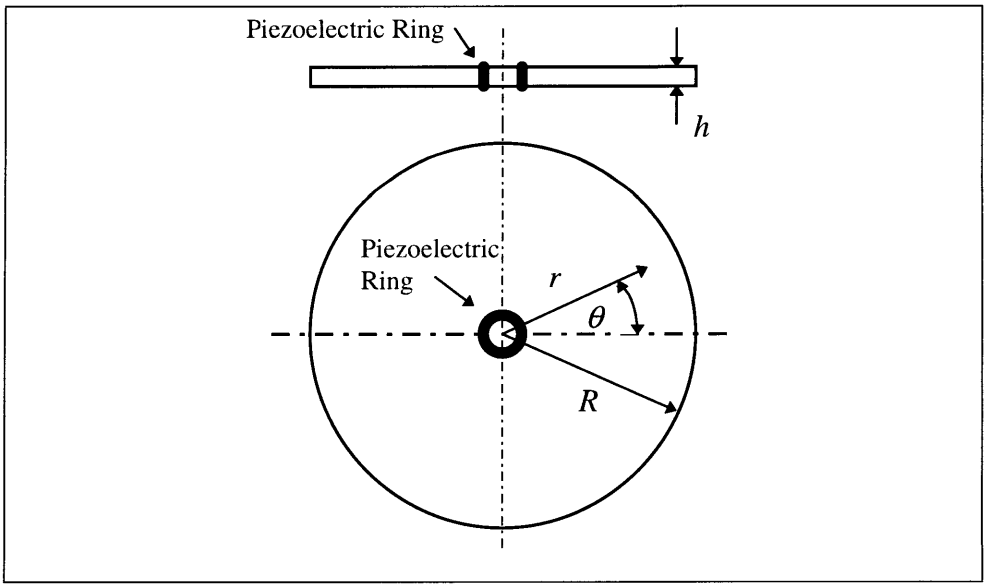

Figure 3.1 Geometry of Circular Plate

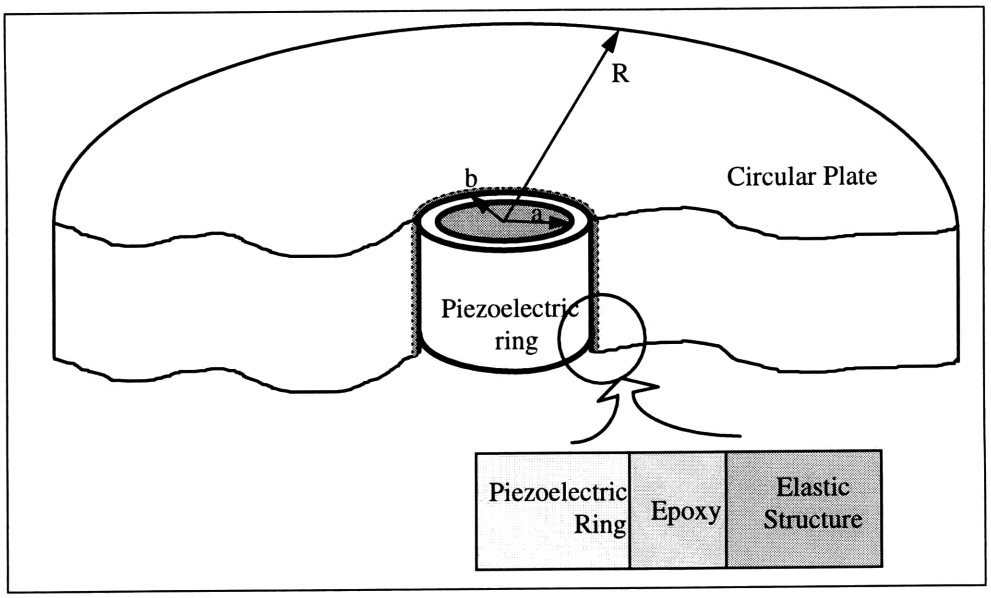

Figure 3.2 Geometry of Piezoelectric Ring Embedded in the Circular Plate

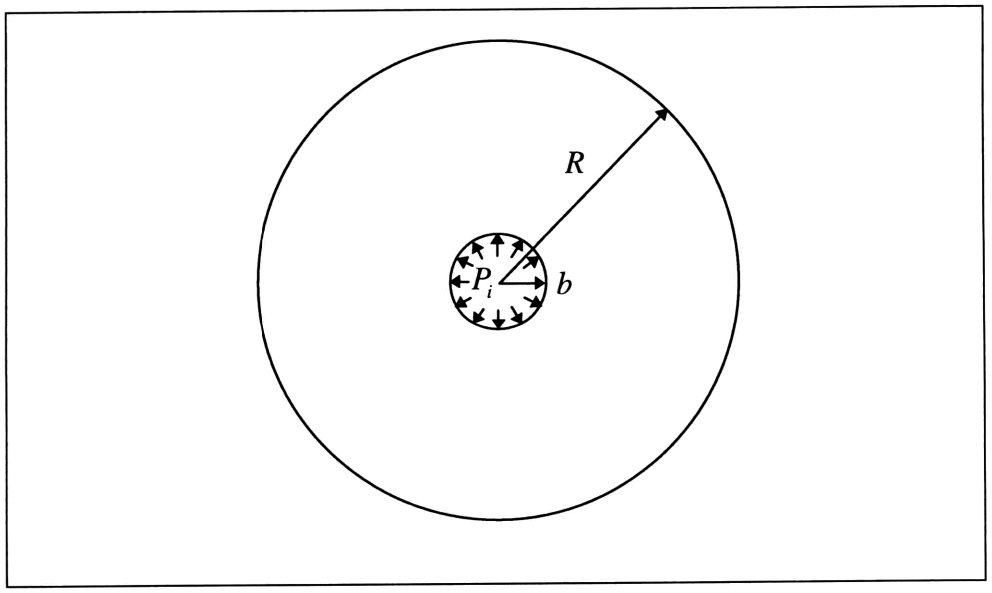

Figure 3.3 Boundary Condition of the Circular Plate

As illustrated in Figure 3.1 and 3.2, a piezoelectric ring was embedded vertically in the center of a circular plate with a thin layer of epoxy, which was less than 0.5 mm in thickness. According to the conclusion of Section 2.3.3, the thickness of the epoxy layer is so thin that can be neglected in the following discussions. The circular plate vibrated primarily in the radial direction when the piezoelectric ring was subjected to an applied voltage and expanded radially. Because of the circular symmetry and the primary expansion in the radial direction, this problem can be reduced to a symmetrical case in one dimension (r), as illustrated in Figure 3.3. Furthermore, assuming the piezoelectric ring excites the circular plate with a dynamic pressure, P_o, at the surrounding surface, as discussed in the previous chapter, the problem simply becomes a circular plate subject to a dynamic pressure at its inner radius, as shown in Figure 3.3. Therefore, by examining elasticity in polar coordinates, the radial velocity response at any radial position due to the dynamic pressure can be calculated. The solution has a form of the first mode Bessel function because of circular symmetry. Finally, by transforming the dynamic pressure in terms of the ring's radial expansion and the applied voltage using Equation 2.29, the transfer function between the radial velocity and the applied voltage can be easily determined. What follows are the details of the derivation for this transfer function. It begins by evaluating the force equilibrium of the circular plate and defining the strain-displacement and the stress-strain relationships in polar coordinates. It ends by applying the boundary conditions and the dynamic pressure of the piezoelectric ring as developed in the previous chapter.

1. Equation of Motion for Circular Plate:

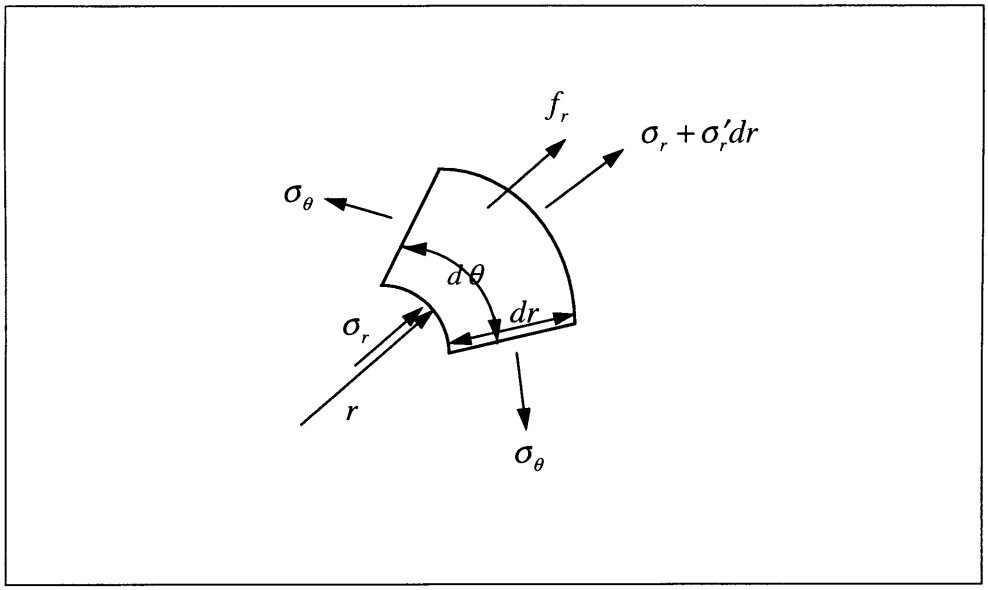

Figure 3.4 Force Equilibrium of in the Circular Plate

As illustrated in Figure 3.4, by examining a circular symmetric infinitesimal element of the circular plate and applying Newton's law, the force equilibrium can be obtained:

$$-\sigma_r r d\theta + (\sigma_r + \frac{\partial \sigma_r}{\partial r} dr)(r + dr)d\theta - \sigma_\theta dr d\theta + f_r r dr d\theta = 0 \qquad (3.1)$$

where the radial body force per unit volume, f_r, is simply the inertia force per unit volume due to the disk density, ρ_D, and its acceleration, $\ddot{u}$:

$$f_r = \rho_D \ddot{u} \qquad (3.2)$$

Ignoring second order terms, therefore, Equation 3.1 can be further reduced to:

$$\frac{\partial \sigma_r}{\partial r} + \frac{\sigma_r - \sigma_\theta}{r} - \rho_D \ddot{u} = 0 \qquad (3.3)$$

Due to the circular symmetry, the strain-displacement relationship of circular plate is the same as that of piezoelectric ring discussed in Equations 2.8 and 2.11:

$$\varepsilon_r = \frac{\partial u}{\partial r} \qquad (2.8)$$

$$\varepsilon_\theta = \frac{u}{r} \tag{2.11}$$

Similarly, the strain-stress relationship is also the same as that of piezoelectric ring, discussed in Equations 2.12 and 2.13:

$$\varepsilon_r = \frac{1}{E_D}(\sigma_r - \nu_D \sigma_\theta), \tag{2.12}$$

$$\varepsilon_\theta = \frac{1}{E_D}(-\nu_D \sigma_r + \sigma_\theta), \tag{2.13}$$

except that E_D and ν_D denote the Young's modulus and Poisson's ratio of the circular disk, respectively. It is helpful to invert the strain-stress relationship into the forms:

$$\sigma_r = \frac{E_D}{1-\nu_D{}^2}(\varepsilon_r + \nu_D \varepsilon_\theta), \tag{3.4}$$

$$\sigma_\theta = \frac{E_D}{1-\nu_D{}^2}(\varepsilon_\theta + \nu_D \varepsilon_r), \tag{3.5}$$

so that the stress-displacement relationship can be obtained in terms of the displacement:

$$\sigma_r = \frac{E_D}{1-\nu_D{}^2}(\frac{\partial u}{\partial r} + \nu_D \frac{u}{r}), \tag{3.6}$$

$$\sigma_\theta = \frac{E_D}{1-\nu_D{}^2}(\frac{u}{r} + \nu_D \frac{\partial u}{\partial r}). \tag{3.7}$$

Replacing the last stress-displacement relationship with the force equilibrium, Equation 3.3, yields the general equation of radial motion for a circular plate:

$$\frac{\partial^2 u}{\partial r^2} + \frac{1}{r}\frac{\partial u}{\partial r} - \frac{u}{r^2} - \frac{\rho_D(1-\nu_D{}^2)}{E_D}\ddot{u} = 0. \tag{3.8}$$

It is usual to define the sound speed, c, in the plate as [15]:

$$c = \sqrt{\frac{E_D}{\rho_D (1 - \nu_D{}^2)}} \tag{3.9}$$

Letting displacement, u, be the dynamic term $u = \bar{u} e^{i\omega t}$ gives $\ddot{u} = -\omega^2 \bar{u} e^{i\omega t}$, so that

$$\frac{d^2\bar{u}}{dr^2} + \frac{1}{r}\frac{d\bar{u}}{dr} + (k^2 - \frac{1}{r^2})\bar{u} = 0, \tag{3.10}$$

where

$$k^2 \equiv \frac{\omega^2}{c^2}, \tag{3.11}$$

or

$$r^2 \frac{d^2\bar{u}}{dr^2} + r\frac{d\bar{u}}{dr} + (r^2k^2 - 1)\bar{u} = 0, \tag{3.12}$$

The last equation is the well-known Bessel equation with the first mode and has a general solution of the form:

$$\bar{u} = C_1 J_1(kr) + C_2 Y_1(kr), \tag{3.13}$$

where J_1 is the first mode of the Bessel function of the first kind, Y_1 is the first mode of the Bessel function of the second kind, and C_1 and C_2 are their corresponding coefficients, respectively. The coefficients C_1 and C_2 may be found by imposing the boundary conditions at the inner and outer radii of the circular plate.

2. Boundary Conditions and Solutions:

It is easily shown in Figure 3.3 that the radial stress at the inner radius, $r = b$, is:

$$\sigma_r = -P_i, \tag{3.14}$$

and the radial stress at the outer radius, $r = R$, is:

$$\sigma_r = 0\ . \tag{3.15}$$

Therefore, using the stress-displacement relationship derived in Equation 3.7 and evaluating at the inner radius, $r = b$, gives:

$$\sigma_r = \frac{E_D}{1-{\nu_D}^2}\left(\frac{\partial u}{\partial r} + \nu_D \frac{u}{b}\right) = -P_t. \tag{3.16}$$

The pressure applied on the plate, P_i, must be equal to the pressure applied on the piezoelectric ring, P_o:

$$P_o = P_t \tag{3.17}$$

Since the dynamic pressure exerted by the piezoelectric ring has been developed in the previous chapter, substituting P_o from Equation 2.29 into Equation 3.16 and retaining the magnitude yields:

$$\frac{E_D b}{(1-{\nu_D}^2)E_R s}\left(\frac{d\bar{u}}{dr} + \nu_D \frac{\bar{u}}{b}\right) = -d_{31}\bar{E}_3 + \frac{\bar{u}}{b}\left(1-\frac{\omega^2}{\omega_R^2}\right). \tag{3.18}$$

Furthermore, introducing a non-dimensional parameter:

$$\bar{E} = \frac{E_R s}{E_D b}, \tag{3.19}$$

and setting the displacement magnitude at the inner radius, $r = b$, to be $\bar{u}_b$ yields:

$$\frac{1}{(1-\nu^2)\bar{E}}\left(\frac{d\bar{u}_b}{dr} + \nu\frac{\bar{u}_b}{b}\right) - \frac{\bar{u}_b}{b}\left(1-\frac{\omega^2}{\omega_R^2}\right) = -d_{31}\bar{E}_3 \tag{3.20}$$

or

$$\frac{d\bar{u}_b}{dr} + \left[\nu - \bar{E}(1-\nu^2)\left(1-\frac{\omega^2}{\omega_R^2}\right)\right]\frac{\bar{u}_b}{b} = -\bar{E}(1-\nu^2)d_{31}\bar{E}_3. \tag{3.21}$$

Similarly, using the stress-displacement relationship derived in Equation 3.7 and evaluating at the outer radius, $r = R$, gives:

$$\sigma_r = \frac{E_D}{1-\nu_D{}^2}\left(\frac{\partial u}{\partial r} + \nu_D \frac{u}{R}\right) = 0, \tag{3.22}$$

or

$$\frac{d\bar{u}_R}{dr} + \nu_D \frac{\bar{u}_R}{R} = 0, \tag{3.23}$$

where $\bar{u}_R$ is the displacement magnitude at the outer radius $r = R$.

Equations 3.21 and 3.23 describe the boundary condition in terms of the radial displacement of the plate. Using these two equations, the coefficients of the general solution thus can be determined by inserting,

$$\bar{u} = C_1 J_1(kr) + C_2 Y_1(kr) \tag{3.13}$$

and its derivative,

$$\frac{d\bar{u}}{dr} = C_1\left[kJ_0(kr) - \frac{1}{r}J_1(kr)\right] + C_2\left[kY_0(kr) - \frac{1}{r}Y_1(kr)\right] \tag{3.24}$$

into Equation 3.21, i.e. at the inner radius, $r = b$, so that:

$$C_1\left[kJ_0(kb) - \frac{1}{b}J_1(kb)\right] + C_2\left[kY_0(kb) - \frac{1}{b}Y_1(kb)\right]$$

$$+ C_1\left[\nu_D - \bar{E}(1-\nu_D{}^2)(1-\frac{\omega^2}{\omega_R^2})\right]J_1(kb)\frac{1}{b} + C_2\left[\nu_D - \bar{E}(1-\nu_D{}^2)(1-\frac{\omega^2}{\omega_R^2})\right]Y_1(kb)\frac{1}{b}$$

$$= -(1-\nu_D{}^2)\bar{E}\ d_{31}\bar{E}_3. \tag{3.25}$$

or

$$C_1\left\{bkJ_0(kb) - J_1(kb)\left[1-\nu_D + \bar{E}(1-\nu_D{}^2)(1-\frac{\omega^2}{\omega_R^2})\right]\right\}$$

$$+C_2\left\{bkY_0(kb)-Y_1(kb)\left[1-\nu_D+\overline{E}(1-{\nu_D}^2)(1-\frac{\omega^2}{\omega_R^2})\right]\right\}$$

$$=-b(1-{\nu_D}^2)\overline{E}\ d_{31}\overline{E}_3\,. \tag{3.26}$$

Similarly, inserting Equation 3.13 and 3.24 into Equation 3.23, i.e. at the outer radius $r=R$, yields:

$$C_1\left[kJ_0(kR)-\frac{1}{R}J_1(kR)\right]+C_2\left[kY_0(kR)-\frac{1}{R}Y_1(kR)\right]+C_1\frac{\nu_D}{R}J_1(kR)+C_2\frac{\nu_D}{R}Y_1(kR)=0 \tag{3.27}$$

or

$$C_1\left[kRJ_0(kR)-(1-\nu_D)J_1(kR)\right]+C_2\left[kRY_0(kR)-(1-\nu_D)Y_1(kR)\right]=0 \tag{3.28}$$

Solving the linear system of Equations 3.28 and 3.26:

$$\begin{bmatrix}A_{11} & A_{12}\\ A_{21} & A_{22}\end{bmatrix}\begin{Bmatrix}C_1\\ C_2\end{Bmatrix}=\begin{Bmatrix}0\\ -b(1-{\nu_D}^2)\overline{E}\ d_{31}\overline{E}_3\end{Bmatrix}, \tag{3.29}$$

the coefficients C_1 and C_2 are given by:

$$C_1=\frac{A_{12}}{\Delta}b(1-\nu_D)\overline{E}\ d_{31}\overline{E}_3, \tag{3.30}$$

$$C_2=-\frac{A_{11}}{\Delta}b(1-\nu_D)\overline{E}\ d_{31}\overline{E}_3, \tag{3.31}$$

where

$$A_{11}\equiv\left[kRJ_0(kR)-(1-\nu_D)J_1(kR)\right],$$

$$A_{12}\equiv\left[kRY_0(kR)-(1-\nu_D)Y_1(kR)\right],$$

$$A_{21}\equiv\left\{kbJ_0(kb)-\left[1-\nu_D+\overline{E}(1-{\nu_D}^2)(1-\frac{\omega^2}{\omega_R^2})\right]J_1(kb)\right\},$$

$$A_{22} \equiv \left\{ kbY_0(kb) - \left[1 - \nu_D + \bar{E}(1-\nu_D{}^2)(1-\frac{\omega^2}{\omega_R^2}) \right] Y_1(kb) \right\},$$

and

$$\Delta = A_{11}A_{22} - A_{12}A_{21}.$$

Since the coefficients C_1 and C_2 have been determined, the radial displacement, $\bar{u}$, for any arbitrary radial position, r, on the circular plate is simply:

$$\bar{u} = C_1 J_1(kr) + C_2 Y_1(kr). \tag{3.13}$$

or

$$\bar{u} = (1-\nu_D^2)\bar{E}b \frac{\left[A_{12}J_1(kr) - A_{11}Y_1(kr)\right]}{\Delta} \; d_{31}\bar{E}_3 \tag{3.32}$$

Replacing the electrical field in terms of the applied voltage and ring's wall thickness, $\bar{E}_3 = -\frac{\bar{V}}{s}$, the transfer function between the radial velocity at any position and the applied voltage is:

$$\frac{j\omega\bar{u}}{\bar{V}} = -j\omega(1-\nu_D^2)\bar{E} \frac{\left[A_{12}J_1(kr) - A_{11}Y_1(kr)\right]}{\Delta} \; d_{31}\frac{b}{s} \tag{3.33}$$

which meets the goal of this section which is the radial response of the circular plate. In order to consider the loss factor η, the Young's modulus E can be replaced by $E(1+i\eta)$.[15]

3. Quasi Static Displacement:

It is helpful to examine the quasi-static displacement. For the quasi static problem, the dynamic term in Equation 2.29 is ignored. The pressure applied on the piezoelectric ring is simply:

$$\overline{P}_o = -\frac{E_R s}{a^2}\overline{u} + \frac{E_R s}{a}\, d_{31}\overline{E}_3 \tag{3.34}$$

As shown in Figure 3.3, the radial stress and tangential stress can be represented as the pressure applied on the inner radius of the plate[11]:

$$\sigma_r = \frac{P_i b^2}{R^2 - b^2}\left(1 - \frac{R^2}{r^2}\right) \tag{3.35}$$

$$\sigma_\theta = \frac{P_i b^2}{R^2 - b^2}\left(1 + \frac{R^2}{r^2}\right) \tag{3.36}$$

Using Equation 2.11 and 2.13, the radial displacement at any radial position on the plate can be represented:

$$\frac{u}{r} = \varepsilon_\theta = \frac{P_i}{E_D}\frac{b^2}{R^2 - b^2}\left[1 - \nu_D + (1+\nu_D)\frac{R^2}{r^2}\right]. \tag{3.37}$$

or

$$\frac{u}{b} = \frac{P_i}{E_D}\frac{r}{b}\frac{b^2}{R^2 - b^2}\left[1 - \nu_D + (1+\nu_D)\frac{R^2}{r^2}\right]. \tag{3.38}$$

Because the pressure applied on the plate must be equal to that on the piezoelectric ring and the inner radius of the plate is much smaller the outer radius, the radial displacement, u_a, at inner radius can be obtained by substituting Equation 3.34 into Equation 3.38:

$$\frac{u_a}{b} = \frac{(1+\nu_D)\overline{E}}{1+(1+\nu_D)\overline{E}}\, d_{31}\overline{E}_3 \tag{3.39}$$

where $\overline{E}$ is defined the same as in Equation 3.18. Since the radial displacement at the inner radius is obtained, the pressure can be also calculated using Equation 3.34

$$P_o = \frac{E_R s}{b}\left[\frac{1}{1+(1+\nu_D)\overline{E}}\right] d_{31}\overline{E}_3 \tag{3.40}$$

Furthermore, the radial displacement at any arbitrary radial position becomes:

$$\frac{\overline{u}}{b} \cong \frac{\overline{E}}{1+(1+\nu_D)\overline{E}} \frac{r}{b} \frac{b^2}{R^2} \left[1-\nu_D+(1+\nu_D)\frac{R^2}{r^2} \right] d_{31}\overline{E}_3 . \tag{3.41}$$

Therefore, the displacement at outer radius of the plate can also be computed:

$$\frac{\overline{u}_R}{b} = 2\frac{b}{R}\frac{\overline{E}}{1+(1+\nu_D)\overline{E}}\ d_{31}\overline{E}_3 \tag{3.42}$$

The radial displacement at any arbitrary radial position was derived above from the static assumption; however, it can be shown that this result is also consistent with the dynamic Equation 3.32 when the excitation frequency, ω, is very low. Introducing a non-dimensional parameter

$$\overline{\omega} = kr , \tag{3.43}$$

for low frequency, $\overline{\omega} \cong 0$, and ignoring the high order terms, the Bessel functions can be expanded in a series at $\overline{\omega} \cong 0$ as

$$J_0 \cong 1, \tag{3.44}$$

$$J_1 \cong 0.5\ \overline{\omega} , \tag{3.45}$$

$$Y_0 \cong 0.637\ \ln\frac{\overline{\omega}}{2}, \tag{3.46}$$

$$Y_1 \cong -\frac{0.637}{\overline{\omega}} . \tag{3.47}$$

Thus,

$$A_{11} \cong \left[\frac{1+\nu_D}{2} \right] \overline{\omega} , \tag{3.48}$$

$$A_{12} \cong \frac{0.637(1-\nu_D)}{\overline{\omega}}, \tag{3.49}$$

$$A_{21} \cong \frac{b}{R}\frac{\overline{\omega}}{2}\left[1+\nu_D+\overline{E}(1-\nu_D^2)\right], \tag{3.50}$$

$$A_{22} \cong 0.637\frac{R}{b}\frac{1}{\overline{\omega}}\left[1-\nu_D+\overline{E}(1-\nu_D^2)\right], \tag{3.51}$$

and

$$\Delta \cong \frac{0.637}{2}(1-\nu_D^2)\frac{R}{b}\left[1+\overline{E}(1+\nu_D)\right]. \tag{3.52}$$

Substituting Equations 3.48-3.52 into Equation 3.32, the radial displacement at the outer radius of the plate,

$$\frac{\overline{u}_R}{b} = \frac{A_{12}J_1(\overline{\omega})-A_{11}Y_1(\overline{\omega})}{\Delta}(1-\nu_D^2)\overline{E}\ d_{31}\overline{E}_3, \tag{3.53}$$

can be reduced to

$$\frac{\overline{u}_R}{b} = 2\frac{b}{R}\frac{\overline{E}}{1+(1+\nu_D)\overline{E}}\ d_{31}\overline{E}_3 \tag{3.54}$$

which is consistent with Equation 3.42. Similarly, the radial displacement at the inner radius of the plate

$$\frac{\overline{u}_b}{b} = \frac{A_{12}J_1(\overline{\omega}\frac{b}{R})-A_{11}Y_1(\overline{\omega}\frac{b}{R})}{\Delta}(1-\nu_D^2)\overline{E}\ d_{31}\overline{E}_3 \tag{3.55}$$

can also be reduced to

$$\frac{\overline{u}_a}{b} = \frac{(1+\nu_D)\overline{E}}{1+(1+\nu_D)\overline{E}}\ d_{31}\overline{E}_3 \tag{3.56}$$

which is also consistent with Equation (3.39).

4. Interference Pattern and Radial Mode Shape:

Equation 3.33 shows that the resonance occurs when the characteristic equation is equal to zero

$$\Delta = 0. \tag{3.57}$$

The characteristic equation is composed of Bessel functions which have roots on the real axis. This implies that resonant peaks occur in the frequency domain. As examples, the radial responses of several plates with different sizes and material are computed using equation 3.33. Figure 3.5 plots the calculated radial velocity response of two PVC circular plates at the outer radius $r = R$; one is 15 cm in radius, and the other is 9 cm in radius. Figure 3.6 also plots the calculated velocity response of two circular plates $r = R$. Both plates are 15 cm in radii; one is aluminum and the other is PVC. The material properties of PVC and aluminum are listed in Table 3.1. The material properties of PVC vary with material, the value listed in Table 3.1 is estimated by experiment[16]; however, the material properties of aluminum are well defined and can be obtained from general texts[17].

As show in Figure 3.5 and 3.6, infinitely many resonant peaks occur and are equally spaced in frequency domain. It is interesting to discuss these interference pattern with several parameters, such as material properties and size of the plate.

First, the sharpness of the resonant peak is related to the loss factor and the excitation frequency. The aluminum plate has much sharper resonant peaks than the PVC plate does because the loss factor of PVC is much higher. In addition, the PVC plate has wider resonant peaks at high frequencies than at low frequencies.

Second, the distance between the two resonant peaks is related to the radius of the plate and the sound speed in the material. The piezoelectric ring radiates waves in the circular plate and these wave are reflected back at the plate edge, so that the resonance occurs when the radiated and reflected waves interfere. The sound wave travels faster in

aluminum than in PVC; therefore, the aluminum plate has wider peak spans for the same radius plate, as illustrated in Figure 3.5. For the same reason, the smaller circular plate has wider peak spans for the same material plate, as illustrated in Figure 3.6.

Third, the magnitude is related to the plate radius and Young's modulus. The stiffer and the larger the plate is, the lower the magnitude.

Finally, as discussed earlier, the resonant peaks correspond to the roots of the characteristic equation. Defining the n th non-dimensional root as $k_n R$, and plotting the displacement magnitude with respect to radius ratio r/R for every root $k_n R$, the n th radial mode shape can then be obtained, as illustrated in Figure 3.7. Therefore, the resonant peak in the frequency domain corresponds to every radial mode shape discussed here.

In this section, the transfer function between the radial velocity of the circular plate and the applied voltage on the piezoelectric ring has been derived; see Equation 3.33. The interference pattern and radial mode shapes implied in Equation 3.33 have also been discussed in detail. In the next section, experimental measurements are compared with Equation 3.33, and the pressure exerted by the piezoelectric ring is estimated.

Table 3.1 Material Properties of the Circular Plate

	PVC	Aluminum
Young's Modulus, E (10^9 N/m^2)	3.0	70
Poisson's Ratio, ν	0.26	0.33
Density, ρ (10^3 Kg/m^3)	1.39	2.7
Loss Factor, η	0.04	0.005
Wave Speed , c (m/s)	1521	5394

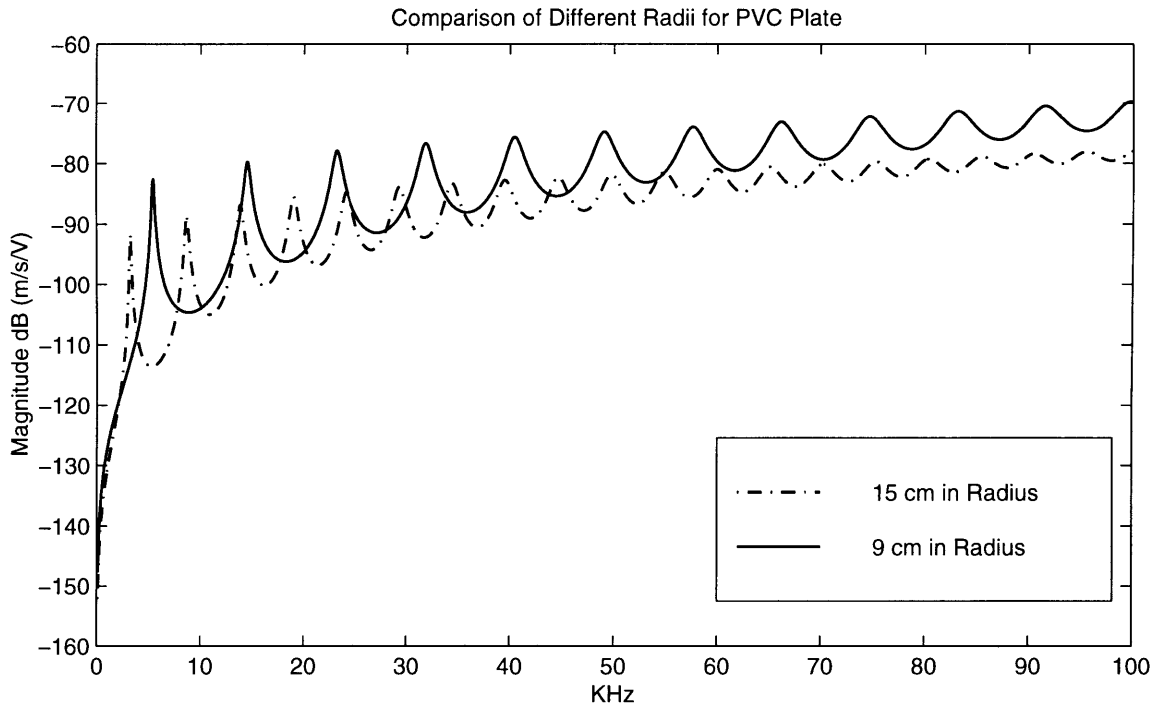

Figure 3.5 Interference Pattern for a Circular Plate in the Linear Frequency Domain: Different Radii

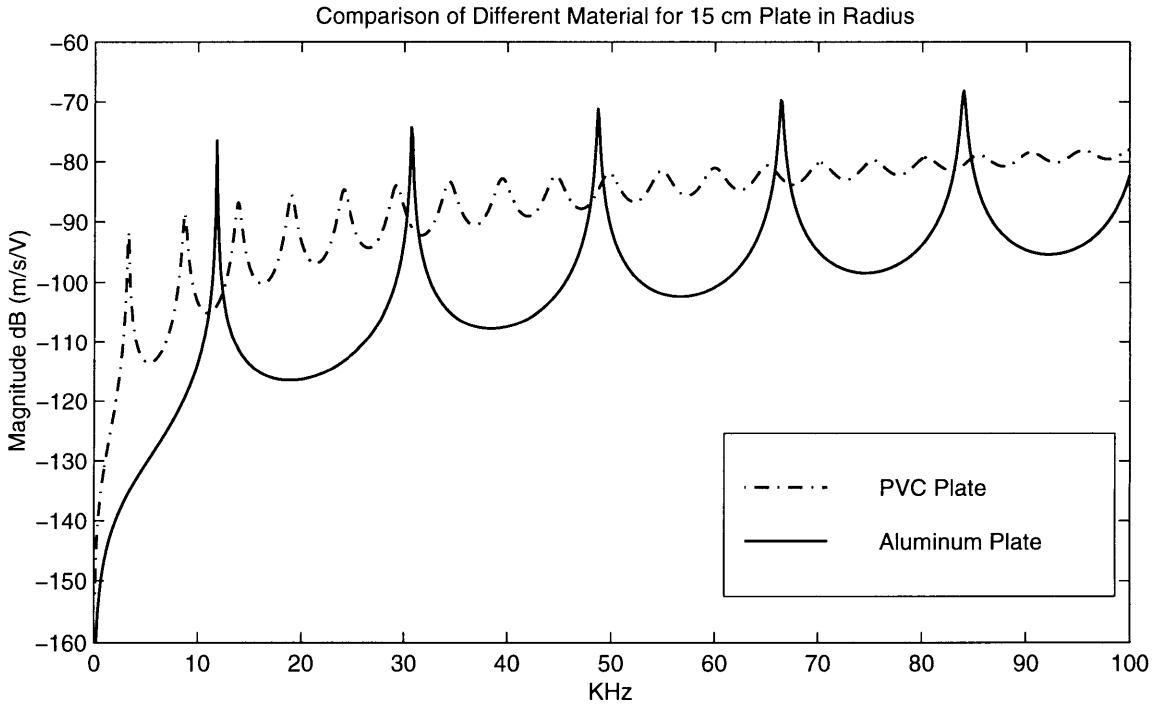

Figure3.6 Interference Pattern of a Circular Plate in the Linear Frequency Domain: Different Materials

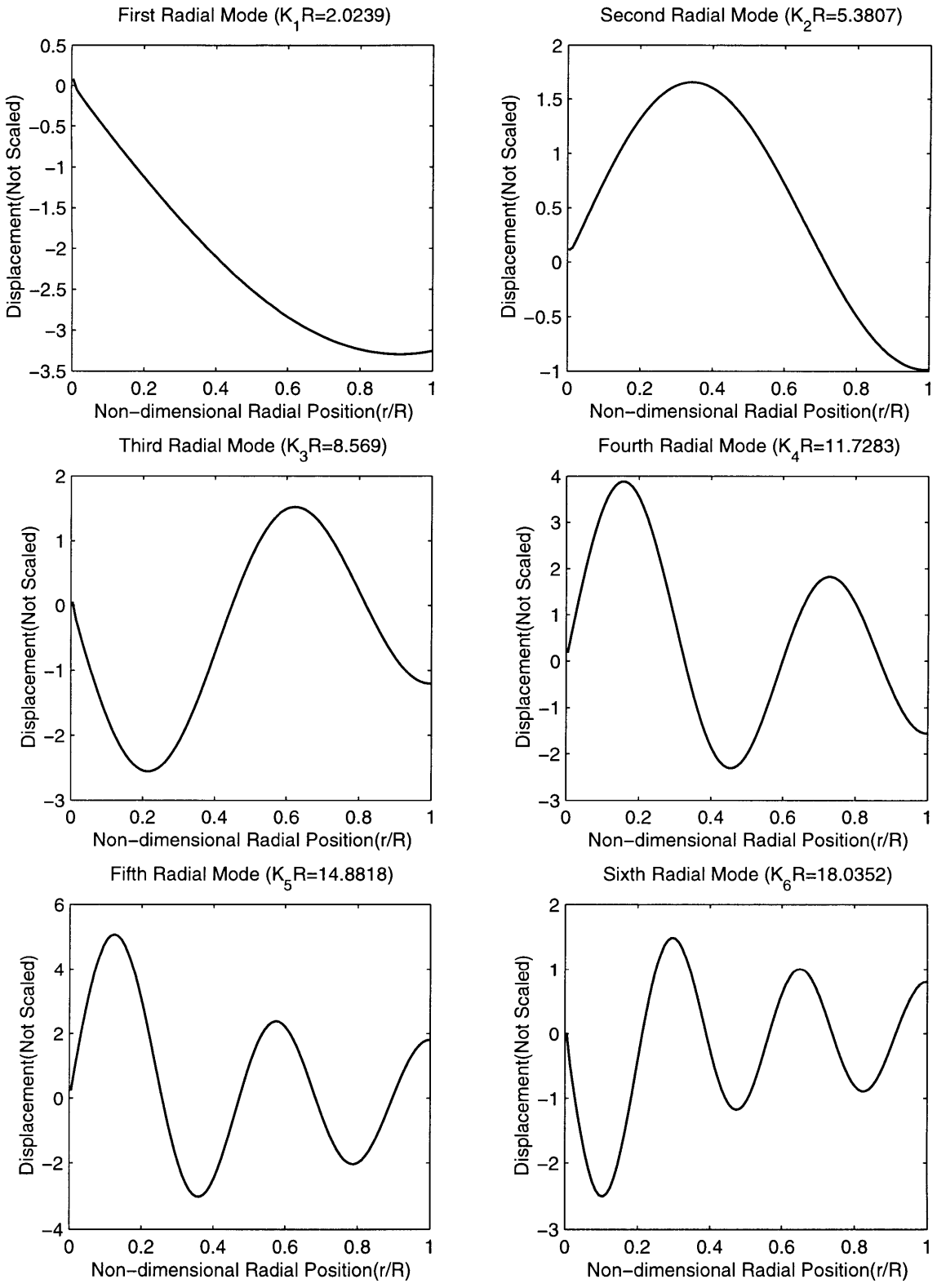

Figure 3.7 First Six Radial Mode Shapes of the Circular Plate

3.2 Pressure Estimation of Piezoelectric Rings in an Aluminum and a PVC Circular Plate

In this section, the radial responses of a PVC and an aluminum circular plate driven by piezoelectric rings embedded in the plate centers are measured and compared to the model of the preceding section. The PVC and the aluminum circular plates are of size 9 and 15 cm in radius, respectively. Their material parameters are summarized in Table 3.1. By comparing to the experimental measurement, Equation 3.33 in previous section can be validated. The pressure exerted by piezoelectric ring can be estimated using Equation 2.29.

Figure 3.8 shows the experimental setup for measuring the radial velocity response. The experiment setup is the same as that in Figure (2.8), except that the piezoelectric ring is now bonded into a circular plate. As illustrated in Figure 3.9, the plate is simply supported by three small plastic balls of size 4 mm in diameter, so that the plate can deform freely in radial direction. The circular plate is excited by the piezoelectric ring with a swept sine voltage signal supplied by the SigLab function generator via the amplifier with a constant gain 13 (22.5 dB). The velocity is then measured by LDI system and fed back to SigLab spectrum analyzer, so that the transfer function between velocity and applied voltage can be obtained by computing the ratio of cross-spectrum and the auto-spectrum. The details of experiment setup and swept sine configuration have been discussed in Chapter II.

The radial velocity response at the outer radius, $r = R$, can be measured directly by pointing the laser beam along the radial direction at the plate edge, as illustrated in Figure 3.8. However, an alternative technique must be used to measure the radial velocity

at any other position for $r < R$. Figure 3.10 illustrates this modified measurement technique. Two velocity response measurements along different directions are required. One is an axial velocity(v_a), which is vertical to the plate surface; the other is a 45° velocity(v_{45^o}), which intersects the radial direction, r, at 45° and is also in the same plane with the radial direction. The measured 45° velocity, v_{45^o}, is contributed to by the projections of the axial velocity, v_a, and the radial velocity, v_r, along the 45° direction, so that:

$$v_{45^o} = \frac{1}{\sqrt{2}}(v_a + v_r), \tag{3.58}$$

and the radial velocity for $r < R$ can be determined by

$$v_r = \sqrt{2}v_{45^o} - v_a. \tag{3.59}$$

In order to determine if Equation 3.33 is valid for all positions on the plate, in addition to measuring the radial response at plate edge, the radial response near the piezoelectric ring is also measured. Figures 3.11(a) and 3.12(a) show the model and the data of the radial response of aluminum plate at $r = 0.15m$ and $r = 7mm$, respectively. Figures 3.11(b) and 3.12(b) show the error analysis between model and data. For the radial response at plate's edge($r = 0.15m$) in Figure 3.11, the error between model and data averages about $1dB$ in the range from 1 to 20 KHz regardless of the resonant peaks. For the radial response at aluminum plate's interior($r = 7mm$) in Figure 3.12, the error between model and data also averages about $1dB$ in the range from 1 ~ 20 KHz regardless of the resonant peaks.

Figures 3.13(a) and 3.14(a) show the model and the data of the radial response of the PVC plate at $r = 0.09m$ and $r = 7mm$, respectively. Figures 3.13(b) and 3.14(b) show

the error analysis between model and data. For the radial response at plate's edge($r = 0.15m$) in Figure 3.13, the error between model and data averages about $2dB$ in the range from 1 ~ 20 KHz regardless of the resonant peaks. For the radial response at PVC plate's interior($r = 7mm$) in Figure 3.13, the error between model and data averages about $3dB$ in the range from 1 ~ 20 KHz regardless of the resonant peaks. The prediction of the radial response at PVC circular plate is not as good as that in aluminum plate because the material properties of PVC are not definitely known. The material properties of PVC used here are estimated. Unlike PVC, the material properties of the aluminum are more accurately known.

According to the comparison discussed above, it can be concluded that Equation 3.33 is validated for all position on the circular plate if the material properties of plate are definitely known. Since Equation 3.33 is validated, the displacement at the outer surface of the piezoelectric ring (or the inner surface of the circular plate) is also validated. Therefore, the pressure exerted by the piezoelectric ring can be estimated using Equation 2.29. Figures 3.15 and 3.16 show the estimated pressures exerted by the piezoelectric rings embedded in the aluminum and the PVC circular plate, respectively. The pressure per unit volt exerted by the piezoelectric ring is estimated as 55 $dB\ re.\ 1\ N/m^2/V$ in a 9 cm radius PVC circular plate and 68 $dB\ re.\ 1N/m^2/V$ in a 15 cm radius aluminum circular plate. As shown in the figures, the pressure is almost independent of frequency away from resonance locations. Furthermore, PVC is more compliant than the aluminum, so the PVC has lower impedance. Thus, the piezoelectric ring is easier to expand in a PVC plate, and the pressure exerted by the ring in the PVC plate is less than that in the aluminum plate.

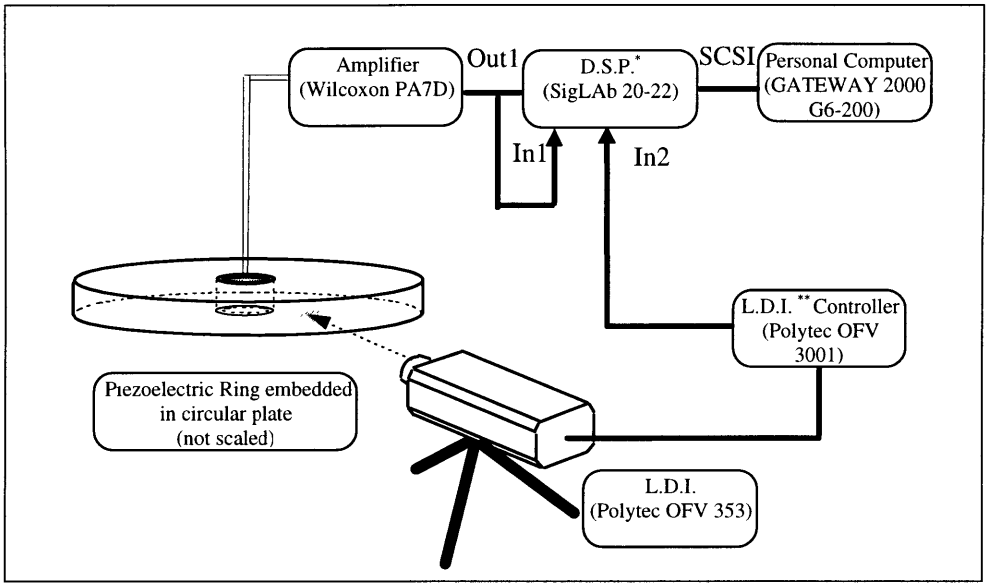

Figure 3.8 Experimental Setup for Measuring the Radial Velocity at Circular Plate Edge

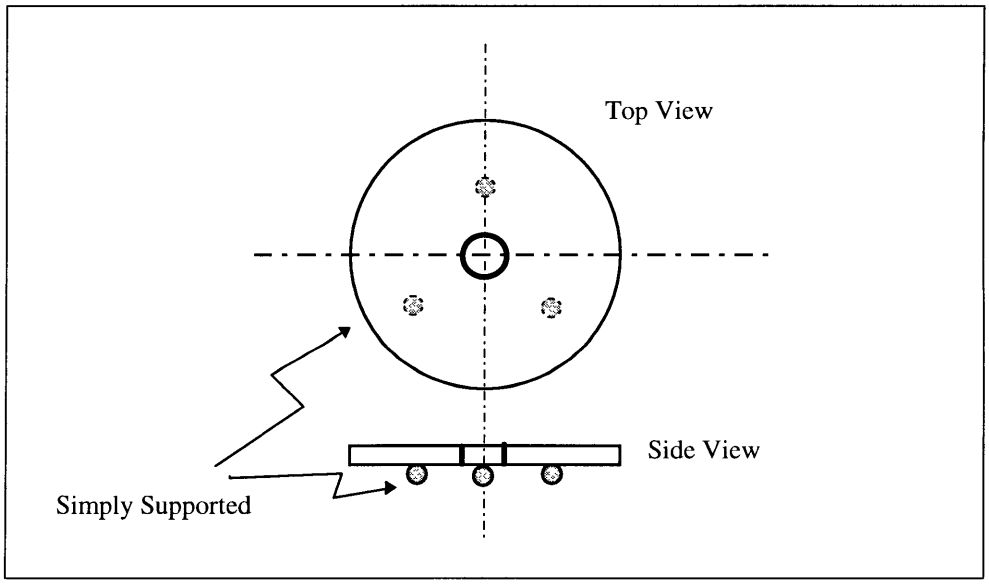

Figure 3.9 Simply Supported Circular Plate

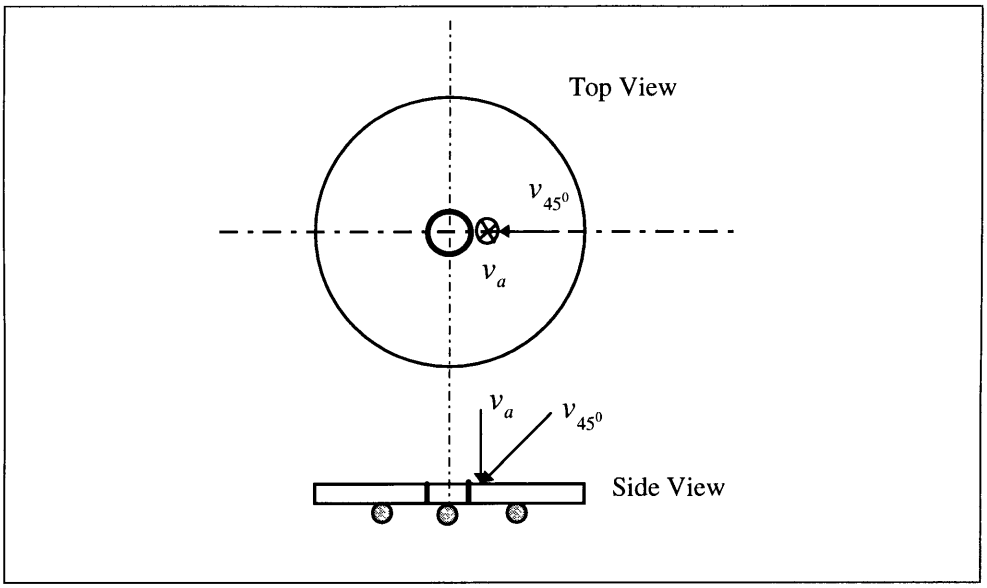

Figure 3.10 Modified Radial Velocity Measurement Technique for r<R

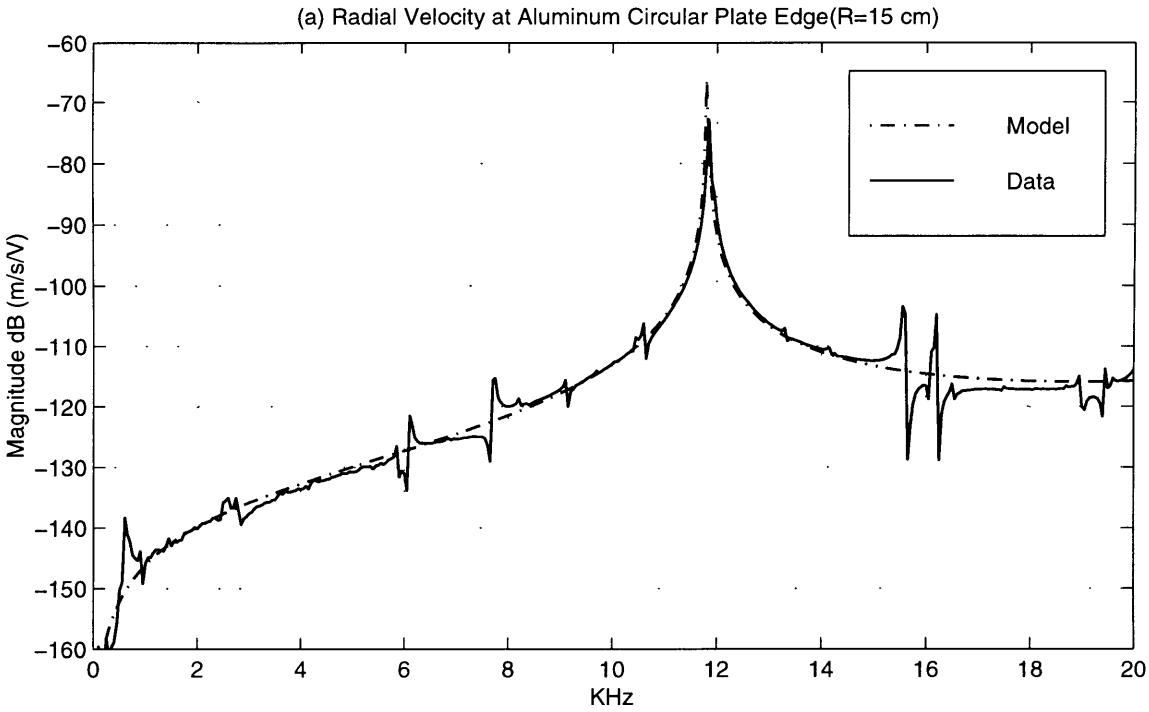

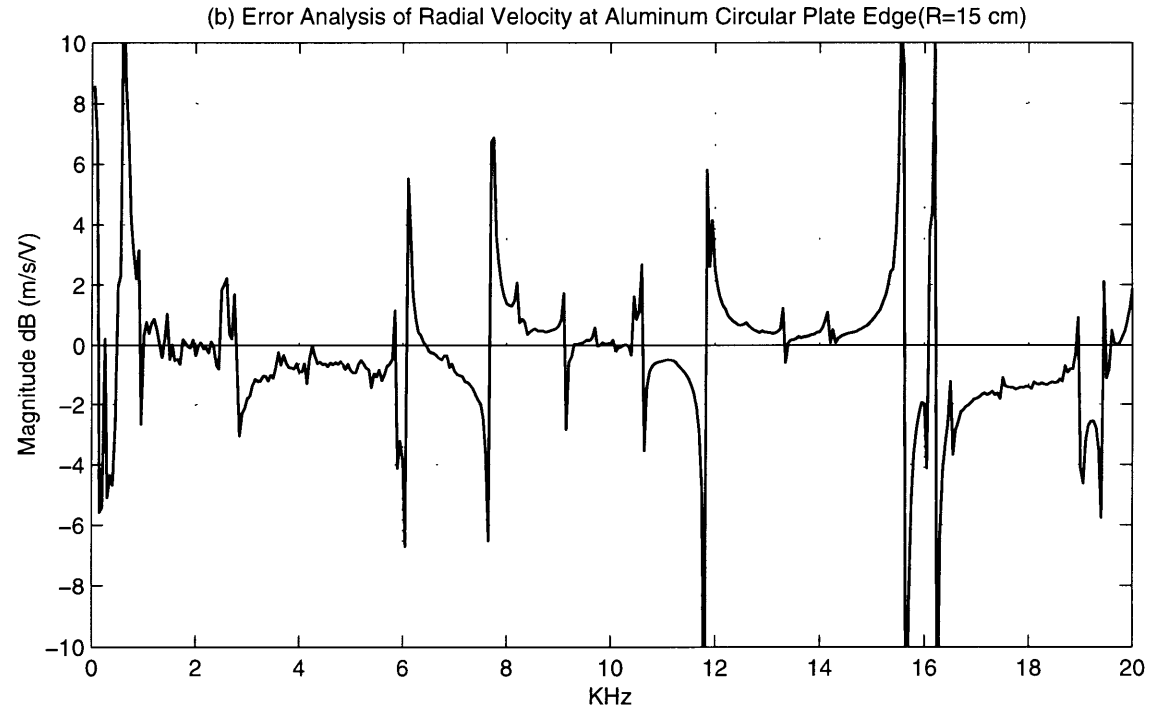

Figure 3.11 Radial Response of the Aluminum Circular Plate at Plate Edge (r=R): (a) Comparison of Model and Data (b) Error Analysis of Model and Data

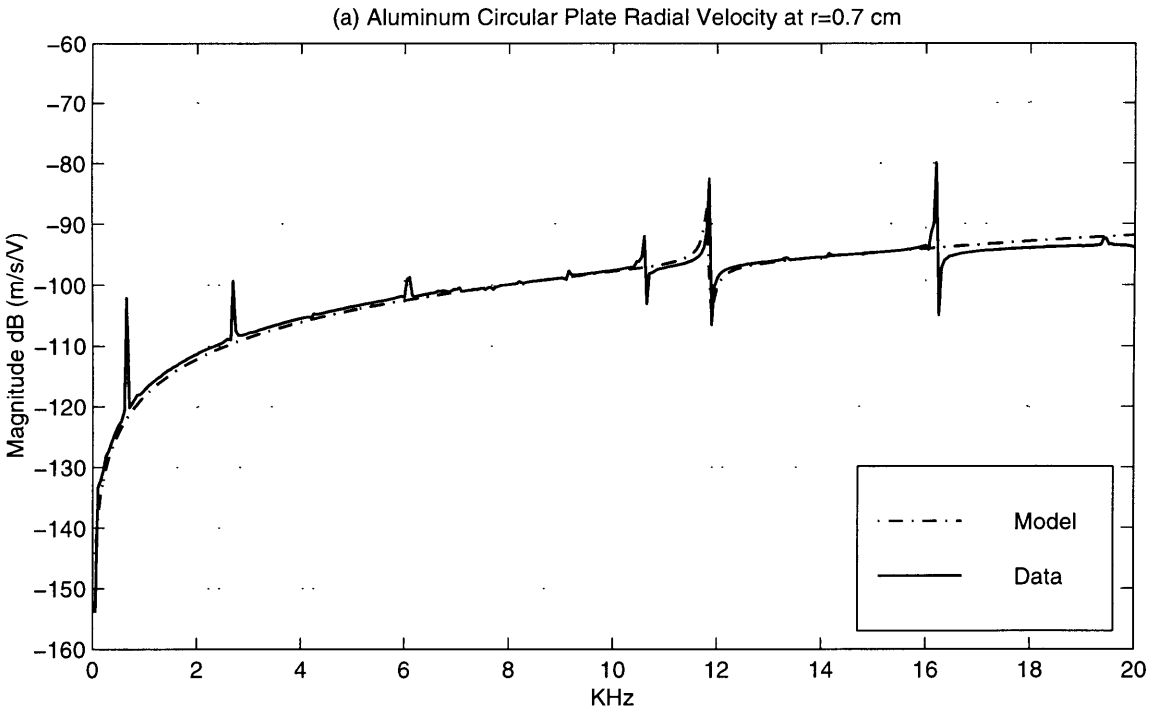

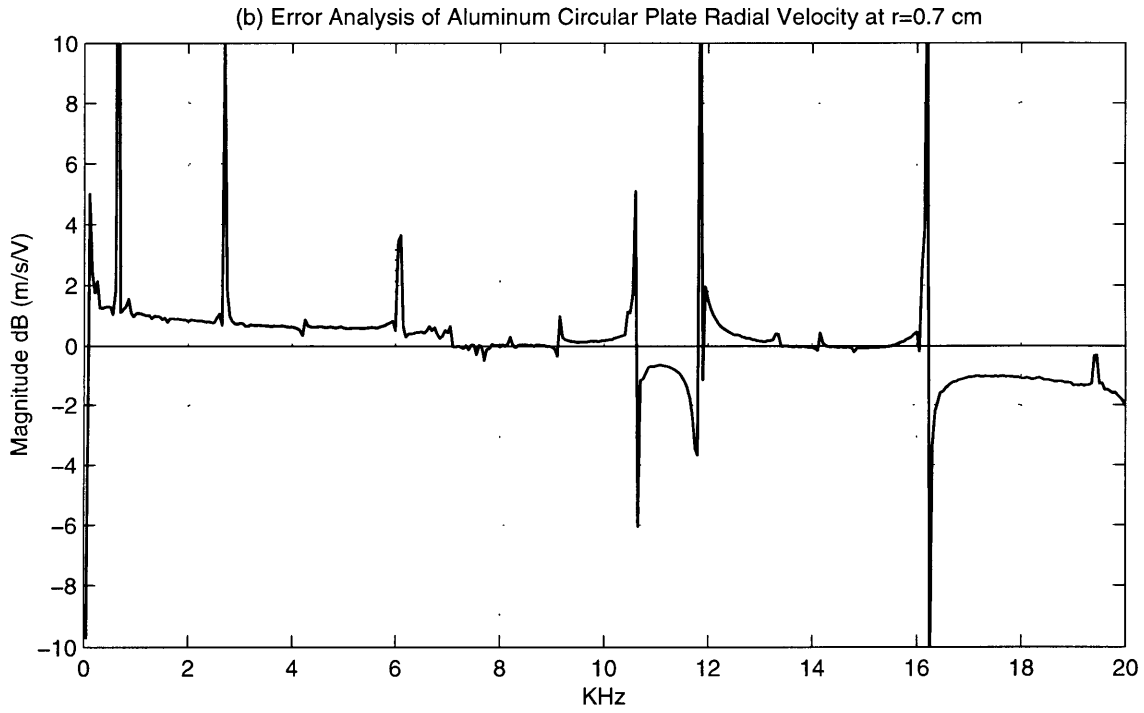

Figure 3.12 Radial Response of the Aluminum Circular Plate at r=7mm (r<R): (a) Comparison of Model and Data (b) Error Analysis of Model and Data

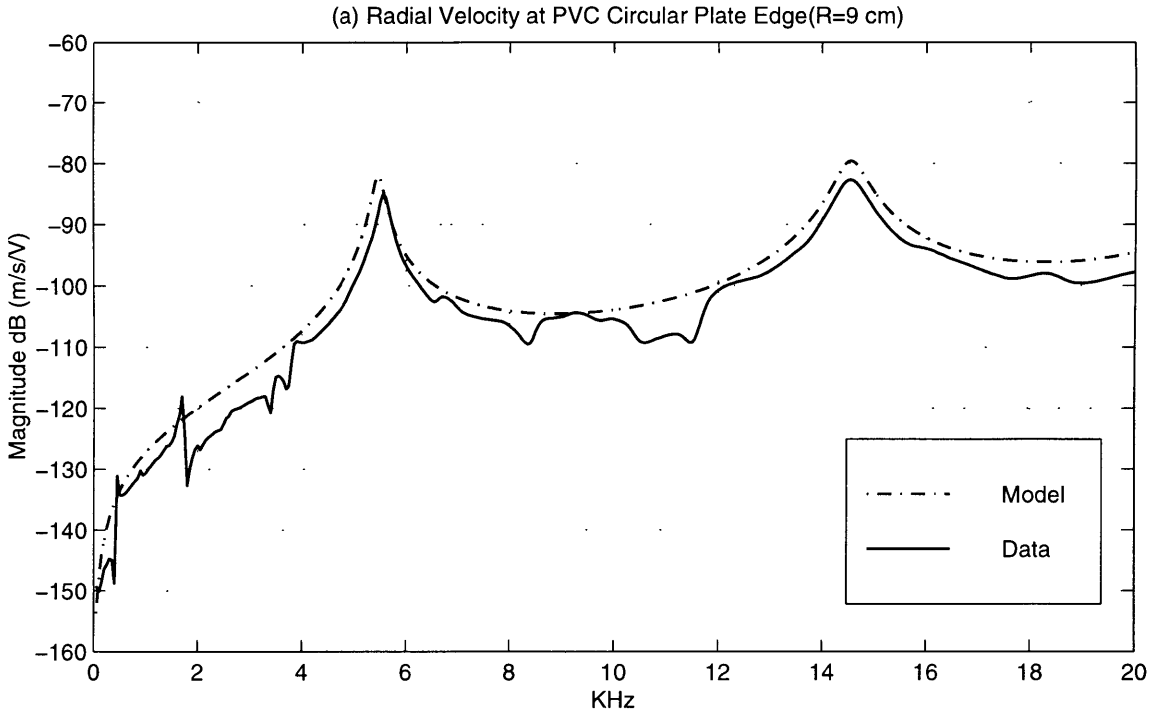

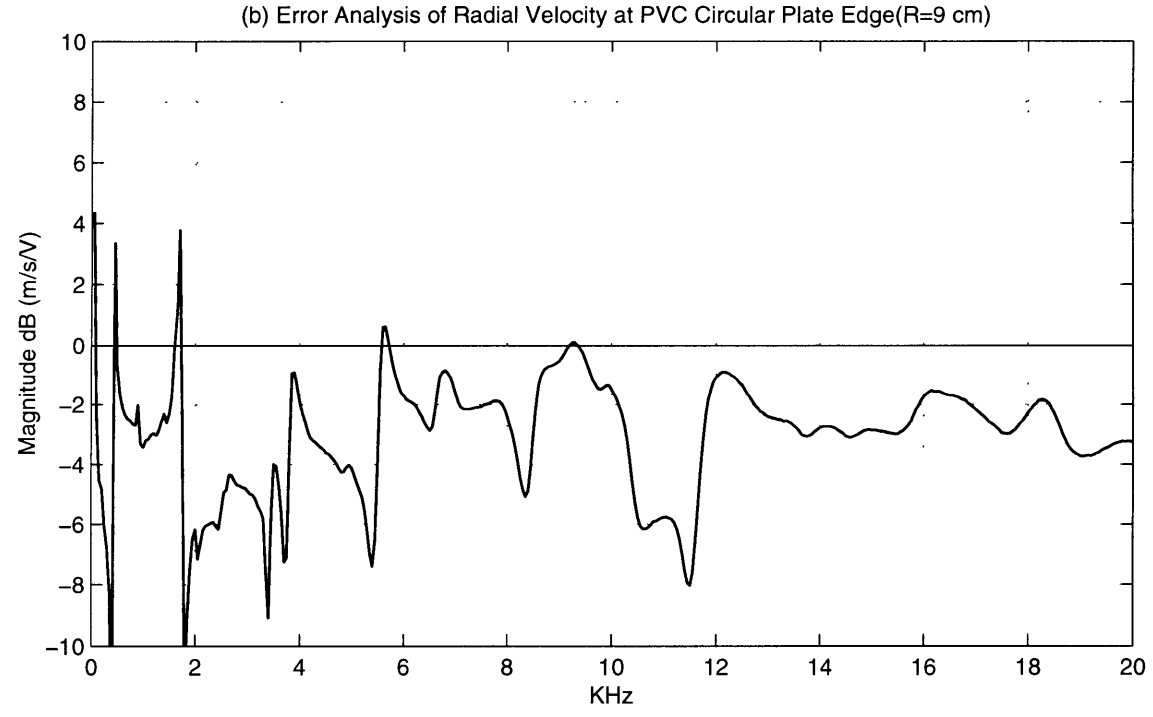

Figure 3.13 Radial Response of the PVC Circular Plate at Plate Edge (r=R): (a) Comparison of Model and Data (b) Error Analysis of Model and Data

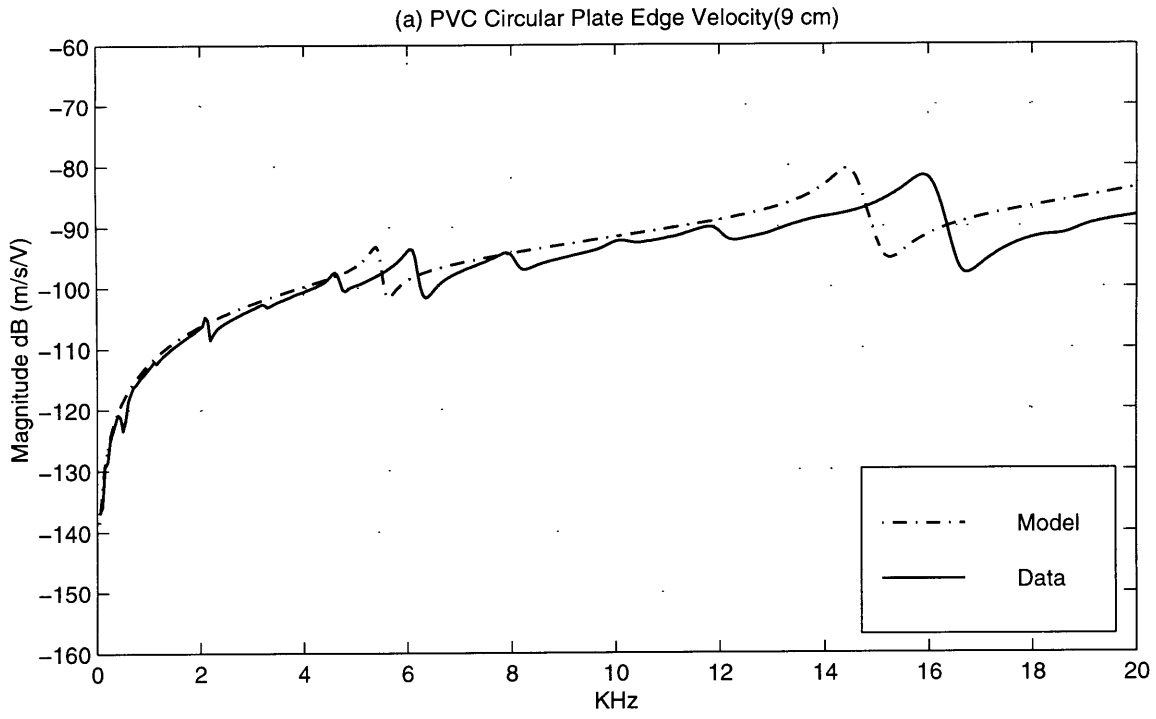

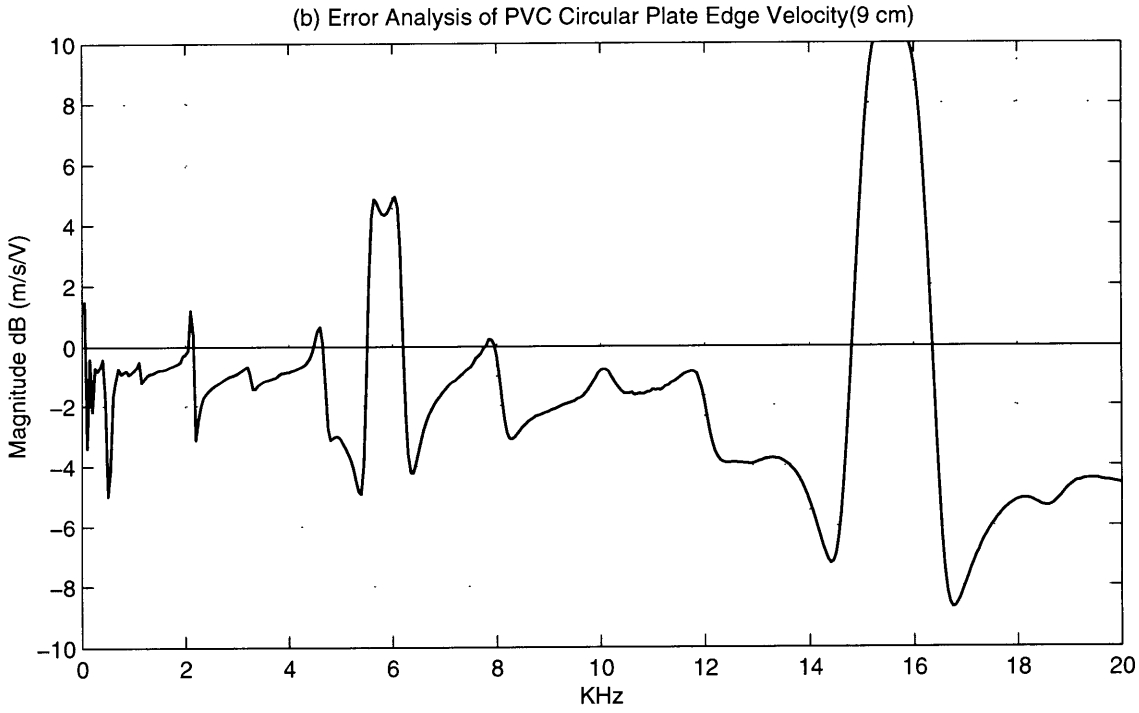

Figure 3.14 Radial Response of the PVC Circular Plate at r=7mm (r<R): (a) Comparison of Model and Data (b) Error Analysis of Model and Data

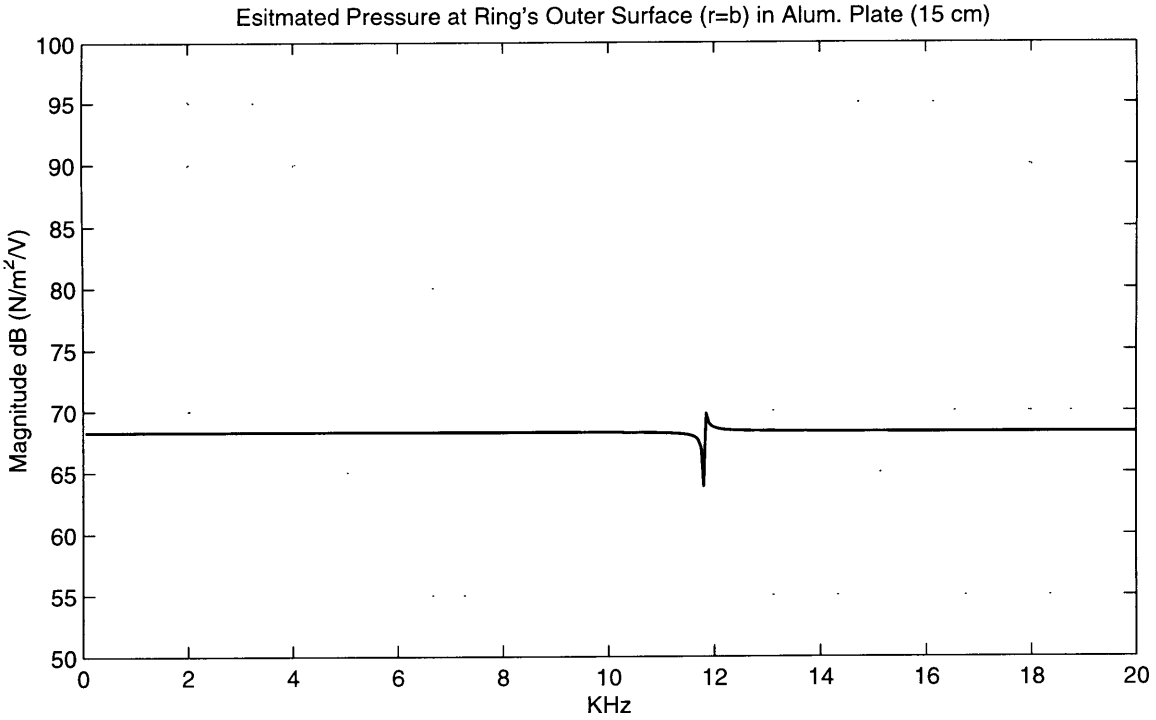

Figure 3.15 Pressure Exerted by the Piezoelectric Ring in the Aluminum Plate

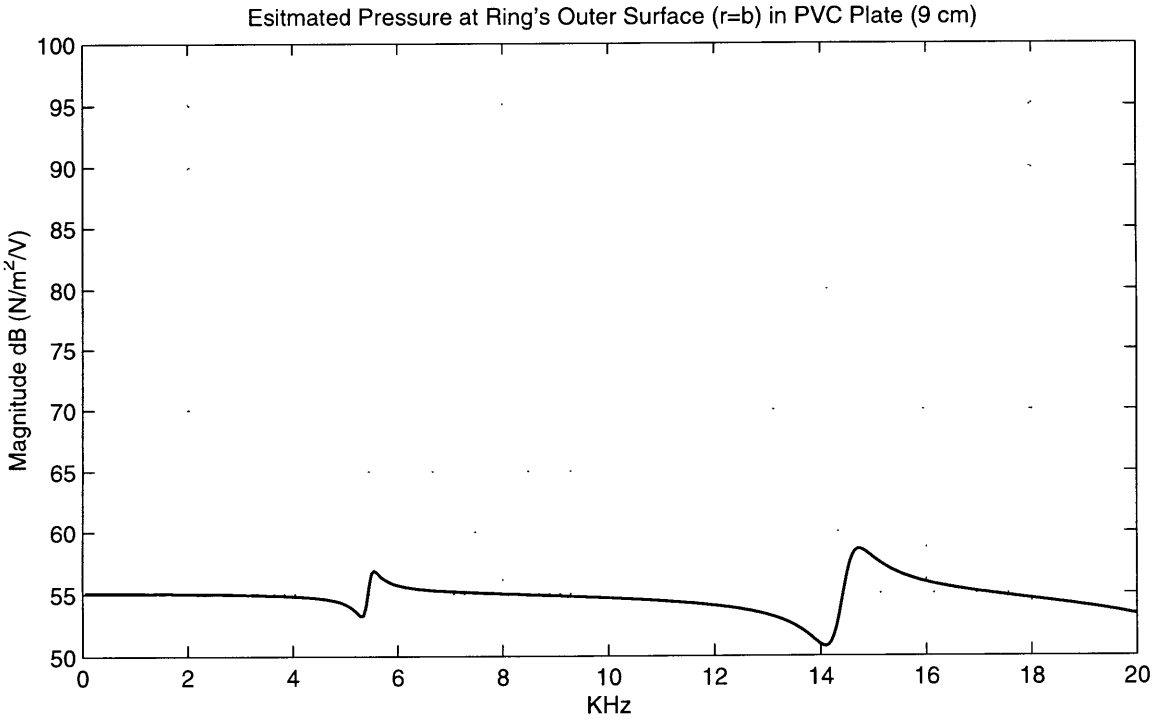

Figure 3.16 Pressure Exerted by the Piezoelectric Ring in the PVC Plate

Chapter 4.

Piezoelectric Rings Embedded in Cylindrical Shells

In this chapter, the pressure exerted by the piezoelectric ring embedded in the cylindrical shell is estimated using the plate model developed in Chapter 3. The basic assumption is that the piezoelectric ring, planted in the cylindrical shell, expands as if it were in a very large circular plate. To validate this assumption, the near field radial response on the shell is measured and compared to the plate model. Once the near field radial response is validated, the pressure exerted by the ring can be estimated. To evaluate this estimation, in the second section, a state space approach developed by Borgiotti[3] is used to predict the far field longitudinal response on the cylindrical shell and compared to the measurement. The input of this state space approach is restricted to a unidirectional point force or modal force, while the piezoelectric ring exerts pressure along all its radial directions. For this reason, the pressure exerted by the ring is integrated into an unidirectional point force, so that it can be used as an input to the model developed by Borgiotti.

Two cylindrical shells with different geometry and materials are discussed in this chapter. Table 4.1 lists the geometric and material parameters of the two cylindrical shells and the piezoelectric rings used in the experiment.

Table 4.1 Parameters of Two Cylindrical Shells and Piezoelectric Rings Used in the Experiment

Parameters of Cylindrical Shells		
Material Type	PVC	Steel
Neck-Down Section	No	Yes
Length (m)	6.07	4.87
Outer Diameter (m)	0.41	0.31
Wall Thickness (m)	0.0047	0.0017
Young's Modulus (GPa)	3.6	200
Poison's Ratio	0.2	0.3
Loss Factor	0.06	1e-4
Density (Kg/m^3)	1.39e3	7.8e3
Quasi-longitudinal Wave Speed (m/s)	1610	5048
Parameters of Piezoelectric Rings		
Material Type	Navy VI Channel 5700	Navy I Channel 5400
Location from the Edge (m)	2.32	1.07
Diameter (m)	0.008	0.0064
Wall Thickness (m)	6.86e-4	7.62e-4
Polarization Mode	3-1 Transverse Mode	3-1 Transverse Mode
Young's Modulus (GPa)	62	82
Density (Kg/m^3)	7.4e3	7.55e3
Piezoelectric Constant (10^{-12} m/V) d_{31}	-250	-135

4.1 Near Field Response and Pressure Estimation of the Piezoelectric Rings in Cylindrical Shells

The goal of this section is to estimate the pressure exerted by a single piezoelectric ring planted vertically in a cylindrical shell. This is a complex problem because the longitudinal axis of the small hole, in which the piezoelectric ring is mounted, is perpendicular to the longitudinal axis of the cylindrical shell. Therefore, two orthogonal coordinates are involved in this problem. However, the ring's radius is much smaller than the cylindrical

shell's radius, so the local curvature near the piezoelectric ring can be treated as small. Therefore, the driving point impedance of the ring in the cylindrical shell can be assumed to be the same as that in a infinite circular plate. Based on this assumption, the problem can be solved by using the plate model developed in the previous chapter and assuming the plate is very large. It is reasonable to assume that if the radius is large it is of the same order as the cylindrical shell's length. To validate this assumption, in this section, the longitudinal response near the piezoelectric ring is measured and compared to the large plate model.

The experimental setup for measuring the near field response is similar to that for the free piezoelectric ring, as illustrated in Figure 2.8. The only difference is that the measurement in this experiment is the near field response of the cylindrical shell. The goal in this experiment is to measure the longitudinal velocity near the outer surface of the piezoelectric ring; however, it is difficult to measure the longitudinal velocity unless two measurements are taken in different directions. The idea is the same as that for measuring the radial response at the circular plate for $r < R$ in the previous chapter. As illustrated in Figure 4.1, v_v is the vertical velocity response and v_{45^o} is the 45° velocity response at the measurement location on the cylindrical shell. v_v, v_{45^o} and the longitudinal direction are in the same plane. The 45° velocity response is contributed to by the projection of the vertical velocity and the longitudinal velocityv_z along the 45° direction, so that

$$v_{45^o} = \frac{1}{\sqrt{2}}(v_v + v_z), \tag{4.1}$$

and the longitudinal velocity can be determined by

$$v_z = \sqrt{2} v_{45^o} - v_v \tag{4.2}$$

Using this algorithm, it is therefore possible to measure the in-plane velocity response on the cylindrical shell.

Now using Equation 3.33 with radius $R = 10m$, which is the same order of the cylindrical shell's length, the near field radial velocity response on the plate, which is equivalent to the near field in-plane velocity on the shell, can be computed. Care must be taken that the plate model is valid for cylindrical shell just outside the piezoelectric ring , because shell curvature must be considered beyond this region.

Figures 4.2(a) and 4.4(a) show the longitudinal velocity responses of steel shell at $z = 5mm$ and $z = 10mm$ in linear frequency domain, respectively. The response at $z = 5mm$ is the nearest possible measurement on the steel shell because the piezoelectric ring is $3.2mm$ in radius and the laser beam focus is not exactly a point but a circle of $3mm$ in radius. Figures 4.2(b) and 4.4(b) also show their error analysis between the model and data at $z = 5mm$ and $z = 10mm$. To investigate the frequency dependence and the error at low frequency, Figures 4.3 and 4.5 show the response in logarithmic frequency domain corresponding to Figures 4.2 and 4.4.

Figures 4.6(a) and 4.8(a) show the longitudinal velocity responses of the PVC shell at $z = 7mm$ and $z = 10mm$ in linear frequency domain, respectively. The response at $z = 7mm$ is the nearest possible measurement at steel shell because the radius of piezoelectric ring is $4mm$. Figures 4.6(b) and 4.8(b) show their error analysis between the model and data at $z = 7mm$ and $z = 10mm$. To investigate the frequency dependence and the error at low frequency, Figures 4.7 and 4.9 show the response in logarithmic frequency domain corresponding to Figure 4.6 and 4.8.

It is shown in Figures 4.3 and 4.5 that the large plate model predicts the near-field longitudinal velocity on the steel cylindrical shell very well with the error averaging $2dB$ from 600Hz to 20KHz. However, Figures 4.7 shows the error averaging $3dB$ from 600Hz to 20KHz for the longitudinal response at $z = 7mm$ on the PVC cylindrical shell and Figure 4.9 shows the error averaging $5dB$ from 100Hz to 20KHz for the longitudinal response at $z = 10mm$ on the PVC cylindrical shell. The reason for the under prediction for the PVC shell's response is probably because the material properties of PVC are not definitely known. Unlike the PVC shell, the material properties of steel are well known. Therefore, the conclusion can be made that the plate model can predict near-field longitudinal velocity response on cylindrical shells as long as the material properties are accurately known.

Since the measurements of the longitudinal velocity response on the cylindrical shells validate the prediction using the plate model, the pressure exerted at the piezoelectric ring's outer surface thus can be estimated using Equation 2.29. Figures 4.10 and 4.11 show the estimated pressures exerted by the rings in the steel and the PVC shells, respectively. The pressure levels are apparently independent of frequency and have an average value for the steel cylindrical shell

$$P_{steel} = 68\ dB\ re.\ 1\ N/m^2/V,$$

and an average value for the PVC cylindrical shell

$$P_{PVC} = 55\ dB\ re.\ 1\ N/m^2/V.$$

These two estimated values thus meet the goal of this thesis.

Note that the pressure for the steel cylindrical shell is as expected higher than that for the aluminum plate, because the driving point impedance of the steel cylindrical shell is

higher than that of the aluminum plate. However, both of them have the same estimated pressure level. This is because the piezoelectric ring used in the steel cylindrical shell had a lower piezoelectric constant than that used in the aluminum plate.

In the next section, the estimated pressures exerted by the piezoelectric rings are integrated into unidirectional forces along the longitudinal direction, so that the state space model developed by Borgiotti can be used to predict the far field longitudinal response on the cylindrical shell.

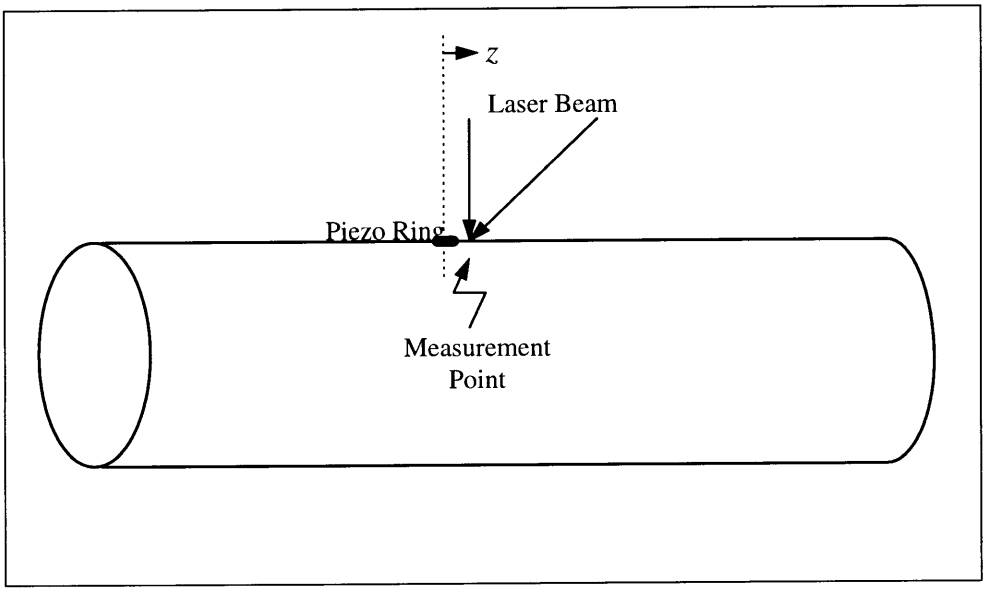

Figure 4.1 Experimental Setup for Measuring the Near Field Longitudinal Velocity on the Cylindrical Shell

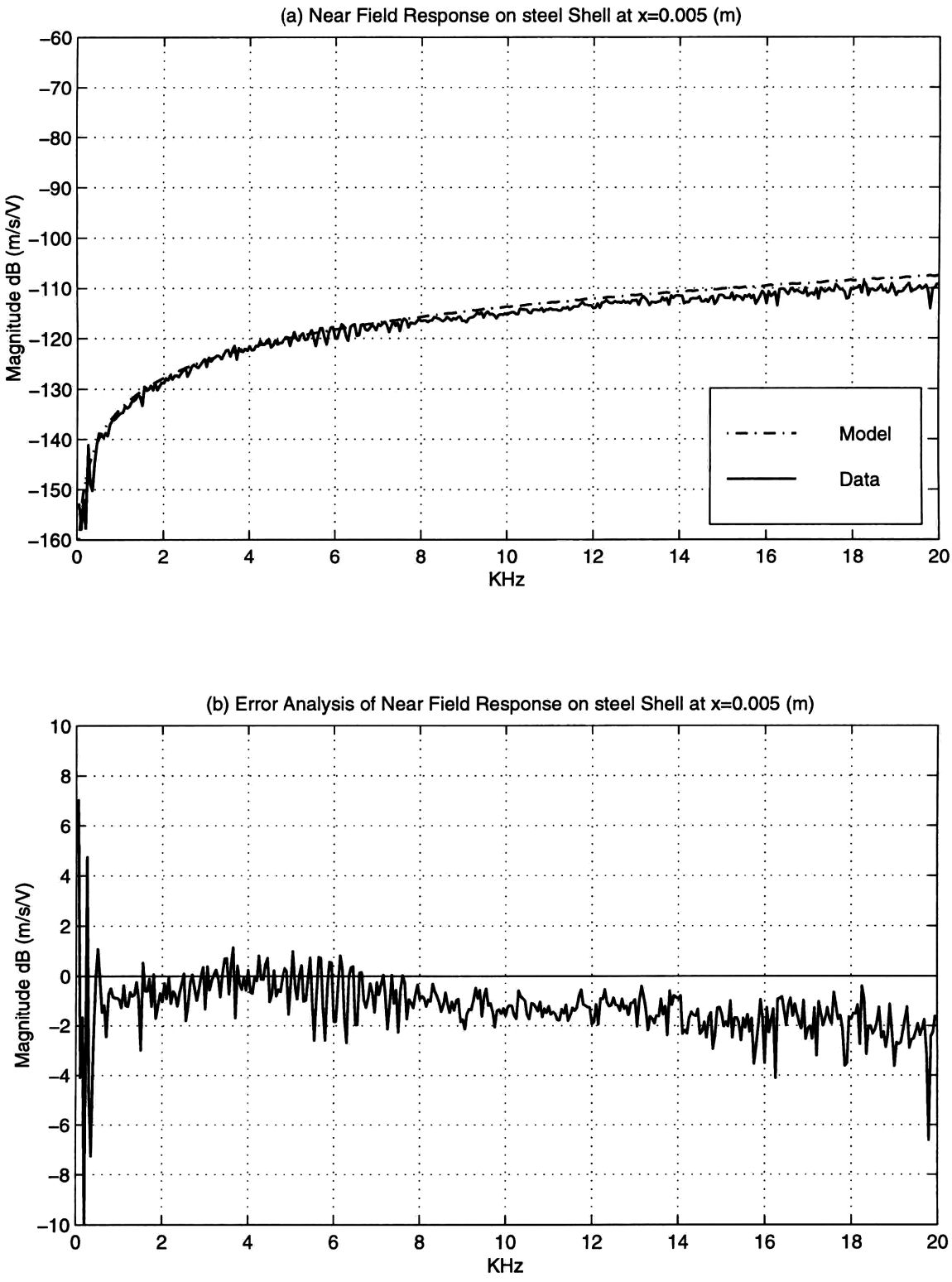

Figure 4.2 Near Field Response at z=0.005m on the Steel Shell in the Linear Frequency Domain (a) Comparison of Model and Data (b) Error Analysis

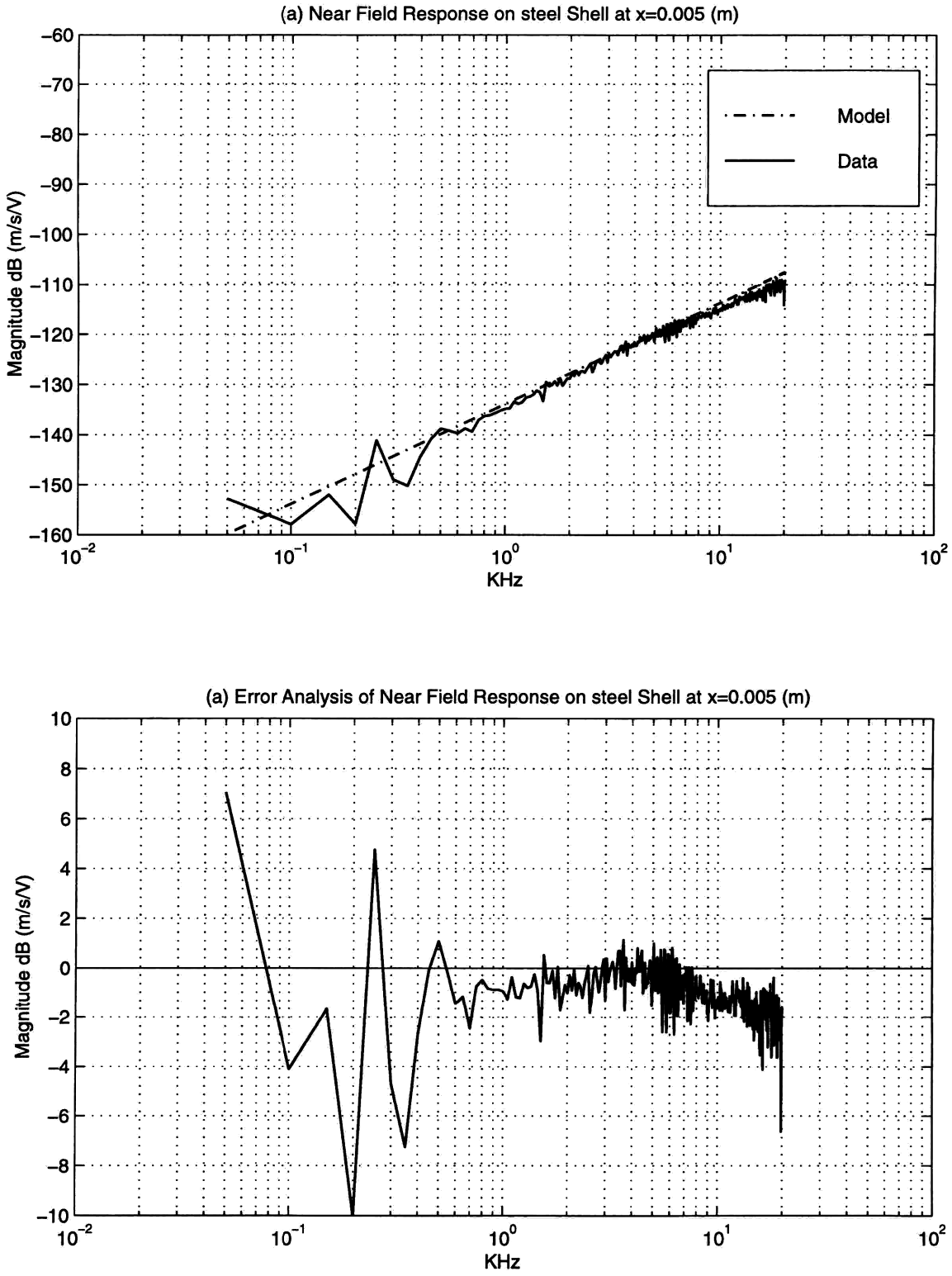

Figure 4.3 Near Field Response at z=0.005m on the Steel Shell in the Logarithmic Frequency Domain (a) Comparison of Model and Data (b) Error Analysis

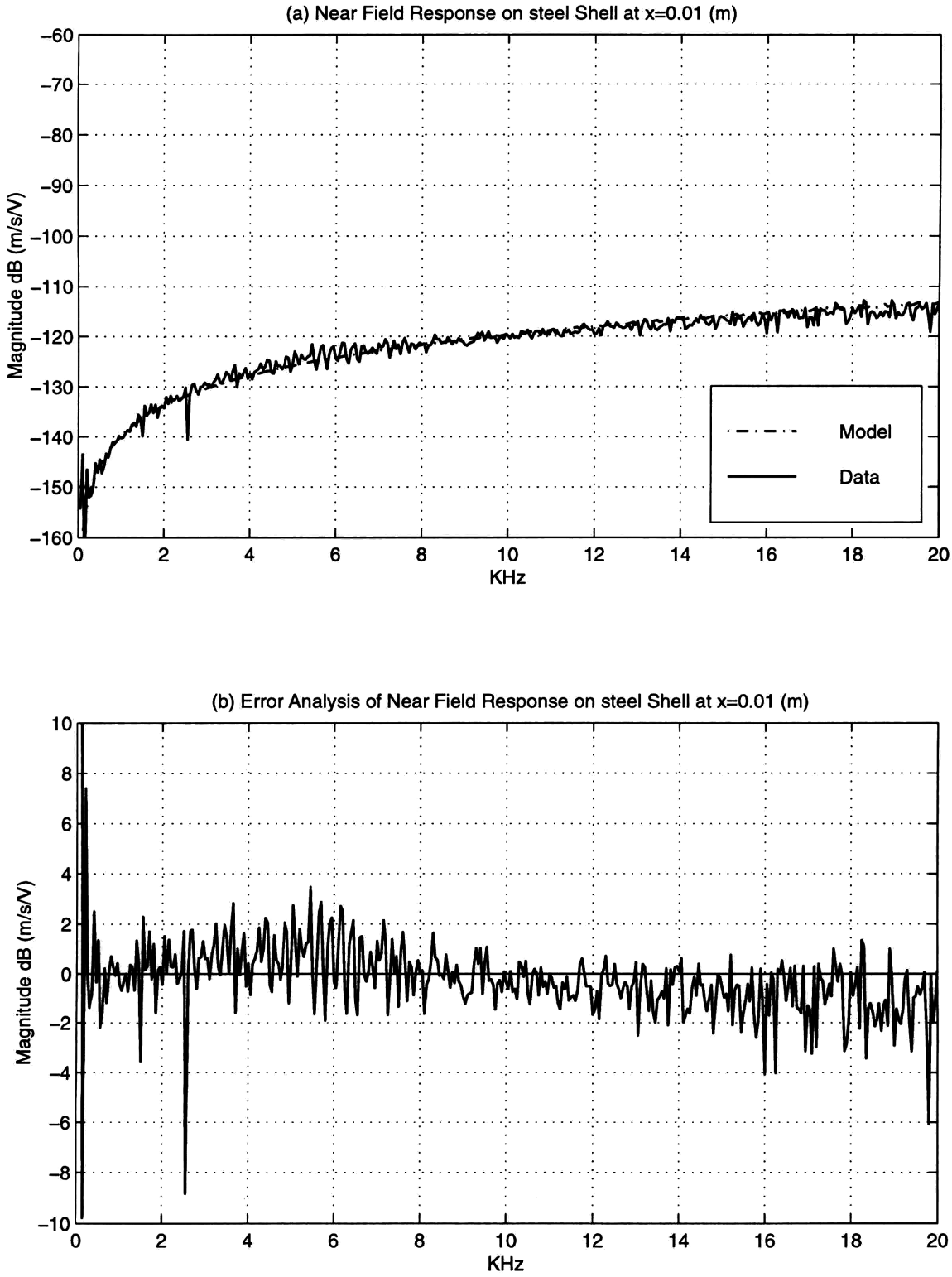

Figure 4.4 Near Field Response at z=0.01m on the Steel Shell in the Linear Frequency Domain (a) Comparison of Model and Data (b) Error Analysis

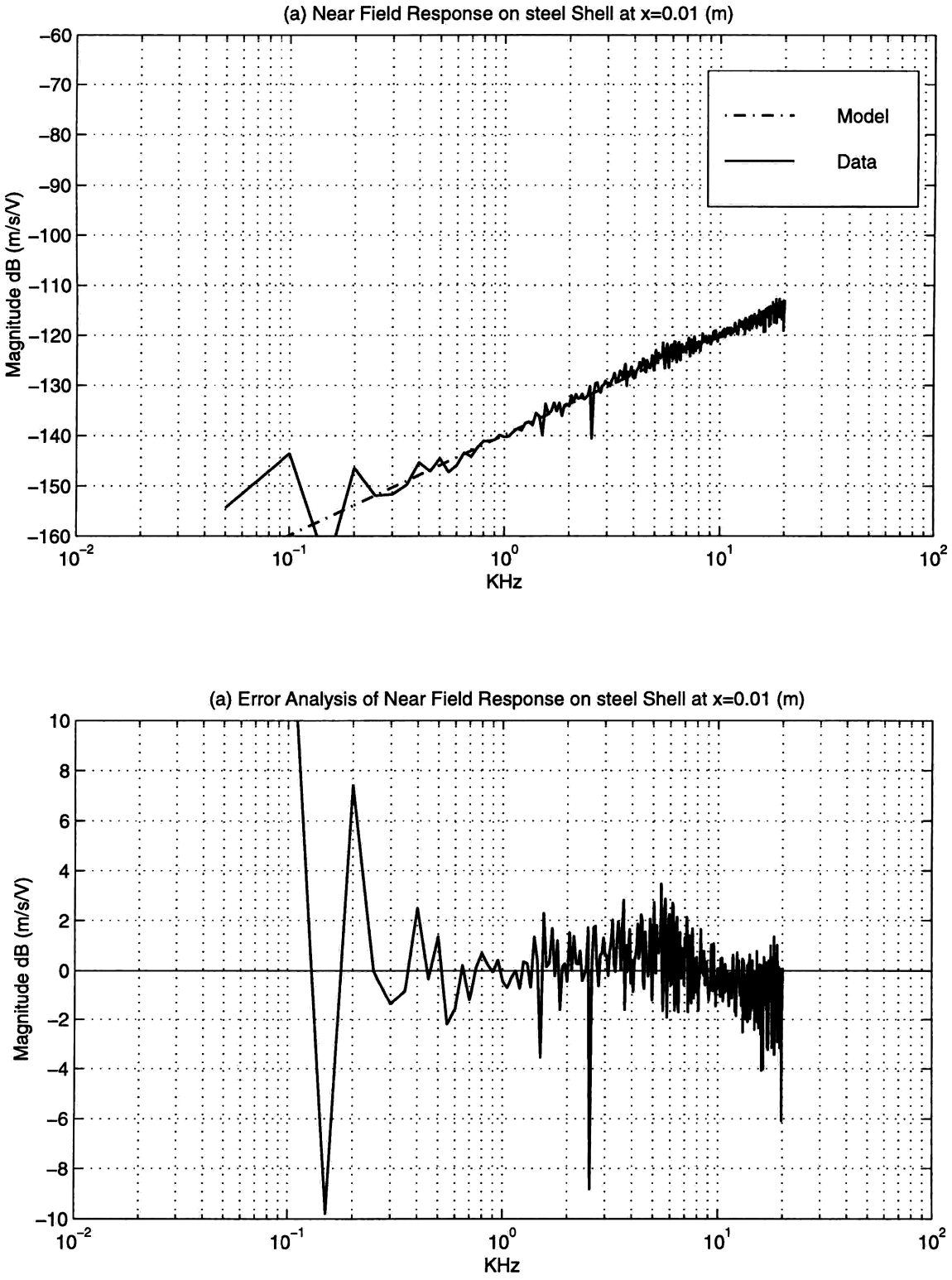

Figure 4.5 Near Field Response at z=0.01m on Steel Shell in the Logarithmic Frequency Domain (a) Comparison of Model and Data (b) Error Analysis

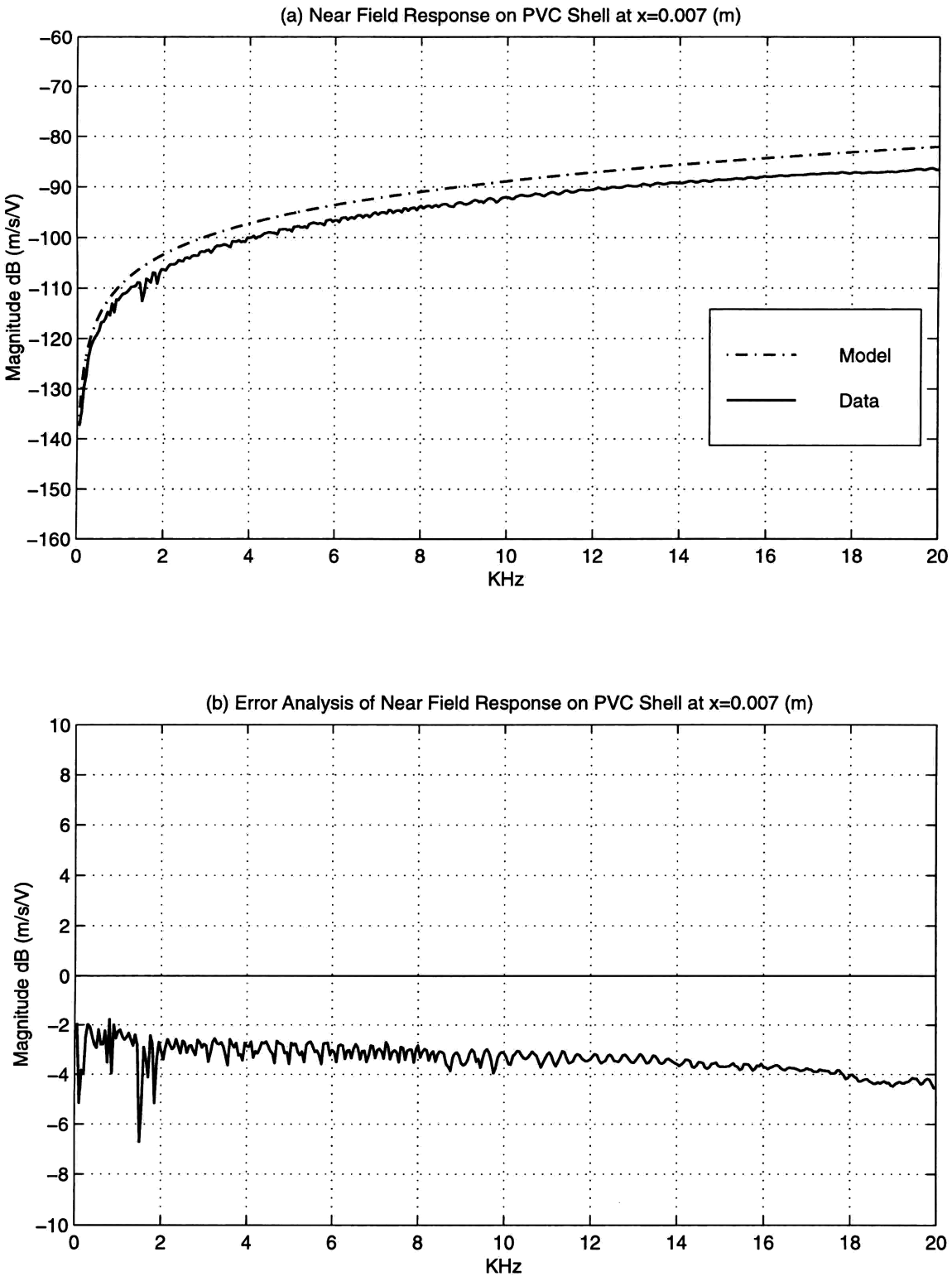

Figure 4.6 Near Field Response at z=0.007m on the PVC Shell in the Linear Frequency Domain (a) Comparison of Model and Data (b) Error Analysis

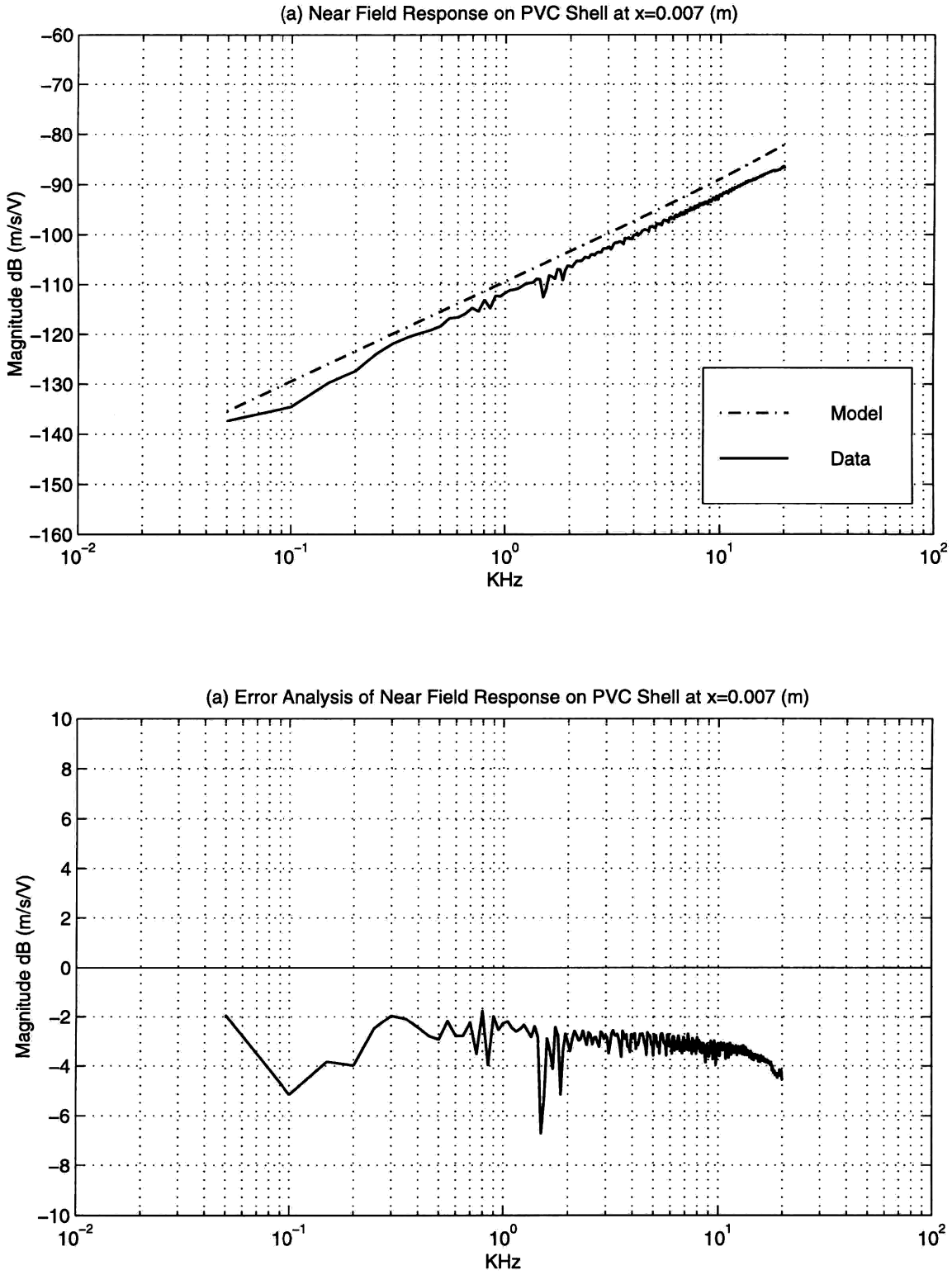

Figure 4.7 Near Field Response at z=0.007m on the PVC Shell in the Logarithmic Frequency Domain (a) Comparison of Model and Data (b) Error Analysis

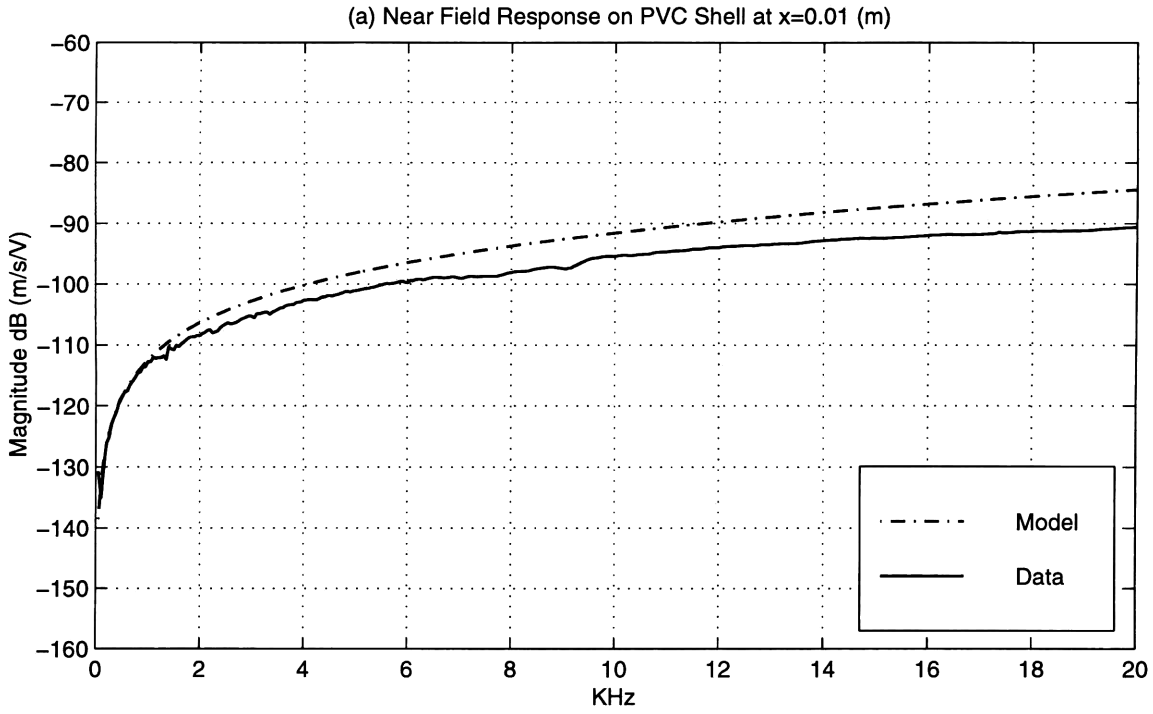

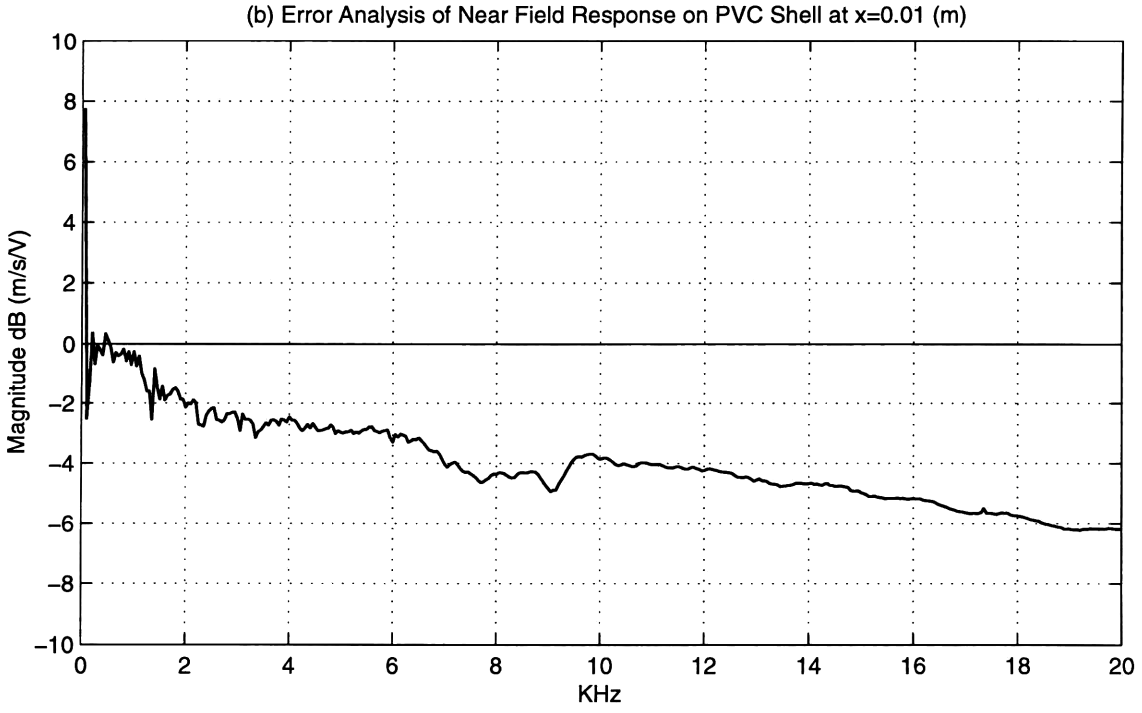

Figure 4.8 Near Field Response at z=0.01m on the PVC Shell in the Linear Frequency Domain (a) Comparison of Model and Data (b) Error Analysis

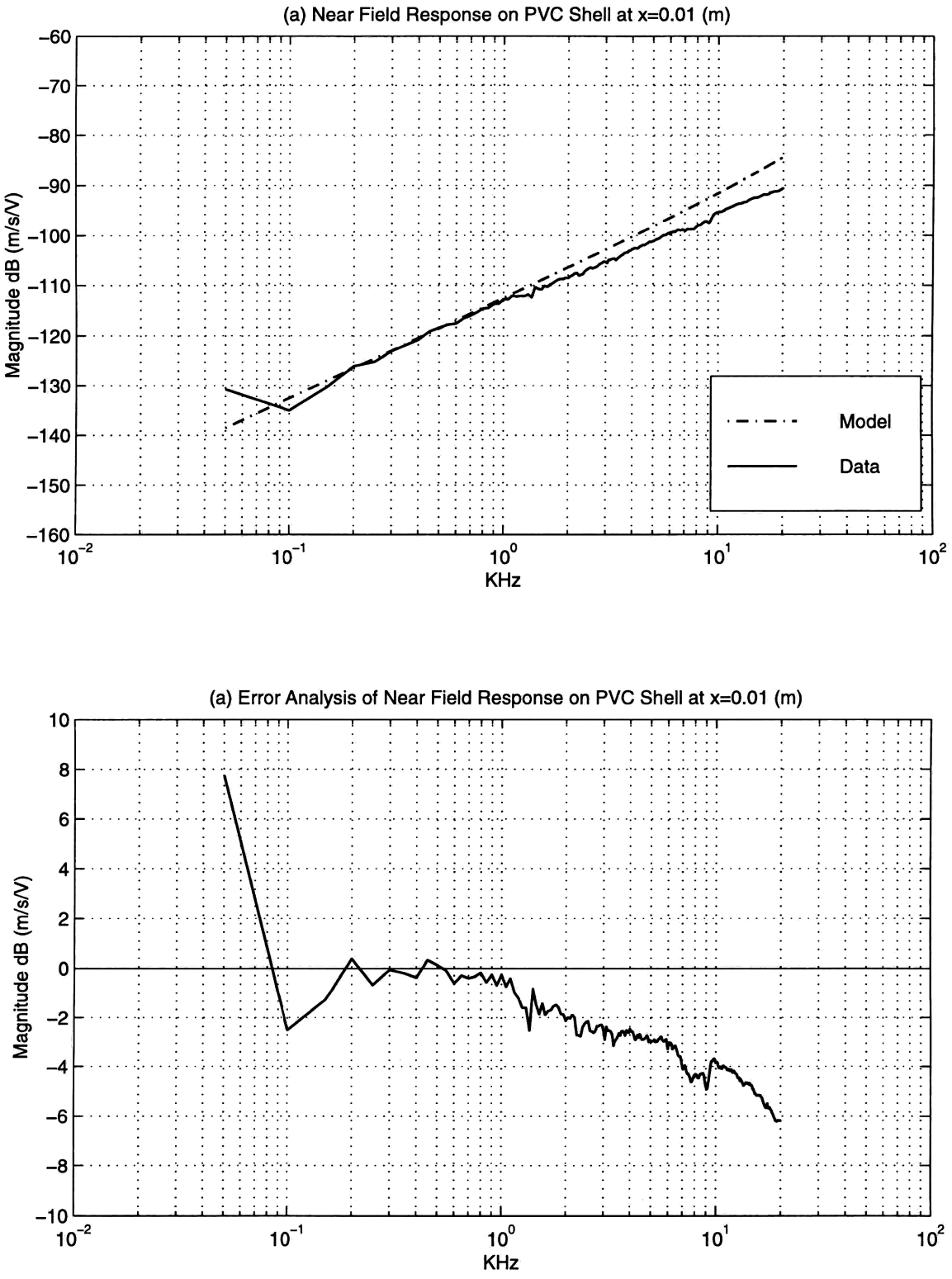

Figure 4.9 Near Field Response at z=0.01m on the PVC Shell in the Logarithmic Frequency Domain (a) Comparison of Model and Data (b) Error Analysis

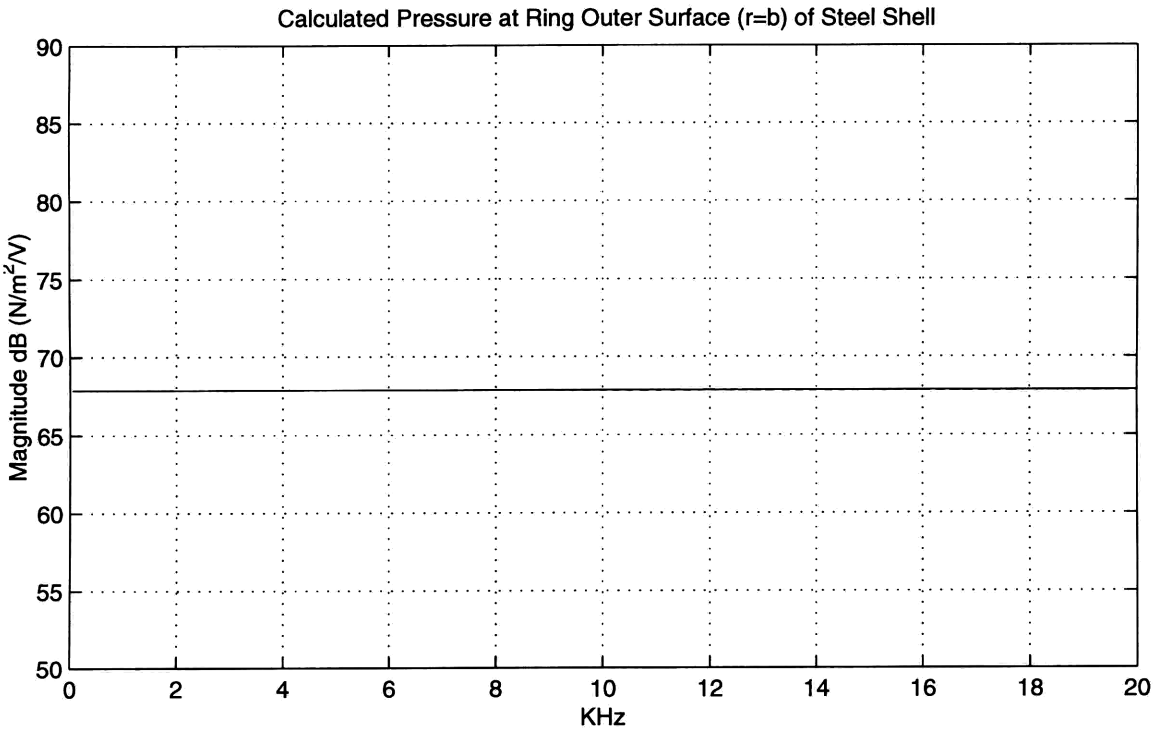

Figure 4.10 Pressure Exerted by the Piezoelectric Ring in the Steel Shell

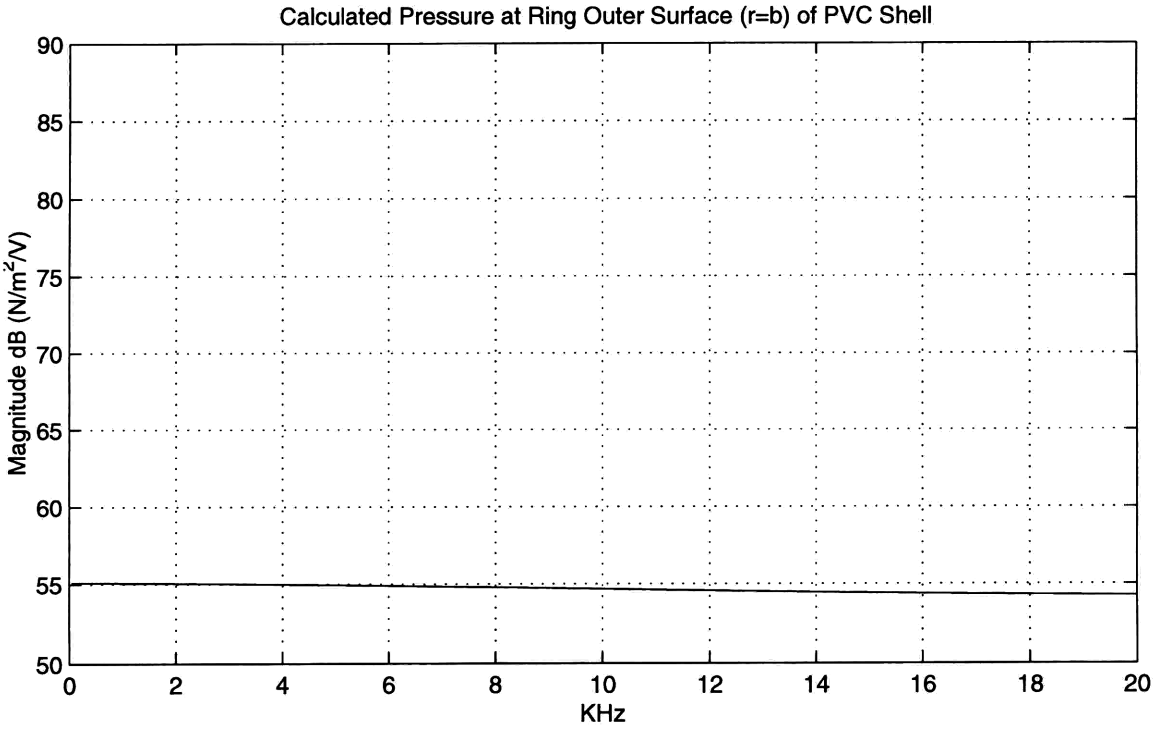

Figure 4.11 Pressure Exerted by the Piezoelectric Ring in the PVC Shell

4.2 Far Field Velocity Response on Cylindrical Shells

The pressure exerted by a single piezoelectric ring embedded in the steel and the PVC cylindrical shells was estimated and validated by comparing the near field response of the measurement to the plate model from the previous section. In this section, it is also interesting to evaluate the far field velocity response on the cylindrical shell. The far field response involves knowledge of wave propagation physics in the cylindrical shell. Borgiotti has introduced "A state vector approach to the wave and power flow analysis of the forced vibration of a cylindrical shell" [3]. This approach can solve the velocity due to a point excitation in any direction at any location on the cylindrical shell. The response due to this point force is a superposition of the response due to infinitely many circumferential modal forces. The difficulty in using this approach to study the far field response excited by the piezoelectric ring is the difference between the unidirectional point excitation in Borgiotti's model and the "compressional" source which exerts forces in all radial directions in the real experimental setup. Therefore, some assumptions must be made to simplify the problem.

It is easier to evaluate the far field response of a symmetric case in which twelve piezoelectric ring sources are excited together and all are in the same phase. Therefore, as illustrated in Figure 4.12, the longitudinal velocity response at a measuring point such as $z = 3.5\,\mathrm{m}$ is contributed by the longitudinal force components exerted by the piezoelectric rings. As illustrated in Figure 4.13, the force exerted by each piezoelectric ring can be decomposed into two longitudinal components. One is in $+z$ direction; the other is in $-z$ direction. These force components can be obtained by integrating the pressure along $\pm z$

directions. Assuming the normal pressure on the outer surface of the piezoelectric ring is P, which is estimated in the previous section, the pressure component in $+z$ direction thus becomes $P\cos\theta$. Integrating this stress component along ring's circumference from $-\pi/2$ to $\pi/2$ gives the total force F exerted by a single piezoelectric ring along z direction

$$F = \int_{-\pi/2}^{\pi/2} P\cos\theta \, dA = 2hrP \tag{4.3}$$

where r and h are the outer radius of the piezoelectric ring and the wall thickness of cylindrical shell, respectively. Assumed that there is no interaction between twelve piezoelectric rings, the total force driven by them along z direction is $12F$. The total force along $-z$ direction is thus $-12F$.

For the far field, the twelve in-phase forces can be treated as two ring forces, i.e. two zero mode circumferential modal forces of magnitude $12F$, respectively. One actuates along $+z$ direction at $z = r$; the other actuates along $-z$ direction at $z = -r$. Using this assumption, the total force per unit circumferential length along $\pm z$ directions is thus $\pm\dfrac{12F}{\pi D}$ and actuating at $z = \pm r$, so the response at far field can be predicted by using Borgiotti's model. Figures 4.14 and 4.15 show the longitudinal response at $z = 3.5m$ on the steel and the PVC shells. In Figure 4.14, using Borgiotti's model and the estimated forces predicts well the longitudinal velocity response on steel shell from 0.5 to 3 KHz. Above 3 KHz, the magnitude level of the predicted response also agrees with experimental measurement. In Figure 4.15, the velocity response and the interference pattern due to the wave propagation in the PVC cylindrical shell are also predicted well

with 3 dB averaged error. Therefore, the estimated forces exerted by piezoelectric rings are validated for the far field velocity response on the steel and the PVC shells.

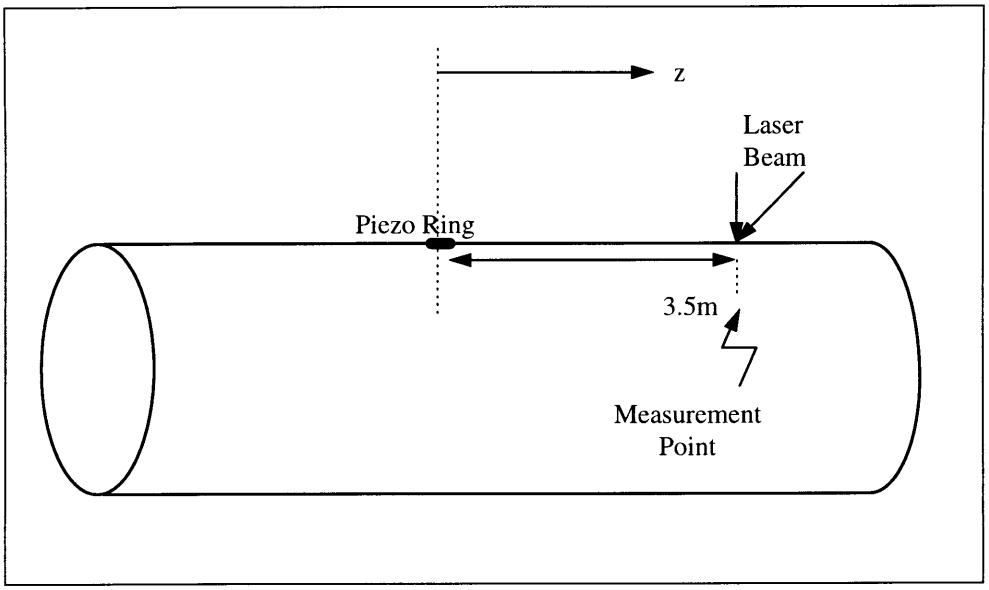

Figure 4.12 Measurement for Far Field Response on the Cylindrical Shell

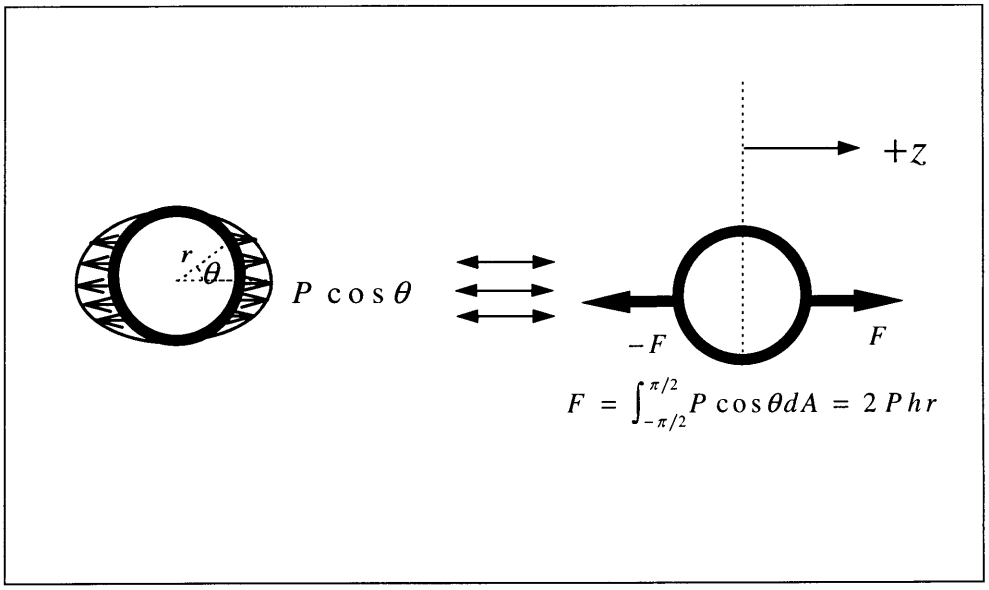

Figure 4.13 Integrating Pressure into a Concentrated Force

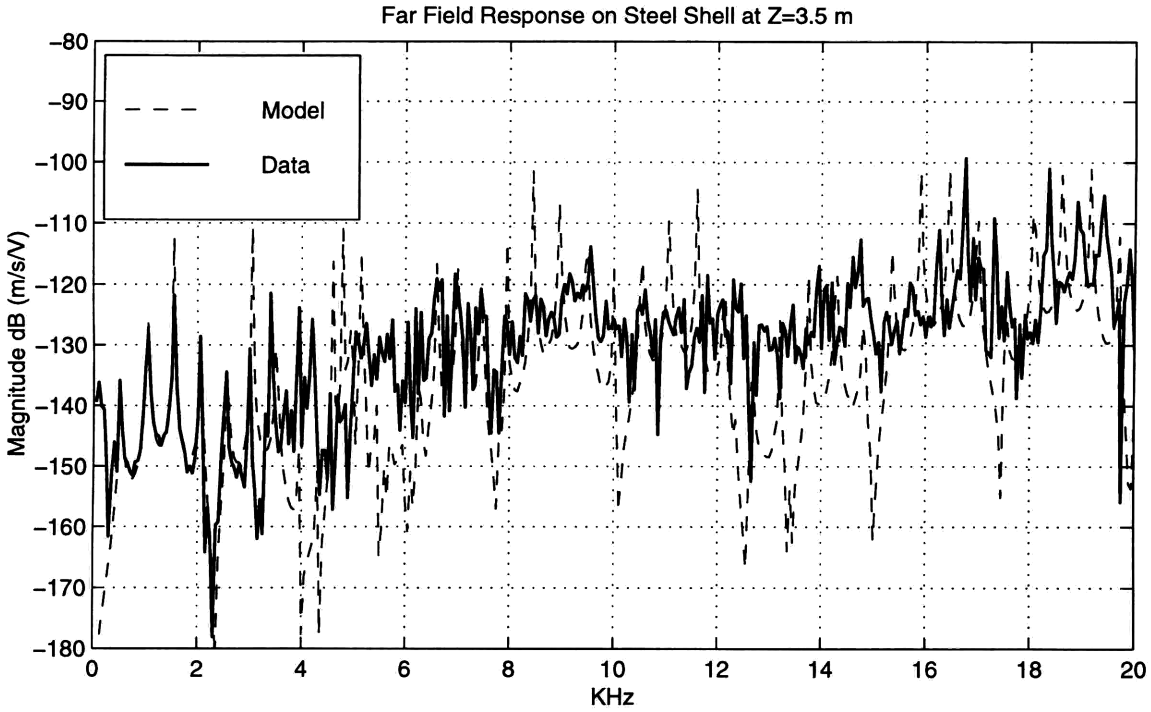

Figure 4.14 Far Field Response at z=3.5m on the Steel Cylindrical Shell

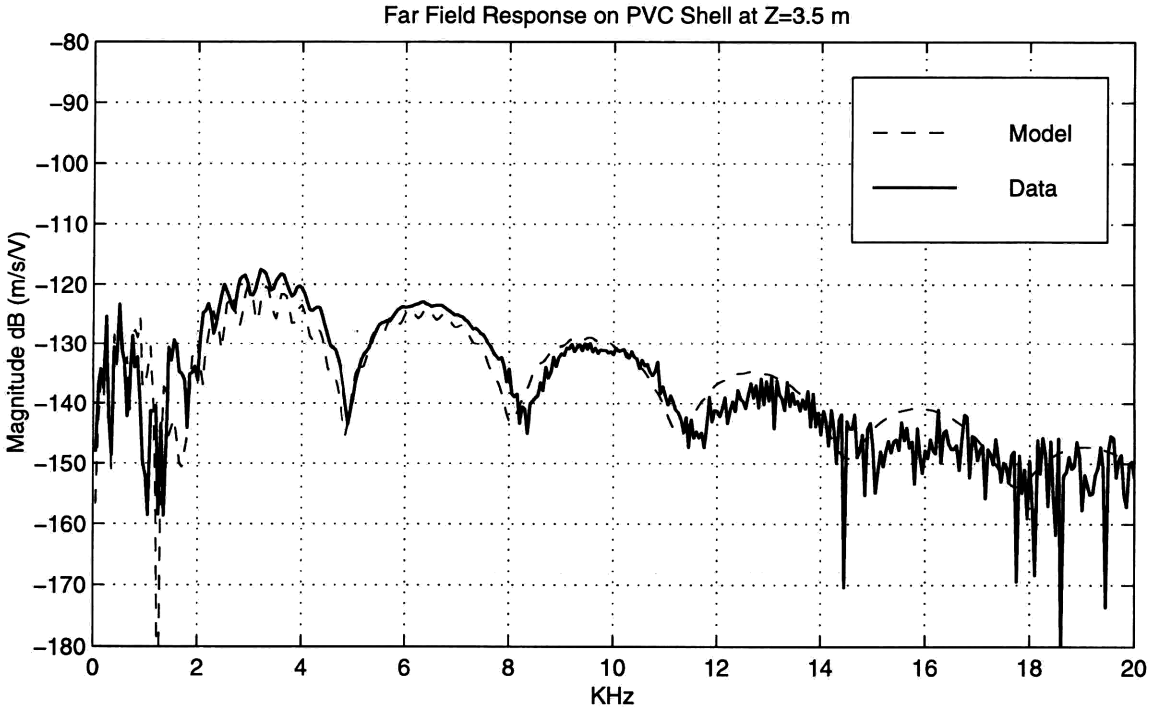

Figure 4.15 Far Field Response at z=3.5m on the PVC Cylindrical Shell

Chapter 5.

Conclusions

5.1 Summary and Conclusions

The goal of this thesis was to estimate the pressure exerted by a piezoelectric ring embedded in a cylindrical shell. The general model of the bonded piezoelectric ring is successfully developed to estimate the pressure exerted by the ring. The model shows that this pressure depends not only on the geometry and the material properties of the piezoelectric ring but also on the radial expansion of the piezoelectric ring which is related to the driving point impedance of the surrounding material. The stiffer or the larger the surrounding material is, the higher the impedance of the surrounding material is, so the less the ring expands.

The dynamic radial expansion at any radial position of the circular plates in which the piezoelectric rings are embedded was also successfully modeled using elasticity theory. The calculated radial velocities at the plate edge and near the outer surface of the ring were validated by experimental measurement. Therefore, the pressure per unit volt exerted by the piezoelectric ring in the circular plate can be estimated using Equation 2.29. The estimated pressure per unit volt exerted by the piezoelectric ring embedded in a 9 cm radius PVC circular plate is about 55 $dB\ re.\ 1\ N/m^2/V$ in the frequency below 20 KHz and almost independent of the frequency except at the two resonant peaks at 5.5 and 14.5 KHz. Similarly, The estimated pressure per unit volt exerted by the piezoelectric ring embedded in a 15 cm radius aluminum circular plate was about 68 $dB\ re.\ 1\ N/m^2/V$ in the frequency range below 20 KHz and almost independent of the frequency except the

resonant peak at 12 KHz. It is reasonable that the pressure exerted by the ring in the aluminum plate is higher than that exerted by the ring in the PVC plate because the stiffness and radius of the aluminum plate are larger than those of the PVC plate; i.e. the impedance of aluminum plate is greater than that of the PVC plate.

Based on this fundamental study of piezoelectric rings in circular plates, the pressure per unit volt exerted by piezoelectric rings in cylindrical shells may be estimated in the same way by assuming that the driving point impedance of the ring in the cylindrical shell is the same as that in a infinite circular plate. Based on this assumption, the calculated longitudinal velocity near the outer surface of the ring in the shell was validated by comparing the calculated velocity to the measured one. The difference between calculated and measured velocity response is about $2dB$ for the known material properties, such as those of steel . The error will grow if the material properties, such as those of PVC, are not exactly known. Since the near field velocity was validated by the experimental measurement, the pressure exerted by the single ring was estimated to be 68 $dB\ re.1\ N/m^2/V$ in the steel shell and 55 $dB\ re.1\ N/m^2/V$ in the PVC shell, and these values are apparently independent of frequency. Using this estimated pressure and Borgiotti's model, the predicted far field longitudinal velocity response on the cylindrical shell was also validated by experimental measurement. Therefore, as shown in Figure 4.10 and 4.11, the goal of this thesis to estimate the pressure exerted by piezoelectric rings orthogonally embedded in cylindrical shells was fulfilled.

5.2 Future Work

The results of the present work provide the future research with the fundamental actuation properties of the piezoelectric rings embedded in the cylindrical shells. The future research can be the design of various modifications to the shell structure, including its frame and bulkheads. A further extension of this research can be made to the study of the modified cylindrical shell in water, which leads the research into a more practical region. Introducing an active control system on the membrane wave control problem by utilizing piezoelectric materials as sensors and actuators can also be an exciting and challenging research area.

Bibliography

[1] C. N. Corrado. *Mid-frequency Acoustic Backscattering from Finite Cylindrical Shells and The Influence of Helical Membrane Waves.* PhD thesis, Massachusetts Institute of Technology, January 1993

[2] I. Dyer and J. R. Fricke, "Structural Acoustics Hull Modification Concepts Proposal for Research," submitted to Office of Naval Research, 10 November, 1994, M. I. T., Department of Ocean engineering.

[3] G. V. Borgiotti and E. M. Rosen. "The state vector approach to the wave analysis of the forced vibration of a cylindrical shell. Part II: Finite cylinders in vacuum." J. Acoust. Soc. Am., 93(2): 864-874, 1993

[4] J. E. Bondaryk, "Modal Excitation and Control of Membrane Waves on Cylindrical Shells," submitted to the Journal of the Acoustical Society of America, June 1997

[5] IEEE Std 176-1978, *IEEE Standard on Piezoelectricity*, The Institute of Electrical and Electronics Engineers, pp. 9-14 (1978)

[6] J. F. Haskins and J.L. Walsh. "Vibrations of ferroelectric cylindrical shells with transverse isotropy. I. Radially Polarized Case." J. Acoust. Soc. Am. 29: 729-734 (1957)

[7] G. S. Kino. *Acoustics Waves*, :Englewood Cliffs,N.J. , Prentice-Hall, 1987.

[8] N. W. Hagood, W. H. Chung and A. H. von Flotow. "Modeling of Piezoelectric Actuator Dynamics for Active Structural Control." J. of Intell. Mater. Syst. And Strut., Vol 1, July, 1990.

[9] N. W. Hagood. Lecture Notes on "Adaptive Materials and Structures." Massachusetts Institute of Technology, 1996.

[10] O. E. Mattiat. *Ultrasonic Transducer Materials*. Plenum Press, New York, 1971, pp.103-109

[11] S. P. Timoshenko and J. N. Goodier. *Theory of Elasticity*. McGraw-Hill Book Company, Inc., New York, 1970, pp. 70-71

[12] Channel Industries, Inc., *Piezoelectric Ceramics Manual,* 839 Ward Drive, Santa Barbara, CA 93111

[13] Polytech PI, Inc., *Vibrometer Operator's Manual*, 23 Midstate Drive, Suite 212, Auburn, MA 01501.

[14] DSP Technology, Inc. , *SigLab User's Guide, Version 2.13*, 48500 Kato Road, Fremont, Ca 94538-7385.

[15] M. P. Norton. *Fundamentals Of Noise And Vibration Analysis For Engineers*, New York, Cambridge University Press, 1989, pp.77

[16] M. Ashby and D. R. H. Jones. *Engineering Materials: An Introduction to Their Properties and Applications.* Pergamon International Library, 1980

[17] J. M. Gere and S. P. Timoshenko. *Mechanics of Materials.* PWS-KENT Publishing Company, Boston, 1990.